WAVE OVERTOPPING OF HYBRID COASTAL STRUCTURES: AN ANALYSIS FOR SAND-COVERED RUBBLE MOUNDS

A Dissertation

by

BADREYAH F A N S ALMARSHED

Submitted to the Office of Graduate and Professional Studies of
Texas A&M University
in partial fulfillment of the requirements for the degree of

DOCTOR OF PHILOSOPHY

Chair of Committee,	Jens Figlus
Committee Members,	Robert Randall
	James Kaihatu
	Wilford Gardner
Head of Department,	Sharath Girimaji

May 2019

Major Subject: Ocean Engineering

ABSTRACT

Considering the accelerating sea level rise, population growth, and coastal developments, the risks associated with extreme storms are expected to increase. To meet this dilemma, hybrid coastal approaches are being employed in various coastal communities. Hybrid coastal approaches can offer protection against flood and coastal erosion while adding recreational value to the coastal areas. Despite all the inherent benefits, many knowledge gaps relevant to their performance still exist. In addition, there is no design framework for these structures. This dissertation focuses on advancing the knowledge of physical processes related to wave-sediment-structure interactions. The first empirical formula to predict wave overtopping rate of a hybrid coastal structure consisting of rubble mound covered by a varying finite sand layer was developed. A physical model experiment consisting of 32 trials, including both the pure rubble mound and the hybrid structures, was conducted in a wave flume with moveable-bed capabilities. A Froude scaling factor of 1:20 was selected to fit the prototype structure properly in the wave flume. Irregular wave trains with significant wave height, H_{m0}, of 9 – 12 cm and peak wave periods, T_p, of 1.64 – 1.9 s were tested. The morphological evolutions of the modeled hybrid structure were captured by laser line scanner measurements. The hydrodynamic conditions were measured by capacitance wave gauges. Acoustic Doppler velocimeters were used to estimate the kinetic energy. An empirical formula to predict the average wave overtopping rate was proposed using nonlinear regression. The analysis and the formula show a high dependency of the average wave overtopping rate on the dimensionless parameter $R_c h_t / H_o^2$. The data correlate well with the proposed equation ($R^2 = 0.72$). The instantaneous wave overtopping rate was found to be best represented by the Weibull distribution where the correlation between the data and the distribution was 0.998. The findings of

this study can aid in understanding the processes related to wave overtopping of a hybrid coastal structure. In addition, this study can help decision makers to select the best protection scheme for their coastal communities, based on the capability of the presented structure in reducing flooding and wave energy.

DEDICATION

I dedicate my dissertation work to my family. A special feeling of gratitude to my loving parents, Mr. and Mrs. Almarshed whose words of encouragement pushed me forward. My sister has never left my side and she was always there for me. I also dedicate this dissertation to my brothers who have supported me throughout the process. I will always appreciate all they have done for me. I dedicate this work and give special thanks to my best friend for being there for me throughout the entire doctorate program.

ACKNOWLEDGEMENTS

Firstly, I would like to express my sincere gratitude to my advisor Dr. Jens Figlus for the continuous support of my Ph.D. study and related research, for his patience, motivation, and immense knowledge. His guidance helped me in all the time of research and writing of this disssteration. I could not have imagined having a better advisor and mentor for my Ph.D. study.

Besides my advisor, I would like to thank the rest of my committee, Dr. Robert Randall, Dr. James Kaihatu, Dr. Wilford Gardner, and Dr. Mohamad Alkhalidi for their guidance and support throughout the course of this research.

My sincere thanks also go to Kuwait University for their financial and academic support.

Thanks also go to my friends, my research group members, my colleagues, and the department faculty and staff for making my time at Texas A&M University a great experience.

Special thanks to my mother and father for their encouragement, and to my sister and brothers for their trust, patience, and love.

CONTRIBUTORS AND FUNDING SOURCES

Contributors

This work was supervised by a dissertation committee consisting of Professor Jens Figlus and Robert Randall of the Department of Ocean Engineering, Professor James Kaihatu of the Department of Civil Engineering, Professor Wilford Gardner of the Department of Oceanography and Professor Mohamad Alkhalidi of the Department of Civil Engineering at Kuwait University.

All other work conducted for the dissertation was completed by the student independently.

Funding Sources

Graduate study was supported by a scholarship from Kuwait University to achieve a Ph.D. degree in Ocean Engineering at Texas A&M University.

TABLE OF CONTENTS

Page

LIST OF FIGURES

Page

LIST OF TABLES

Page

CHAPTER 1

INTRODUCTION

1.1 Background

In light of increasing storm risks due to climate change and sea level rise, the protection of infrastructure and coastal developments becomes a major concern for federal, state, and local governments, stakeholders, and research institutions. Risks associated with extreme flooding and coastal erosion call for innovative defenses that can provide protection during extreme events and adapt to climate and environmental changes. One option of such innovative defenses is a hybrid coastal structure. This structure combines coastal defenses, ecology, and planning approaches where the benefits of each element are married to form a single defense system. A hybrid coastal structure is a feasible Engineering-with-Nature® (EWN) solution that could be designed and shaped according to the recreational, ecological, and habitat-based needs of coastal communities. Thus, this type of defense system would enhance and enrich the use of natural resources and add environmental and socioeconomic benefits while at the same time providing the required safety measures against flooding and storm events.

Recently, more attention has been drawn toward hybrid coastal structures as an alternative to traditional defenses (Basco, 1998; Irish et al., 2013; Voorendt, 2015; Boudreau et al., 2018; Nordstrom, 2018). Hybrid coastal structures come in different shapes and varieties. In a broader sense, researchers have used the term multifunctional flood defenses for systems that incorporate protection, erosion control, ecosystem benefits and other functions (Voorendt, 2017). Sutton-Grier et al. (2015) defined the hybrid coastal approach as a combination of natural (e.g., sand dunes,

coral reefs, oyster beds, and mangroves) and built infrastructure (e.g., seawalls, revetments, levees, and dikes). According to Boers (2012), a hybrid coastal approach is a combination of sand dunes with a hard structure that acts as a flood defense. Here, the latter definition of a hybrid coastal structure will be used where dynamic (e.g., sand dune or sand cover) and static (e.g., hard structure) components work together to fulfill various functional requirements. Despite different configurations of such structures, many researchers agree on the inherent benefits of enhancing the protection and restoration of ecosystems while offering the desired level of infrastructure protection. A hybrid structure can protect coastal areas against chronic erosion due to sea level rise, wave and tidal currents, and positive gradients in alongshore sediment flux. Also, it can reduce wave energy attacking the static element by providing an erodible sand layer that acts as a buffer and forms a sand deposit in the foreshore (Figure 1).

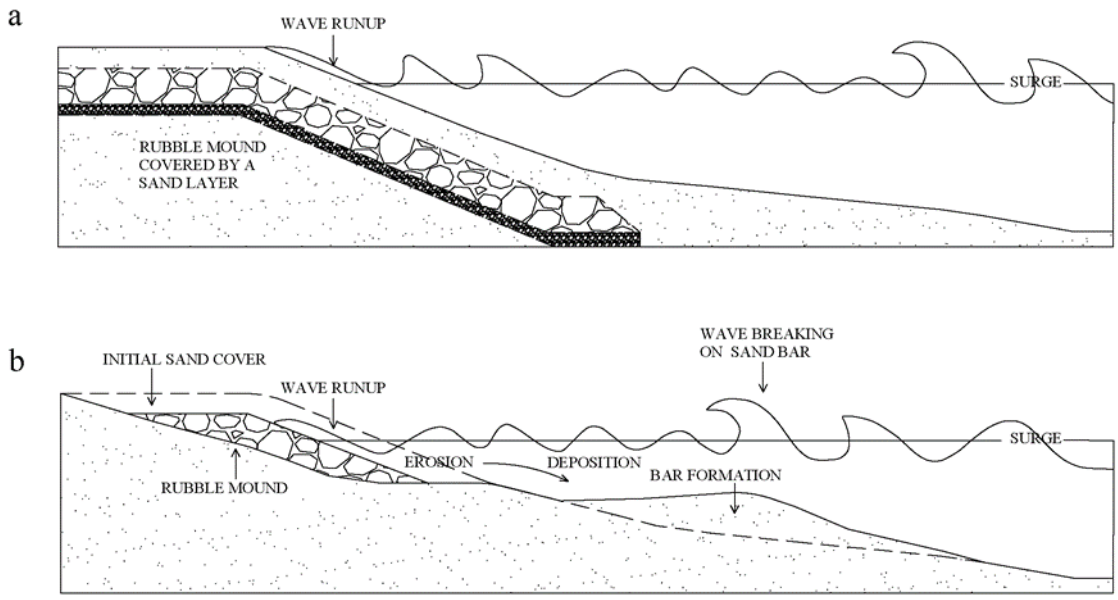

Figure 1 Schematic of a hybrid coastal structure type consisting of a sand layer covering a hard core. (a) An example of a hybrid coastal structure where a rubble mound structure and sand cover are integrated into a single system. During extreme storm conditions, the sand layer can act as a buffer and forms sediment deposits in the foreshore, which can reduce the wave energy hitting the structure (b).

Several examples of hybrid structures exist and are mainly found in Europe and the United States. However, some of these structures are not intended by design to be hybrid coastal structures. Rather, they fit into that category accidentally as they provide an efficient protection against storm impacts. An example of a hybrid structure in the United States is the relic seawall, along the Bay Head coast in New Jersey. The relic seawall has been buried underneath a sand dune via natural processes and nourishment activity (Figure 2). During superstorm Sandy, this hybrid structure provided significant protection for the island against wave forces and inundation compared with the adjacent parts of the island without a hybrid structure (Irish et al., 2013;

Smallegan et al., 2016). Basco (1998) reported on a dune system with a buried seawall that successfully offers protection for naval infrastructure facing the Atlantic Ocean in Dam Neck, Virginia (Figure 3). Another example is an embedded rubble mound structure in a sandy cover in Maui, Hawaii (Figure 4). This hybrid solution is adding recreational value to the beach, reducing coastal erosion in the upland area, and protecting the island from potential risks associated with sea level rise (Boudreau et al., 2018). Additional examples of hybrid structures are employed in Europe such as a dike-in-dune defense system in Noordwijk, the Netherlands (Figure 5). This hybrid structure protects the coastal communities behind it from flooding while the hybrid nature allows it to blend in with the natural fabric of the area (Arcadis, 2012; Voorendt, 2017). Another example in Katwijk, the Netherlands, is a rubble mound dike consisting of basalt blocks on top of a filter layer and geotextile and covered by a sand layer. This hybrid system includes a parking garage that was constructed within the dune shape, as shown in Figure 6, to optimize the use of space near the coastal boulevard (Voorendt, 2015). It is worth noting that such hybrid structures are preferred over traditional shore protection solutions because of the potential flood protection, economic, and social benefits. Moreover, it can be viable protection solutions in areas with limited spaces.

Figure 2 Photo of an “accidental” hybrid coastal structure along the narrow beach of Bay Head, New Jersey, consisting of a relic seawall underneath a sand cover. The hard core has been exposed after wave-induced erosion of the seaward face of the sand cover triggered by superstorm Sandy. Photo courtesy of Jon Miller.

Figure 3 Photo of buried seawall in a sand dune in Dam Neck, Virginia during construction. Photo reprinted from Basco (1998).

Figure 4 Rubble mound before it was covered with sand in Maui, Hawaii. Photo reprinted from Boudreau et al. (2018).

Figure 5 A photo of an engineered hybrid coastal structure along Noordwijk, the Netherlands, during the construction processes. The structure consists of a sand core that is covered by basalton blocks that are then covered by sand again. Photo courtesy of Henk Jan Verhagen.

Figure 6 Photo of a dike-in-dune system with a parking garage in Katwijk, the Netherlands. Photo by Badreyah Almarshed.

Other hybrid coastal structures configurations have been introduced in different locations. In Norderney, Germany, a composite coastal protection system was employed to protect the island against storm surge and erosion. The composite defense consists of groins, a dune revetment, innovative wall elements on the upper section of the revetment, and a crest wall (Figure 7). The combination of wall elements and vertical segments reduced wave runup and overtopping (Thorenz and Blum, 2011). The latter hybrid system overcame the constraint of limited space and helped meet the tourism requirements of the area. Accordingly, such innovative coastal defenses are vital to adapt to rising sea levels and the lack of space for protecting coastal infrastructure.

Another example of a composite defense system is in Ostend, Belgium. The defense system consists of a seawall, a sandy foreshore, and a groin system. The groin system accelerated erosion of the beach instead of preserving the touristic nature of the area. Subsequently, soft and hard coastal protection measures, such as beach nourishment, dunes, vertical walls, and storm surge barriers, have been studied with the existing seawall to assess how well they reduce the risk of flooding, their potential environmental impacts, and their costs. Among the studied coastal protection alternatives in Ostend, the beach nourishment was found to be the most cost-efficient in the long term (Mertens et al., 2011). Although beach nourishment is an option for reducing the impacts of severe storms, it is not always applicable, especially in areas that are close to harbors (Van Doorslaer et al., 2009) because there is a high possibility that part of the eroded beach nourishment sediment will accumulate in the basin and/or the entrance of the harbor.

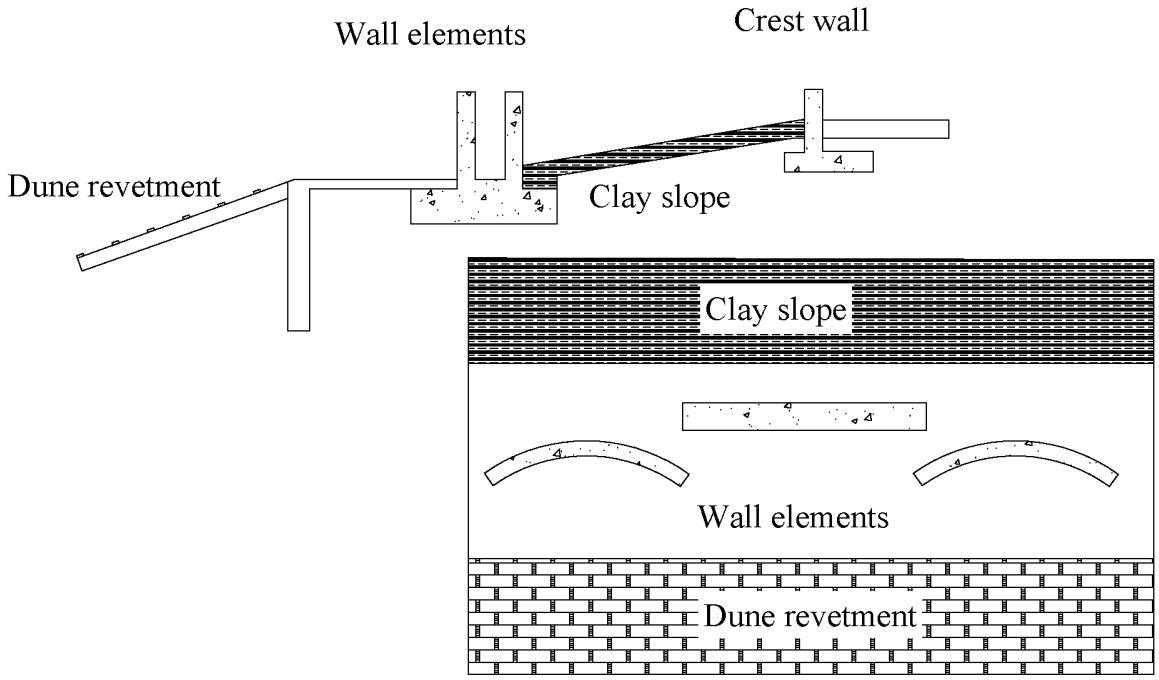

Figure 7 Schematic of the composite defense system in Norderney, Germany. The defense system combines hard and soft defense approaches together to reduce coastal flooding and erosion. Photo adapted from Thorenz and Blum (2011)

Although hybrid coastal structures have become more common recently, there are still no generally applicable guidelines or design criteria. Research on hybrid concepts has many gaps, especially in estimating the hydrodynamic responses, erosion processes, and environmental impacts of these hybrid structures. Also, the replenishment or maintenance plans for such structures are not well-examined. Most importantly, the interaction between the soft and hard elements of a hybrid structure is still obscure.

Some research efforts related to hybrid structures are focusing on the morphological response during a storm (e.g., Boers et al., 2011; Van Thiel de Vries, 2012; Figlus et al., 2015; Nederhoff et al., 2015; Smallegan et al., 2016; Muller, 2017). Only a few studies investigated the wave hydrodynamics during wave overtopping regimes (Kim, 2017; Kobayashi and Kim, 2017). In addition, current design practices treat hard and soft protection applications separately without evaluating how the combined protection may help in reducing storm impact and affect the cross-sectional design of the hard element.

This research aims to fill some of the knowledge gaps in hydrodynamic and morphodynamic processes of a hybrid structure consisting of a rubble mounds buried under a sand cover. The motivation behind this research is to introduce a framework outlining knowledge gaps and open research questions related to hybrid structures and to evaluate the performance of hybrid structures as a risk reduction measure under wave attack. This research aims to develop a functional design equation to estimate the wave overtopping over a hybrid coastal structure based on hydrodynamic and morphodynamic responses during a storm event. The outcomes of the research can help decision makers to adopt such hybrid strategies for coastal communities in light of the potential threat of accelerated sea level rise. It is worth noting that some vulnerable coastal cities are considering risk reduction measures that are environmentally friendly and aesthetic. One example is the proposed hybrid protection plan for the Greater Houston/Galveston metropolitan area. A surge barrier consisting of a core-enhanced dune is one potential option within a coastal spine system that would protect the greater Houston/Galveston region from storm surge impacts (Ebersole et al., 2015; U.S. Army Corps of Engineers, 2018).

1.2 Identified Research Problems and Objectives

Hybrid coastal defenses are being constructed in various locations around the world without explicit design guidance. Traditional coastal defenses (i.e., hard coastal structures and sand dunes), that are constructed to specific parameters and they required maintenance or adaptation to withstand the effects of changing water level and the added effects of tide, storm surge, and hydrodynamic conditions. Hybrid coastal defenses can be flexible in adapting to future climate and environmental changes. They can be designed and shaped (changed in the future easily) according to ecological, habitat and environmental requirements in a coastal area. Also, hybrid approaches can be integral parts of coastal sediment feeder systems (i.e., mega nourishments), and may play a vital role in erosion control and can be a practical solution to deal with the architectural considerations for touristic areas. However, lack of knowledge about the effectiveness of hybrid defenses for flood mitigation, potential cost benefits, and maintenance plans can make these defense systems controversial.

There are some known constraints of working with hybrid approaches. First, most of the hybrid approaches are new, and their performance is not well evaluated during storm events. Second, there are no explicit design guidelines or formulae for wave overtopping and runup over the crest of a hybrid coastal structure, and therefore the optimum crest height of the hybrid structure cannot be calculated. The existing studies of hybrid structures mainly investigated dune evolution due to high water levels and surge during storms. The effectiveness of hybrid structures in enhancing storm protection for coastal communities is not well treated.

The three significant problems that were considered in working with hybrid coastal structures are:

1. Existing literature on wave overtopping and runup covers hard coastal structures only (e.g., impermeable or permeable, smooth or rough slopes, continuous or composite slopes, etc.). For hybrid structures, it is expected that the covering sand layer influences wave overtopping and wave runup characteristics over the crest of a hybrid coastal structure. Different wave runup and wave overtopping behaviors are expected due to beach profile evolution by wave-induced erosion and overwash processes.

2. The current practice treats hard and soft defenses separately, neglecting the fact that combining multiple elements within a coastal structure may alter the required design crest level.

3. The accuracy of current prediction formulas for wave overtopping over a hard-coastal structure have not been verified for hybrid structures.

The overall objective of this research is to provide a better understanding of the fundamental dynamic processes during wave overtopping events and develop a practical design tool for hybrid coastal structures based on total overtopping discharge volumes. This research also aims to investigate the morphological responses of the sand cover to identify any changes that may occur in hydraulic loading and wave overtopping behavior during an extreme event. The current research provides detailed insight into the overtopping phenomenon for rubble mound structures covered by a sand layer. The intention here is to provide prediction formulae for the average and instantaneous wave overtopping discharge rates.

The research objectives are summarized as follows:

1. Estimate the morphological evolution of hybrid coastal structures consisting of a rubble mound and with different sand cover thicknesses and under various hydrodynamic forcing conditions.

2. Evaluate the effects of initial sand cover layer thickness and resulting changes of the beach profile in front of hybrid structures on wave overtopping rates.

3. Compare the performance of the hybrid structure in reducing wave overtopping discharge and dissipating wave energy with that of pure rubble mound structures under the same hydrodynamic forcing conditions.

4. Establish a functional relationship between wave overtopping discharge rates and the geometrical parameters of hybrid structures including height and sand cover thickness.

The research hypotheses to be tested are:

1. If sand cover layer over a fixed height rubble mound structure reduces wave overtopping discharge volumes, then hybrid coastal structures with thicker sand cover layer provide better protection against flooding compared to traditional coastal structures during wave attack. This hypothesis can be explained as follows:

    a. Under wave-induced erosion and overwash processes, it is thought that as waves approach the hybrid structure, the initial sand cover ramp effect (i.e., the sand cover layer reduces the roughness and the porosity of a rubble mound structure) changes to a dissipation effect through submerged sand berm/bar formation near the toe of the structure as the sand layer evolves during storm impact.

    b. A greater volume of sand covering the hard structure while maintaining a fixed surge level is presumed to provide better protection against wave overtopping once the beach profile reaches its equilibrium state. This can be explained by the ability of the sand bar/berm to increase the dissipation of wave energy hitting the exposed rubble mound structure. However, in real storms the sand cover effect might be

reduced since the gradual increase of surge levels and wave energy will erode the dune and move sediment further offshore before wave overtopping occurs.

2. The presence of a dynamic sand cover as part of the hybrid structure alters the water depth and the hydraulic conditions that will eventually influence wave overtopping discharge over the crest. Therefore, new parameters may be necessary in the prediction formula for hybrid structures.

1.3 Research Approach

Wave overtopping at a hybrid coastal structure is a complex phenomenon. Both hard and soft elements of a hybrid structure can influence the physical processes relevant to overtopping discharge rates. Prediction methods for wave overtopping discharge of hybrid structures are not available. Research investigating wave overtopping can be divided into two categories; small or large physical model experiments (either fixed-bed or movable bed models), or numerical model tests. In physical model tests, a scale model is built and the water volume of overtopped waves is collected. In numerical model tests, it is inevitable to make assumptions and simplifications in terms of the governing equations and the geometry of the simulated structure. Currently, the available numerical modeling capabilities cannot be used to accurately predict wave overtopping for a certain coastal structure. It is quite challenging to numerically simulate the complicated rubble mound and sand cover interactions. Many assumptions have to be made in order to investigate overtopping over a hybrid structure using numerical models. Therefore, the current study investigates the wave overtopping discharge rate at hybrid structures through physical model experiments. Physical model testing is used mainly to investigate complex phenomena that cannot be addressed analytically and to obtain empirical prediction formulae. Improving numerical model

capabilities to incorporate overtopping of sand-covered rubble mounds will be a next step but is beyond the scope of this dissertation.

This dissertation is organized as follows. Chapter 2 presents a literature review related to hybrid structure processes and discusses design implications for rubble mound structures and engineered sand dunes. The chapter also presents the state-of-the-art of hybrid coastal structure approaches and design. Chapter 3 describes the research methodology including experimental setup, laboratory instruments, and data processing. Chapter 4 presents the results including wave hydrodynamics, cross-shore profile evolution, and average and instantaneous wave overtopping discharge rates. In addition, the influence of different variables on wave overtopping discharge are discussed and a comparison between the performance of hybrid and rubble mound structures during storm events in terms of wave overtopping is presented. Finally, the findings, conclusions, and recommendations from this study are presented in Chapter 5.

CHAPTER 2

LITERATURE REVIEW

This study is intended to serve as a stepping stone for further hybrid structure research and design efforts. First and foremost, it raises awareness surrounding the lack of proper criteria and formulae to design hybrid coastal structures and the need to develop such design approaches. Hybrid coastal defenses come in different shapes, configuration, and varieties. In the scope of this study, one type of hybrid coastal defense consisting of a sand cover on top of a rubble mound structure is investigated. Dune and beach systems are often used on the ocean side of hard structures to provide an extra line of defense and to preserve the landscape. Hard coastal structures are more effective than soft defenses alone at preventing severe storm damage to infrastructure from wave impact and flooding during their design life. However, in certain situations where space or sand material is scarce, the need to combine the two approaches into one structure may arise. To this end, it becomes essential to develop functional design formulations relevant to the hydrodynamic and morphodynamic processes. The following sections review the current design approaches for rubble mound structures and engineered sand dunes separately before attempting to combine them into a single structure.

2.1 Functional Design Implications of a Rubble Mound Structure

Coastal structures are constructed along the shoreline to minimize the wave-induced erosion and flooding associated with extreme events. Hard coastal structures including seawalls and rubble mounds are constructed parallel to the shoreline and they mainly protect landward areas from waves and flooding. This research focuses mainly on rubble mound structures because they

are widely used, can be adapted to work with most coastal water depths, and can be repaired readily (U.S. Army et al., 1978). Rubble mound structures consist of large armor units (e.g., quarry stones or concrete elements) covering the filter and core layers. This armor is responsible for the rough surface of rubble mound structures and significantly affects wave runup, energy dissipation, and overtopping.

2.1.1 Wave runup

Wave runup is a complex phenomenon that depends on local water levels, incident wave conditions, and the nature of the beach or structure. It is defined as the maximum vertical extent of wave uprush on a beach or structure above the still water level (Van der Meer et al., 2016). Wave runup has a significant impact on the design of various natural and artificial coastal defenses, having led to numerous studies on this issue over the past few decades (e.g., Miche, 1944; Hunt, 1959; Takada, 1970; de Waal and Van der Meer, 1992; Ahrens et al., 1993; Hedges and Reis, 2004; Van der Meer et al., 2016). Based on a linear Lagrangian equation of motion in shallow water, Miche (1944) derived an equation for calculating wave runup for breaking waves. Based on laboratory data, Hunt (1959) established a non-dimensional wave runup formula for breaking waves on smooth, rough, and composite slopes. Takada (1970) improved Miche's formula for wave runup and breaking waves by including the slope effect. de Waal and Van der Meer (1992) proposed the following empirical formula for wave runup and overtopping on smooth and rocky slopes:

$$\frac{R_{u2\%}}{H_s} = 1.6\,\xi'_{op} \quad \text{with a maximum of } 3.2 \tag{2. 1}$$

with

$$\xi'_{op} = \frac{tan\alpha}{\sqrt{\frac{H_S}{L_{op}}}} \quad (2.\ 2)$$

where $R_{u2\%}$ is the 2% wave runup height (a 2% wave runup height is a vertical height measured above the still water level that is exceeded by 2% of incident waves), H_s is the significant wave height at the toe of the structure, ξ'_{op} is the surf similarity parameter, $tan(\alpha)$ is the slope of the coastal structure, and L_{op} is the deep-water wavelength associated with the peak spectral wave period T_p.

Ahrens et al. (1993) proposed design formulae for significant and 2% wave runup based on a large data set for smooth and impermeable slopes ranging from 1:1 to 1:4 for both breaking and non-breaking waves. Hughes (2004) developed a formula for wave runup that focuses on a dimensionless maximum depth-integrated wave momentum flux. In that study wave runup was investigated for regular, irregular, and solitary waves on smooth, impermeable slopes for both breaking and nonbreaking waves. Table 1 presents further details on select wave runup investigations and model tests. The table shows how wave runup prediction models have been evolving over the years. In earlier models, many parameters were not included in the prediction formulae potentially influencing the accuracy of wave runup prediction (e.g., structure porosity and cross section, wave breaking characteristics, and oblique wave attack).

Table 1 Collection of wave runup formulae for coastal structures

Authors / Applicability	Formula
Miche (1944) For surging waves	$\frac{R}{H_0} = \frac{R}{H_1}.\frac{H_1}{H_0} = \sqrt{\frac{\pi}{2\theta}} \sqrt{\frac{\sinh\frac{4\pi h_1}{L_1}\cdot\coth\frac{2\pi h_1}{L_1}}{\sinh\frac{4\pi h_1}{L_1}+\frac{4\pi h_1}{L_1}}} + \pi\frac{H_0}{L_0}\frac{\sinh\frac{4\pi h_1}{L_1}}{\sinh\frac{4\pi h_1}{L_1}+\frac{4\pi h_1}{L_1}}\cdot\left(\coth\frac{2\pi h_1}{L_1}\right)^3 \times\left\{1+\frac{3}{4\left(\sinh\frac{2\pi h_1}{L_1}\right)^2}-\frac{1}{4\left(\cosh\frac{2\pi h_1}{L_1}\right)^2}\right\}$
Hunt (1959) For impermeable, smooth structure with a continuous slope. Impermeable slopes for surging waves. Rough, porous structure with a continuous slope. For composite slopes where the waves break at the upper slope.	$\frac{R}{H} = \frac{2.3\ tan\alpha}{\sqrt{\frac{H}{T^2}}} \quad \begin{cases} i^2 < \frac{H}{T^2} \\ H \approx H_o \end{cases}$ $\frac{R}{H} = 3 \quad \begin{cases} i^2 > \frac{H}{T^2} \\ H \approx H_o \end{cases}$ $\frac{R}{H} = \frac{2.3\ tan\alpha}{\sqrt{\frac{H}{T^2}}}\ (\emptyset)$ $\frac{R}{H} = \frac{2.3\ tan\propto}{\sqrt{\frac{H}{T^2}}}\left(\frac{tan\alpha_1+tan\alpha_2}{2}\right)S \quad \begin{cases} i^2 < \frac{H}{T^2} \\ H \approx H_o \\ S \approx 0.8\ to\ 0.9 \end{cases}$
Takada (1970) For surging waves with $\frac{H_0}{L_0} > \sqrt{\frac{2\theta}{\pi}}\cdot\frac{sin^2\theta}{\pi}$ $\cot\theta < 8$	$\frac{R}{H_0} = \frac{\varphi}{(\cot\theta)^{2/3}}$ $\varphi = \sqrt{\frac{\pi}{2\theta_c}} \sqrt{\frac{\sinh\frac{4\pi h_1}{L_1}\cdot\coth\frac{2\pi h_1}{L_1}}{\sinh\frac{4\pi h_1}{L_1}+\frac{4\pi h_1}{L_1}}} + \pi\frac{H_0}{L_0}\frac{\sinh\frac{4\pi h_1}{L_1}}{\sinh\frac{4\pi h_1}{L_1}+\frac{4\pi h_1}{L_1}}\cdot \left(\coth\frac{2\pi h_1}{L_1}\right)^3 \times\left\{1+\frac{3}{4\left(\sinh\frac{2\pi h_1}{L_1}\right)^2}-\frac{1}{4\left(\cosh\frac{2\pi h_1}{L_1}\right)^2}\right\}(\cot\theta)^{2/3}$
de Waal and Van der Meer (1992) For wave runup on plane smooth slopes. Adapted wave runup formula for shallow water, structure roughness, oblique wave attack, and berm.	$\frac{R_{u2\%}}{H_s} = 1.6\ \xi'_{op}$ with a maximum of 3.2 $where \quad \xi'_{op} = \frac{tan\alpha}{\sqrt{\frac{H_s}{L_{op}}}}\frac{R_{u2\%}}{H_s} = 1.6\ \gamma_f\gamma_h\gamma_\beta\xi_{p,eq}$ $where \quad \xi_{p,eq} = \gamma_{berm}\ \xi_{p,eq}$

Table 1 Continued

Authors / Applicability	Formula
Ahrens et al. (1993) For breaking waves (plunging or spilling on slopes). For nonbreaking waves (surging/collapsing). Significant wave runup	$\frac{R_{u2\%}}{H_{mo}} = \frac{2.26\xi_{op}}{(1+0.324\xi_{op})} \quad for\ (\xi_{op} \leq 2.5)$ $\frac{R_{u2\%}}{R_s} = 1.6 \pm 0.24 \quad for\ (\xi_{op} \geq 4.0)$ $\frac{R_s}{H_{mo}} = e^{\left(2.48X_p + 0.446(\cos\alpha)^{3.5} + 0.19\Pi\right)} \quad for\ (\xi_{op} \geq 4.0)$
Hughes (2004) For regular wave runup on smooth and impermeable plane slopes. For irregular wave runup on smooth and impermeable plane slopes: a) Nonbreaking/ surging/ collapsing waves $\left(\frac{H_{mo}}{L_p} < 0.0225\right)$ b) Plunging/ spilling waves $\left(\frac{H_{mo}}{L_p} > 0.0225\right)$ c) Plunging/ spilling waves (for any value of $\frac{H_{mo}}{L_p}$)	$\frac{R}{h} = 3.84\ tan\alpha\ \left(\frac{M_F}{\rho g h^2}\right)^{0.5}$ $\frac{R_{u2\%}}{h} = \left[1.75 - e^{-(1.3\cot\alpha)}\right]\left(\frac{M_F}{\rho g h^2}\right)^{0.5} \quad for\ 1/4 \leq tan\alpha \leq 1$ $\frac{R_{u2\%}}{h} = 4.4(tan\alpha)^{0.7}\left(\frac{M_F}{\rho g h^2}\right)^{0.5} \quad for\ 1/5 \leq tan\alpha \leq 2/3$ $\frac{R_{u2\%}}{h} = 4.4(tan\alpha)^{0.7}\left(\frac{M_F}{\rho g h^2}\right)^{0.5} \quad for\ 1/30 \leq tan\alpha \leq 1/5$

2.1.2 Wave overtopping

Wave overtopping is one of the most important and complex phenomena affecting the integrity of coastal defenses. In the modern design of flood defense structures, the allowable wave overtopping is used rather than a 2% wave runup due to difficulties in estimating loads on the crest and inner slope of a hard structure using 2% wave runup (Pullen et al., 2007). Wave overtopping discharge is generally related to the wave runup assessment. When extreme wave runup exceeds the crest level of a coastal structure, wave overtopping occurs (Figure 8). This phenomenon may only occur for a few waves during a storm. For most coastal structures the required crest elevation

is determined based on the allowable overtopping discharge rate. In this sense, the overtopping discharge rate is a primary factor in the design of coastal structures and has a potential impact on its cost (CIRIA et al., 2007). Overtopping discharge may cause damage to coastal defenses and pose a danger to buildings, vehicles, and people on or behind the structure. The critical values of wave overtopping for designing hard structures, such as breakwaters, seawalls, dikes, and dams, are expressed in detail in the EurOtop manual (Van der Meer et al., 2016), Rock manual (CIRIA et al., 2007) and the Coastal Engineering manual (US Army Corps of Engineers, 2002). Research on wave overtopping of rubble mound structures has been the subject of numerous investigations over the last few decades (Aminti and Franco, 1988; Van der Meer, 1993; Besley, 1999). Although a substantial number of physical model studies have been carried out with the aim of determining overtopping discharge as a function of the geometry of the structure, construction materials, and hydrodynamic parameters, none of these studies have covered all potential situations. The main parameter when assessing wave overtopping is the mean discharge per unit length, q. The most widely used tools for predicting the mean wave overtopping discharge are empirical formulae. Owen (1980) established a formulation framework that continues to be in use today. It evaluates the mean overtopping discharge of impermeable smooth, straight, and bermed slopes. His formula takes into account the roughness of the slope, the geometry of the structure, and the wave steepness as follows:

$$\frac{q}{T_m.g.H_{mo}} = a \exp\left(-b\left(\frac{R_c}{T_m\sqrt{g.H_{mo}}}\frac{1}{\gamma_f}\right)\right) \quad (2.\ 3)$$

where q is the mean overtopping discharge, g is the acceleration of gravity, H_{mo} is the significant wave height, R_c is the freeboard, T_m is the mean wave period, γ_f is a correction factor

accounting for the roughness of the structure, and *a* and *b* are empirical coefficients derived from physical model test results (Owen, 1980). Owen's method has some drawbacks, however. It is not applicable to permeable rubble mound structures and it is applicable only for $0.05 < \frac{R_c}{T_m\sqrt{g.H_{mo}}} < 0.6$ and for a limited deep-water wave steepness between 0.035 and 0.055 (CIRIA, 2007).

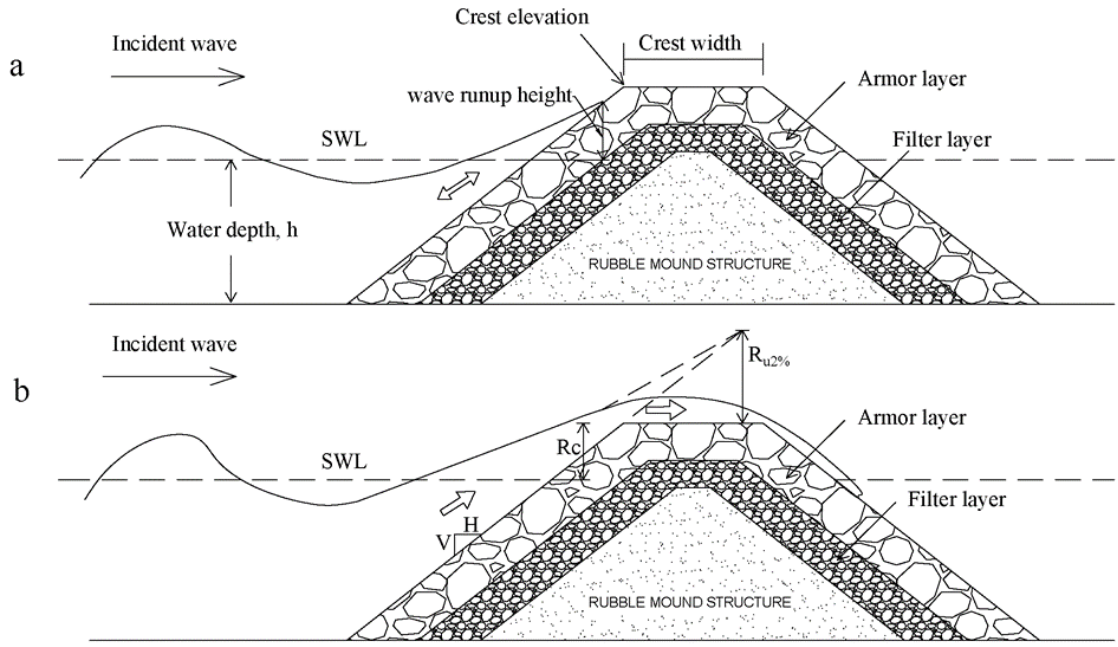

Figure 8 Wave runup occurs when waves break against the shore and water starts to rush up and down a sloped structure as shown in (a). If wave runup exceeds the crest elevation of the structure, overtopping occurs as shown in (b).

Jensen (1984) analyzed wave overtopping data collected in laboratory tests where the spatial distribution of wave overtopping was evaluated behind the crests of seven different breakwater configurations. Bradbury and Allsop (1988) studied the effects of various crown walls

on the performance of an armored rock slope. Based on a hydraulic model test for random waves, Aminti and Franco (1988) introduced a design diagram and formulae for the prediction of overtopping discharge for different rubble mound breakwater configurations with a crown wall. Ahrens and Heimbaugh (1989) developed three overtopping models based on laboratory tests of irregular wave overtopping for a variety of seawall and revetment configurations. These models showed that the overtopping discharge strongly depends on a dimensionless freeboard parameter related to the freeboard through local hydrodynamic conditions at the structure's toe. Based on a parametric laboratory study Pedersen and Burcharth (1992) investigated wave forces on structures and developed a prediction formula for the mean overtopping rate over rubble mound breakwater walls. Van der Meer and Janssen (1995) proposed wave overtopping formulae for smooth, rough straight slopes for breaking waves

$$\frac{q}{\sqrt{gH_s^3}}\sqrt{\frac{s_{op}}{tan\alpha}} = 0.06\exp\left(-5.2\frac{R_c}{H_s}\sqrt{\frac{s_{op}}{tan\alpha}}\frac{1}{\gamma_b\gamma_d\gamma_\beta\gamma_f}\right) \quad (2.\ 4)$$

and for nonbreaking waves

$$\frac{q}{\sqrt{gH_s^3}} = 0.2\exp\left(-2.6\frac{R_c}{H_s}\frac{1}{\gamma_b\gamma_d\gamma_\beta\gamma_f}\right) \quad (2.\ 5)$$

Van der Meer (2002) provided a prediction method for wave overtopping of breakwaters. In this method, a distinction is made between breaking waves and nonbreaking waves. Also, spectral wave characteristics were incorporated in the formulae for breaking waves as

$$\frac{q}{\sqrt{gH_{mo}^3}} = \frac{0.067}{\sqrt{tan\alpha}}\gamma_b\xi_{m-1,0}\exp\left(-4.3\left(\frac{R_c}{\xi_{m-1,0}H_{mo}\gamma_b\gamma_f\gamma_\beta\gamma_v}\right)\right) \quad (2.\ 6)$$

and for nonbreaking waves as

$$\frac{q}{\sqrt{gH_{mo}^3}} = 0.2 \exp\left(-2.3\left(\frac{R_c}{H_{mo}\gamma_f\gamma_\beta}\right)\right) \quad (2.\ 7)$$

where the variables are defined as follows:

The parameter γ_b is the correction factor for a berm. A berm is the part of the front face of a coastal structure between the crest and toe where the slope is significantly reduced over some distance. The slope of the berm varies between 0 and 1:15. The inclusion of a berm can reduce the overtopping discharge and lead to lower required crest levels. The berm correction factor depends on the width of the berm and the vertical difference between the middle of the berm and the still water level. The maximum value for the berm correction factor is 1.

The parameter γ_d is a correction factor for shallow foreshores. For slopes of 1:100 physical model results exist and γ_d can be calculated using an empirical equation (Van der Meer and Janssen, 1995). For other slope values γ_d is set to unity.

The parameter γ_β is the correction factor for oblique wave attack. It captures the effects of oblique wave approach on wave runup and overtopping. It differs for long-crested waves and short-crested waves. The factor ranges from 0.736 to 1 for short-crested waves and from 0.6 to 1 for long-crested waves. Further details can be found in the EurOtop manual (Van der Meer et al., 2016).

The parameter γ_f is the correction factor for the roughness of the slope. Typically, the seaward slope of the coastal defense will consist of grass, asphalt, concrete, or natural rock. The maximum value for the factor of surface roughness is 1.

The parameter γ_v is the correction factor for a vertical wall on the slope. This factor is used in the presence of a small vertical wall at the top of the slope. For a steep wall sloping at 45^o, the reduction factor is 1, and for a steeper wall sloping between 45^o and 90^o, it can be calculated as $\gamma_v = 1.35 - 0.0078\alpha_{slope}$. If no roughness, obliqueness, or presence of the berm was used throughout the model test, these correction factors are assumed to be 1. H_{mo} is the spectral wave height and $\xi_{m-1,0}$ is the Iribarren parameter based on the spectral wave period $T_{m-1,0}$ ($T_{m-1,0}$ = m_{-1}/m_0 with $m_n = \int_0^\infty f^n s(f)\, df \; where \; n = -1 \; or \; 0$). The first negative moment of the spectral wave period is used to evaluate wave runup and overtopping to account for the increased relevance of lower wave frequencies in the spectrum to runup. This spectral wave period is the preferred parameter for all kinds of wave spectra including double-peaked and bimodal spectra. The Iribarren parameter is defined as $\xi_{m-1,0} = \frac{tan\alpha_{wall}}{\sqrt{\frac{2\pi H_{mo}}{g T^2_{m-1,0}}}}$.

Hedges and Reis (2004) proposed a method to predict the wave overtopping of smooth and rough seawalls by random waves. The model showed discrepancies when predicting the overtopping rate for relatively low and high freeboard values compared to the models of Owen (1980) and Van der Meer and Janssen (1995), but it predicted similar or slightly higher overtopping rates in the middle range of freeboards where most of the data fall. The discrepancies between the models occur outside the middle range of the freeboards where data are scarce. Andersen and Burcharth (2006) investigated the spatial distribution of wave overtopping behind the crest of

multiple configurations of a rubble mound breakwater. Their study showed that overtopping discharge decreases when wave steepness increases. Table 2 presents further details on wave overtopping investigations based on model tests of various coastal structure configurations exposed to regular and irregular waves, along with the resulting overtopping prediction equations. The listed wave overtopping equations in Table 2 give an overview of average discharge wave overtopping prediction methods. Through the years, the prediction of the average wave overtopping discharge has been enhanced by including the effect of various parameters in the equations. The overtopping discharge rate is not constant owing to the intermittent nature of waves and runup. Therefore, in more recent studies, attention has been drawn toward the effect of instantaneous wave overtopping discharge on the design of coastal structures (Hughes and Thornton, 2016). The instantaneous wave overtopping discharge is defined as the product of the layer thickness and flow velocity time series occurring during an individual wave overtopping event. The significance of the instantaneous wave overtopping discharge plays out in the form of cumulative erosion affecting inner slope stability (Van der Meer et al., 2014).

Another prediction tool called the overtopping Neural Network (NN) was introduced by (Verhaeghe et al., 2003) to evaluate the mean wave overtopping discharge for various coastal structures. The NN is a data-driven tool where more than 10000 physical model tests were integrated to generate this prediction tool (Van der Meer et al., 2009). Based on hydrodynamic and structural parameters, NN can predict whether an overtopping event will be created. Then NN can calculate the mean overtopping discharge under the given conditions (Van Gent et al., 2007). The prediction of NN tool is affected to large extent by the applied database. Therefore, the conceptual design obtained from the NN is used for preliminary design stages only.

Table 2 Models and formulae to compute overtopping discharge rates.

Authors/ Applicability	Formula
Owen (1980) For impermeable, smooth, rough, straight and bermed slopes.	$\frac{q\sqrt{\frac{s_{m0}}{2\pi}}}{\sqrt{gH_s^3}} = ae^{-b(\frac{R_c}{\gamma H_s\sqrt{\frac{s_{m0}}{2\pi}}})}$
Jensen (1984) For calculating the intensity of overtopping behind seven different break-water structures.	The intensity of overtopping as a function of distance x behind a breakwater is: $q(x) = q_o 10^{-\frac{X}{\beta}}$ The total amount of overtopping is: $Q = \int_0^\infty q_o 10^{-\frac{X}{\beta}} dx \quad t\text{hus } Q = q_o\,\beta/\ln(10)$
Bradbury and Allsop (1988) For armored rock slopes with crown walls.	$\frac{q}{gH_sT_{m0}} = a\left[\left(\frac{R_c}{H_s}\right)^2\sqrt{\frac{s_{m0}}{2\pi}}\right]^{-b}$
Ahrens and Heimbaugh (1989) For seven variable seawall/ revetment configurations.	$\frac{q}{\sqrt{gH_s^3}} = ae^{-b\left(\frac{R_c}{(H_s^2L_{p0})^{1/3}}\right)}$
Pedersen and Burcharth (1992) For rubble mound breakwater walls.	$\frac{qT_{m0}}{L_{m0}^2} = a\frac{H_s}{R_c}$
Hedges and Reis (2004) For impermeable, smooth, rough, straight and bermed slopes exposed to irregular waves.	$\frac{q}{\sqrt{gR_{max}^3}} = A\left[1-\frac{R_c}{R_{max}}\right]^B \quad for\ 0 \le \frac{R_c}{R_{max}} < 1$ $\frac{q}{\sqrt{gR_{max}^3}} = 0 \quad for\ \frac{R_c}{R_{max}} \ge 1$
Van der Meer and Janssen (1995) For impermeable, smooth, rough, straight and bermed slopes. breaking waves nonbreaking waves	$\frac{q}{\sqrt{gH_s^3}}\sqrt{\frac{s_{op}}{tan\alpha}} = 0.06\exp\left(-5.2\frac{R_c}{H_s}\sqrt{\frac{s_{op}}{tan\alpha}}\frac{1}{\gamma_b\gamma_d\gamma_\beta\gamma_f}\right)$ $\frac{q}{\sqrt{gH_s^3}} = 0.2\exp\left(-2.6\frac{R_c}{H_s}\frac{1}{\gamma_b\gamma_d\gamma_\beta\gamma_f}\right)$
Van der Meer (2002) For impermeable, smooth, rough, straight and bermed slopes. breaking waves nonbreaking waves	$\frac{q}{\sqrt{gH_{mo}^3}} =$ $\frac{0.067}{\sqrt{tan\alpha}}\gamma_b\xi_{m-1,0}\exp\left(-4.3\left(\frac{R_c}{\xi_{m-1,0}H_{mo}\gamma_b\gamma_f\gamma_\beta\gamma_v}\right)\right)$ $\frac{q}{\sqrt{gH_{mo}^3}} = 0.2\exp\left(-2.3\left(\frac{R_c}{H_{mo}\gamma_f\gamma_\beta}\right)\right)$
Andersen and Burcharth (2006) Landward distribution of average overtopping rate behind a rubble mound break-water with a crown wall.	$\frac{q_{passing\,x}}{q_{total}} =$ $\exp\left(-1.1s_{0p}^{-1.05}\left(\frac{max(x/\cos(\beta)-2.7h_{level}s_{0p}^{0.15},0)}{H_{m0}}\right)\right)$

2.2 Engineered Sand Dunes

Sand dunes are an integral part of a balanced coastal defense system. They are a sediment buffer and reservoir at the same time, providing sediment material for profile adjustment during storm impact. Moreover, sand dunes can reduce risks of coastal erosion and flooding. Dunes are a natural habitat for a variety of species, and they can add recreational value to beaches (Bruun, 1998; Nordstrom and Arens, 1998). Natural or engineered dunes are part of a dynamic coastal system because they can protect coastal areas from wave action and allow shoreline oscillation during low and high energy wave conditions (French, 2001). Natural dunes are usually modified to fulfill a specific protection criteria or replaced by engineered sand dunes (Nordstrom et al., 2000; Saye et al., 2005). A sand dune can be constructed using sand from the beach or hind-dune areas. However, if the local sediment supply is scarce then importing sand is another option for constructing dunes. Hydraulic placement of dredge material is another alternative to provide sediment for building a sand dune. Sand dunes are suffering from losses due to coastal developments and the associated coastal infrastructures, sea level rise, and storm events (Hanley et al., 2014). If these dunes are maintained and replenished frequently, risks associated with flooding and coastal erosion could be reduced.

2.2.1 Dune-Storm Interaction

Sand dunes are susceptible to erosion when water levels rise significantly above the elevation of the dune toe during a storm as shown in Figure 9. A significant increase in the water levels alters the balance in the mean water surface and the radiation stresses. This can generate an undertow (a bed return flow) that is capable of transporting sand from the dune to the subaqueous portion of the beach face (often resulting in the formation of sand bars) (Houser, 2009). Further

migration of sand offshore through surf zone leads to additional dune scarp and lower beach slope (Lee et al., 1998). After the storm, the subaqueous profile changes toward an equilibrium shape based on the post-storm conditions. The sand moves back onshore, and the beach profile undergoes a gradual accretion during low energy conditions. This recovery process can restore the subaqueous pre-storm profile in its entirety if adequate sediment supply is readily available. In addition, the presence of vegetation can trap sand deposits from overwash and aeolian transport (Houser and Hamilton, 2009). Overwashed and breached dunes, however, may only recover via aeolian processes or engineered restoration efforts. If sediment has been lost from the beach/dune system, the remaining material may not be sufficient to withstand future wave attack leading to an increased possibility for overwash and inundation to occur.

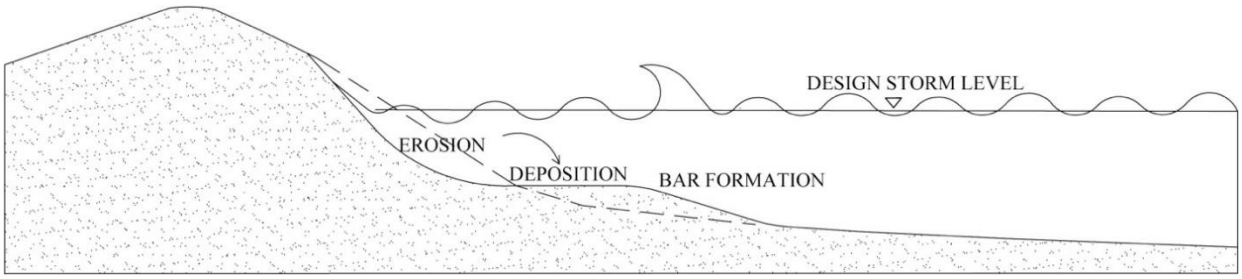

Figure 9 Dunes undergo morphological changes during a storm as water level and wave height are elevated. During high energy wave conditions, dune profile is narrow due to erosion induced by wave action. The eroded sediment is transferred offshore and deposited in offshore sandbars. The low energy dune profile is wide because sand slowly moves to the beach and the sand dune can recover.

Sallenger Jr (2000) classified erosion and accretion of sand dunes during a storm impact into four regimes as follows:

- The swash regime: Wave runup levels reach the foreshore and sediment is moved and deposited offshore.
- The collision regime: Wave runup collides with the base of the dune. Dune sediment is eroded and transported offshore.
- The overwash regime: Wave runup levels exceed the crest of the dune. The overwash sediment is deposited on the back side of the dune.
- The inundation regime: Storm surge levels completely submerge a barrier island. The dune is impacted by wave action and sediment is transferred landward as long as water level gradients are negative (higher water on the ocean side versus the bay side).

In some cases, especially during the waning stages of a storm, a positive water free-surface gradient may occur, reversing the flow direction from the inundation regime by driving a mean flow from the bay to the ocean (Sherwood et al., 2014). This phenomenon is called storm surge ebb. The storm surge ebb flow can scour the deposited material and may affect the sediment budget of the beach-barrier-bay system (Harter and Figlus, 2017). The ability of a dune to recover after a storm varies and depends on the response of the barrier island to sea level rise, the change in frequency and/or magnitude of storm surges (Houser et al., 2015), the supply of sediment (Bauer and Davidson-Arnott, 2003; Robin, 2005; Woodruff et al., 2013), the beach width, wetting and drying cycles, the growth and state of existing vegetation, as well as its capability to trap wind-blown sediment (Houser and Hamilton, 2009). Houser et al. (2008) investigated the longshore morphology of a sand dune along Santa Rosa Island in northwest Florida. They found that longshore variation in dune morphology, shoreline erosion, and storm impact are controlled by transverse ridge and island width. In addition, the authors showed that overwash penetration is larger for the narrower portions of the island at lower elevations. In contrast, the portions of the island with higher elevations and a wider extension experienced fewer overwash penetrations.

Erosion of dunes and beaches may occur over several hours and days. However, the recovery of a dune can take years, even decades and depends on the extent to which dune erosion occurs. The recovery process of a dune can be affected by many factors including wind, wave, and tidal processes, sediment entrapment by vegetation, availability of sediment, and the frequency of storm events (Christiansen and Davidson-Arnott, 2004; Houser et al., 2015). Dunes may require maintenance after a storm because the natural recovery processes are relatively slow even with the presence of adequate sediment supply in the intertidal zone. Davidson-Arnott (2010) classified the level of disturbance of a foredune and the corresponding natural recovery rate of sand dunes according to the extent of the erosion as follows:

- Minor disturbance: Where waves reach the base of the foredune, there will be minor erosion, and recovery occurs within a few months to a year.
- Moderate disturbance: Where waves erode embryonic dunes and/or dune ramps and scarp the base of the foredune, recovery occurs within 2–5 years.
- Severe disturbance: Where waves erode a dune severely, generating a vertical scarp. The recovery may range from 5–10 years.
- Catastrophic disturbance: Waves breach a dune completely and transport and deposit sediment to the backside of the dune as overwash fans; the recovery may take more than 10 years.

2.2.2 Restored Sand Dune Design

Dunes of any size are beneficial in reducing storm impact, even if it is only via delayed or reduced flooding. However, larger dunes can provide more protection to the areas behind them because the stored sand in a dune requires more time to erode, thus delaying the severe impacts of extreme storms (Wootton et al., 2016; Sigren et al., 2018). The design parameters of a dune are the crest height, crest width, frontal dune volume, side slopes, and grain size distribution. In

general, an attempt is made to keep the grain size distribution close to that of the native material as that material is thought to be close to the equilibrium situation for the specific location based on the prevailing dynamics at the site. The design parameters of a dune are selected based on economic optimization. The crest height of a sand dune is calculated based on a surge elevation, wave setup, and wave uprushes with a factor of safety (Bruun, 1998). Although the crest width and side slopes of a dune depend on different hydrodynamic parameters, the constructability limitations and the angle of repose of the fill material affect the selection of the dune width and slopes (US Army Corps of Engineers, 2002). Typically, the dune geometry needs to meet certain design criteria to ensure adequate storm protection. In the United States, the Federal Emergency Management Agency (FEMA) established a general criterion for sand dunes based on an analysis of hurricane-related dune erosion. According to FEMA, the critical parameter for protection against the 100-year still water elevation is the amount of stored sand in the cross-sectional area of the frontal half of a primary dune (Federal Emergency Management Agency, 1995) as indicated in Figure 10. Dunes with crest elevations below the 100-year storm water level will rapidly erode and overwash and will not provide a significant amount of protection. However, dunes that are slightly above the 100-year stormwater elevation will be scraped and eroded. Hallermeier and Rhodes (1986) and Dewberry and Davis (1989) found that 540 ft^3 of sand per linear foot is required to resist a 100-year storm. Consequently, FEMA introduced a minimum cross-sectional area of frontal sand dunes of 540 ft^3/ft. This criterion is referred to as the FEMA 540-rule (Coulton et al., 2005). More recently, however, FEMA recommended increasing the cross-sectional area to 1100 ft^3/ft. This new recommendation was made for the following reasons: (1) the 540-rule does not account for the long-term erosion that affects dunes and beaches, (2) the 540-rule does not account for cumulative effects of multiple storms occurring within a short period of time, and (3) the 540-

rule is based on analysis that underestimates dune erosion 50 % of the time (Federal Emergency Management Agency, 2011). It should be noted that FEMA criterion is not a design guideline, rather a tool to assess mainly the flood insurance requirements.

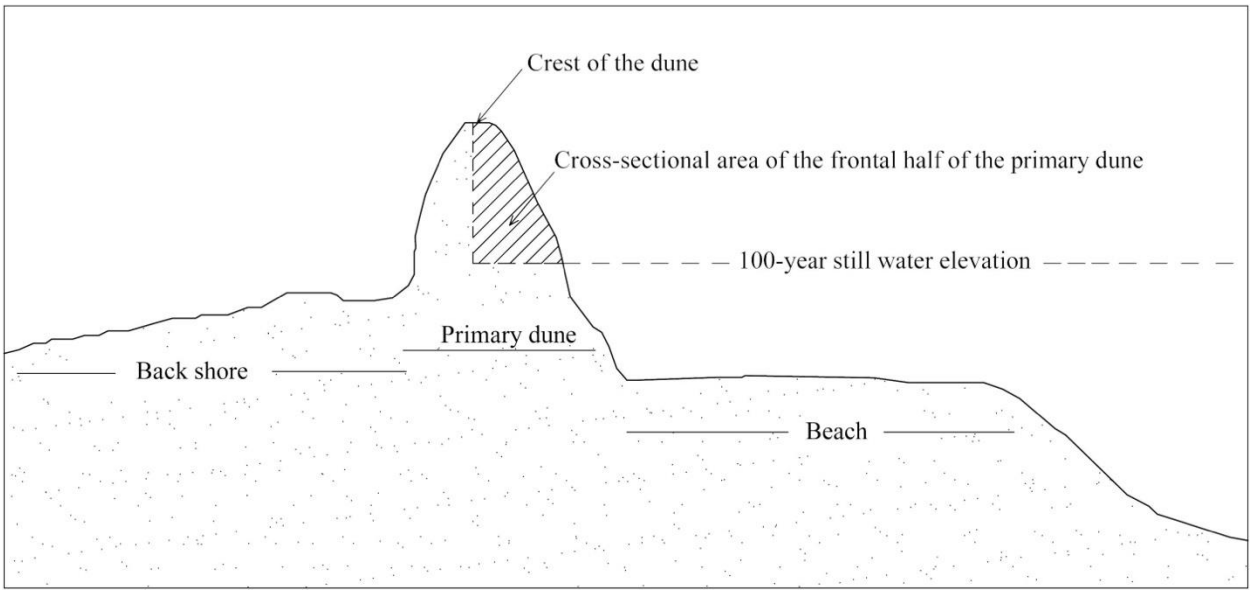

Figure 10 Schematic cross-section of a dune and beach. The frontal dune cross-sectional area above the 100-year still water elevation is indicated by the hatched area. photo modified from (Federal Emergency Management Agency, 2011)

In Dutch practice, several models were developed to predict dune erosion during storm conditions. Based on the results of small-scale and large-scale experiments, Vellinga (1983) developed a predictive computational model for dune and beach erosion during storm surges. According to Vellinga (1983), the initial beach profile reshapes during a surge to an equilibrium profile (erosion profile) and can be described by the following equation:

$$\left(\frac{7.6}{H_{os}}\right) y = 0.47\left[\left(\frac{7.6}{H_{os}}\right)^{1.28}\left(\frac{w}{0.0268}\right)^{0.56} x + 18\right]^{0.5} - 2.00 \quad (2.\ 8)$$

where:

H_{os} = actual significant deep-water wave height in m;

w = fall velocity of the sand particles in m/s;

x = cross-shore distance from dune foot in m;

y= depth below storm surge level in m.

The profile extends from the dune foot at the storm surge level where $x = 0$ and $y = 0$

$$\text{to} \qquad x = 250\left(\frac{H_{os}}{7.6}\right)^{1.28}\left(\frac{0.0268}{w}\right)^{0.56} \text{ and } \quad y = 5.72\left(\frac{H_{os}}{7.6}\right) \quad (2.\ 9)$$

Van de Graaff (1986) proposed a probabilistic method for designing sand dunes that includes seven characteristic parameters: maximum storm surge level, significant wave height during the maximum height of the surge, mean particle diameter (D_{50}) of the dune material, shape of the initial dune profile, storm duration, squall oscillation (sometimes called seiches) and gust bumps (short-term rises of the water level caused by passage of a front or heavy shower), and the accuracy of the computation. However, the surge level is the most significant factor for the erosion of dunes.

In Dutch practice guidelines, the size of an engineered dune design is primarily evaluated with a probability of failure of 10^{-5} per year. The probability of failure is the most critical factor in designing sand dunes in low-lying areas such as the Netherlands. According to Van de Graaff (1989), the minimum crest elevation of a dune is computed by:

$$h_0 = CL + 0.12\hat{T}\sqrt{H_s} \quad (2.\ 10)$$

however,

$$h_0 \geq CL + 2.5 \quad (2.\ 11)$$

CL = storm surge level + (2/3) decimation height (2. 12)

The decimation height is the water level with a probability of exceedance 10 times smaller than that of the storm surge level minus the actual storm surge level. The parameter h_0 is the minimum dune crest level above Normal Amsterdam Peil, NAP (also known as standard Amsterdam Datum), *CL* is the computational level above NAP. $\hat{T}$ is the peak period of the wave spectrum, and the significant wave height at the computational level is H_s.

2.2.3 Advances in the Modeling of Dune and Beach Profiles

During severe storms, substantial portions of a dune erode rapidly under the impact of waves and from overwash processes. Estimating the erosion volume of a dune is essential in coastal areas because sand dunes are widely used as a coastal risk-reduction solution to minimize damages from storm surges and large waves. Several methods are employed to predict dune erosion. Some of these methods are analytical while others are based on physical model experiments or numerical studies. Currently, empirical and process-based models are primarily used to estimate dune profile evolution and erosion volumes associated with a storm. An empirical model evaluates the pre-storm dune profile and the erosion volume based on the post-storm profile. Process-based models describe the evolution of the beach and dune profile in time and space based on numerical formulations of the dominant physical processes.

In the early 1980s, two of the most widely used methods for predicting the erosion of a dune were those of Vellinga (1983) and Kriebel and Dean (1985). Vellinga (1983) presented an empirical model based on extensive physical model studies to assess dune erosion during storm surges. This model predicts the post storm dune erosion profile based on storm surge level, wave conditions, and sediment grain size characteristics. Kriebel and Dean (1985) developed a numerical model for predicting time-dependent erosion of beaches and dunes during severe storms. This model solved the dynamic equations governing cross-shore sediment transport and the conservation of sand. However, neither the Vellinga (1983) model nor the Kriebel and Dean (1985) model is general enough to cover all beach profiles, storm surge levels, and wave conditions. In addition, neither of those models provides detailed descriptions of wave runup, wave overtopping, and bar formation, and both of them are intended for monotonic profile shapes only. Larson and Kraus (1989) proposed a semi-empirical model based on equilibrium equations similar to that used in the model by Kriebel and Dean (1985). Although the Larson and Kraus (1989) model does not fully resolve surf zone hydrodynamics and sediment transport processes, it schematizes the processes in a way that allows for more realistic storm erosion simulations. Thus, it overcomes some of the shortcomings of previous models and includes the ability to reproduce bar formation. Steetzel (1991) developed a mathematical model to predict the cross-shore sediment transport rate during storm surges. The model is able to determine the amount of erosion for coastal profiles under extreme wave attack. Larson et al. (2004) established an analytical model to predict the erosion and recession of coastal dunes based on a wave impact approach, where the dune profile evolution could be estimated by waves directly hitting the dune (Overton et al., 1987). Van Gent et al. (2008) and Van Thiel de Vries et al. (2008) completed large-scale dune erosion studies to examine the physical forces driving dune erosion during major storm events. Based on these

physical model experiments, Van Gent (2008) updated the empirical model of Vellinga (1983) to account for the effects of the wave period.

Although overwash processes are essential in predicting dune profile evolution and assessing flood risk, in the previous experiments overtopping and overwash were not considered when modeling dune erosion during extreme storms. A comprehensive review of coastal overwash in relation to physical and numerical studies is presented by Donnelly et al. (2006). Despite the importance of dune and beach profile changes during overwash regimes, only a few small-scale (Hancock and Kobayashi, 1994; Kobayashi et al., 1996; Kobayashi et al., 2009; Figlus et al., 2011) and large-scale (Williams et al., 2012; Blenkinsopp et al., 2016; D'Alessandro and Tomasicchio, 2016; Matias et al., 2016) experiments for coastal dune overwash have been conducted to date.

To aid dune design, process-based models (e.g., XBeach or CSHORE) are being employed to estimate the short-term evolution of beach and dune systems under storm conditions. The XBeach model (Roelvink et al., 2009) solves 2DH equations for wave propagation, flow, sediment transport, and evolution of bathymetry, for time-varying hydrodynamic conditions and employs an avalanching algorithm based on the critical slope of wet sand to simulate dune scarp retreat. The time- and depth-averaged, cross-shore morphodynamic model CSHORE (Johnson et al., 2012) offers another alternative to simulate beach and dune profile evolution over short and medium (several months) time-scales based on offshore hydrodynamic parameter input and an initial profile. While a detailed explanation of numerical model setup and capabilities for both of these models is beyond the scope of this overview, the reader is kindly referred to the references cited within this document. However, in the following section, the current capabilities of the two models related to hybrid coastal structure simulations are presented.

2.3 Hybrid Coastal Structures: State-of-The-Art and The Path Forward

With the introduction of hybrid coastal defenses, where a hard structure and sand dune and/or buffer are combined into a single system, valuable coastal areas can fulfill multiple functions related to storm protection and ecosystem preservation. Stronkhorst and Lagendijk (2012) pointed out that one of the main strengths of hybrid coastal protection approaches is the combination of the benefits they can yield. Yet, research on hybrid concepts has many gaps, especially in estimating the hydrodynamic responses, erosion processes, and environmental impacts of hybrid structures. A few studies of hybrid systems have been conducted. These studies cover various aspects of hard and soft component interaction and are presented here, ranging from purely physical model experiments to numerical investigations.

Van Gent (2008) presented a large-scale physical model experiment to explore the effects of a dune revetment on dune erosion and compared it to the situation of a dune without a revetment. Two different dune configurations were tested. One configuration was a sloping dune revetment, and the other was a horizontal and vertical revetment representing a seaside boulevard with a sandy beach. The results showed that after the failure of the revetment, the amount of dune erosion was similar to that of a dune without a revetment. In addition, the duration for which the revetment provided protection depended on the strength of the revetment. Van Geer et al. (2009) performed a laboratory experiment to measure dune erosion of two hybrid setups using a video-based technique. The first setup consisted of four parallel concrete dikes with three narrow sand beaches and a dune section on either side of the alongshore array of dikes and narrow sand beaches as shown in Figure 11a. The second setup contained two concrete dikes, two dune revetments separated by a narrow sandy beach, and a sand dune adjacent to one of the dikes as shown in Figure

11b. A narrow sandy beach in the setup was intended to simulate a breach. The experiment was conducted in a 3D wave basin with an area of 25 x 25 m surrounded by two wave-damping beaches at the edges of the test area. In this experiment, dikes enhanced the dune erosion and increased the rate of retreat of the dune crest, especially along a breach. In addition, larger peak waves lead to an increase in the eroded dune volume. The experiment is mentioned here since it highlights some of the complexities involved in understanding combinations of hard and soft coastal defense systems. In particular, the used dune revetments resemble the hybrid structures under investigation in this dissertation. Boers et al. (2011) reported on dune erosion and foot scour of hybrid structures investigated by Van Geer et al. (2009) (Figure 11). The test showed significant dune erosion near hard structures. It was presumed that the presence of a hard structure increased the concentration of wave loading leading to an additional increase in dune erosion (varying between 27% in the areas of transition from dune to dike segments and 88% in the areas of narrow beaches between dikes). In addition, it was noticed that the scour in front of the dike was much less, while no change was noticed in front of the dune revetment when compared to previous studies.

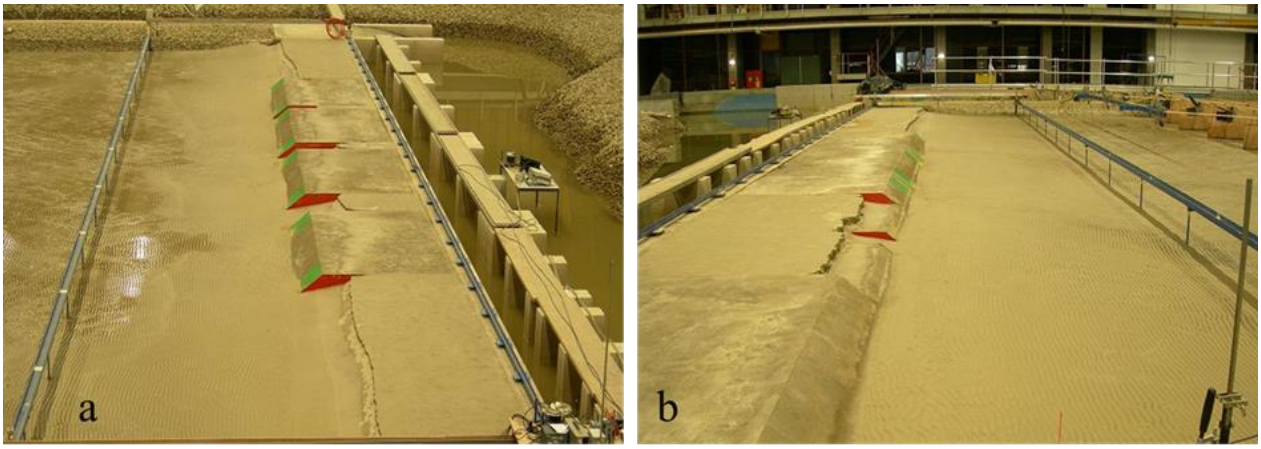

Figure 11 Photo of two different hybrid coastal structure setups tested by Van Geer et al. (2009) and Boers et al. (2011). a) A hybrid structure consisting of four parallel concrete dikes with three breaches and two dune sections on either side of the dike array. b) A hybrid structure containing two concrete dikes, a breach separating two dune revetments, and a sand dune that is constructed adjacent to the dikes. Photo reprinted from Van Geer et al. (2009).

Van Thiel de Vries (2012) extended the numerical morphodynamic model XBeach (Roelvink et al., 2009) to assess the morphological evolution of a partial dune revetment due to wave forcing. In this experiment, the revetment did not extend all the way to the crest of the dune, but rather left a section above it exposed. The numerical model was used to assess the erosion of this exposed dune portion above the revetment as observed during physical wave flume model tests conducted by Steetzel (1987). The flume dimensions were 230 x 5 x 7 m (length x width x height). In the experiment, waves broke before reaching the revetment, and some of the wave energy was reflected while some produced overtopping. As the waves ran up the revetment and overtopped it, the water mass slowed down and a portion of it flowed back due to gravity. This can cause scouring in front of the hard structure depending on backwash velocity and scour depth. The overtopped waves scarped the exposed dune face above the revetment, and the eroded

sediment was deposited in front of the revetment creating a submerged sand mound as shown in Figure 12. The extended numerical model predicted the erosion above the revetment well. However, the scour depth in front of the dune revetment was underestimated since some of the physical processes related to the formation of scour (i.e., wave reflection, wave run-down, and the effect of accumulated sand deposits near the toe of the revetment) were not incorporated in the model. For cases where the revetment stayed in place without collapsing the submerged mound affected wave runup characteristics. This investigation was focused on morphodynamic changes of the system consisting of a revetment fronting the lower portion of a sand dune but did not further discuss modifications to wave runup and overtopping resulting from this hybrid setup.

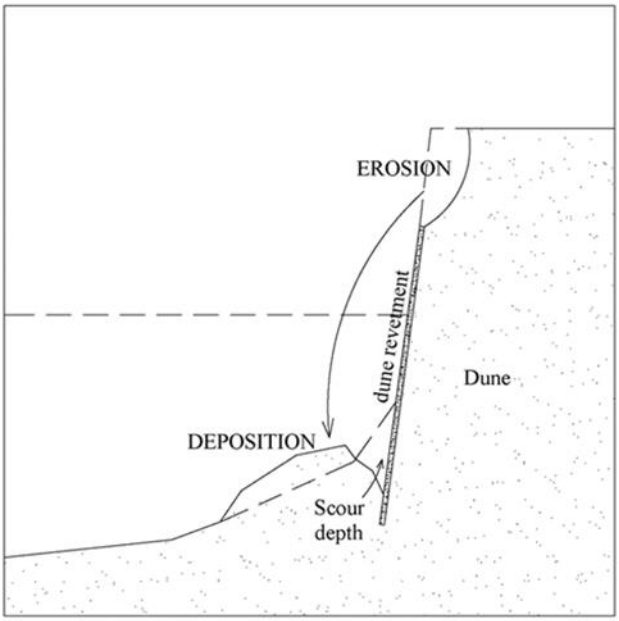

Figure 12 Schematic of setup and morphological response of a hybrid structure consisting of a revetment partially protecting the front face of a sand dune (adapted from Van Thiel de Vries, 2012).

Figlus et al. (2015) presented small-scale physical model experiments on morphological changes of a sand dune and three sand dune-covered core alternatives (rubble mound revetment, a clay levee, and a T-wall) under wave conditions with no overtopping. The results indicated that all the core alternatives reduced the erosion of the dune compared to a plain dune. The rubble mound core offered more reinforcement for the sand dune against erosion, but water seepage was observed through the pores of rocks. The clay core was able to restrain water seepage due to its low permeability. The T-wall blocked the seepage flow, but a scour hole at the toe of the structure was observed due to wave reflection from the vertical wall. Kobayashi and Kim (2017) performed small-scale physical model experiments on wave overtopping and overwash over four different test series consisting of 1) a sand beach with a berm, 2) a sand beach with a narrow dune, 3) a rock seawall, and 4) a rock seawall buried in a sand dune. The tests showed that the narrow sand dune could only provide limited protection under wave attack with no overtopping. The rock seawall reduced wave overtopping and overwash even under moderate damage conditions (rock settlement). For the case of a rock seawall buried in a sand dune, before the sand cover eroded by swash action the sand cover decreased the structure roughness and porosity. Thus, wave overtopping and overwash were increased slightly. However, after the rock seawall was exposed, it was nearly as effective as the rock seawall with no sand cover in reducing wave overtopping and overwash. Kobayashi and Kim (2017) examined the findings of the physical model experiment conducted by Kim et al. (2017) using the cross-shore numerical model CSHORE by Kobayashi (2016). Similar to other process-based models, this model has some limitations in predicting wave overtopping and overwash in situations involving a rock seawall due to the presumption of no

settlement of the rock seawall. Muller et al. (2018) investigated the impact of a sand cover over the Galveston, Texas, seawall in reducing the hydraulic loads during a storm via the use of XBeach. The study showed that a greater volume of sand cover over the seawall can reduce wave height in the surf zone up to 40%. This was explained by changes in the bed elevation (shallower depth) due to wave-induced dune erosion that enhanced the dissipation of wave energy in the shallower surf zone. In addition, Muller et al. (2018) investigated the effects of a sloped dike (side slope of 1v:5h) embedded in a sand dune on the dissipation of wave energy in the surf zone and compared the results to those from a similar setup using a sand-covered vertical seawall. Results indicated that the volume of sand covering and fronting the respective hard structures influenced wave energy dissipation in the surf zone as the sand profile was adapting to the hydrodynamic forcing conditions. Using the XBeach model, Nederhoff (2014) and Nederhoff et al. (2015) investigated the morphological effects of a buried seawall with respect to cross-shore and alongshore morphodynamic processes. According to the model, a substantial scour depression formed at the base of the seawall during the storm peak surge; however, the depression was subsequently filled in as the storm subsided. This agrees with post-Sandy elevation profiles presented by Miller et al. (2009). The model also found that the combination of seawall, beach, and dune effectively limited the erosion of the fronting beach, but that it increased erosion on adjacent areas by up to 32%. Using a Boussinesq-type wave model Irish et al. (2013) assessed the effectiveness of the buried seawall in reducing wave forces during the peak of a storm. It was found that the portions of the beach including the hybrid setup fared better against storm-induced erosion than the adjacent stretches of coastline without the buried relic seawall. Walling et al. (2016) compared the structural damage observed in Bay Head during Superstorm Sandy to that which occurred in the neighboring town of Mantoloking. The research showed that the relic seawall in Bay Head played an important

role in reducing damages. In addition, the research indicated that the beach area and the proximity of a structure to the pre-storm shoreline played a significant role in determining the amount of damage that was sustained. Using the XBeach model Smallegan et al. (2016) investigated the morphological response of a barrier island and the capabilities of sand dunes in reducing wave action during Hurricane Sandy. The model was used to measure the morphological response of the island and to evaluate the effect of the dune in reducing wave forces compared with the hybrid setup (seawall covered by a sand dune). The study showed that the hybrid setup reduced the horizontal erosion of the island by 5 m compared to the locations featuring sand dunes only. The hybrid setup decreased wave forcing and prevented inundation of the island compared to the adjacent dune setup with no hard core.

Hybrid structures performance in reducing wave overtopping volumes compared to other traditional risk reduction measures is not investigated. Although hybrid structures have employed at a different location around the world, the effect of the hard component (e.g., rubble mound, vertical wall) on the overall design is not examined yet. There is no design frame for those hybrid structures. Some of those structures were not envisioned by design to be a hybrid structure, rather the fulfill the criteria accidentally. The design of several hybrid structures was based on treating each element (i.e., soft and hard) of the structure separately. A prediction formula that can translate the effects of both elements in reducing overflow volume can be beneficial for future coastal protection plans. This can help coastal communities to assess the performance of hybrid structures and decide whether they can fit well in their future protection plans.

CHAPTER 3

METHODOLOGY

Wave overtopping is a complex phenomenon that is influenced by various hydraulic and structural parameters. The wave overtopping process over a hybrid structure is more complicated, since additional parameters related to the morphological response of the sand cover affect overtopping discharge. As an example, the erosion and overwash (flow of water and sediment over the crest of coastal dune or beach during a storm event) processes shown in Figure 13 alter the water depth. Consequently, the wave hydrodynamics near the toe of the structure are influenced. The effects of water depth in addition to the crest freeboard and the side slope of the structure, should be integrated into overtopping discharge calculations of a hybrid structure. Owing to the complexity of the wave overtopping process associated with hybrid structures, a physical model approach is chosen here instead of a numerical model treatment of the problem. Future research will address the numerical modeling aspects, but these are beyond the scope of this dissertation. Currently available process-based numerical models are not capable yet to investigate all the combined dynamic processes relevant to wave overtopping of a hybrid structure comprised of a rubble mound and sand cover.

The physical modeling experiments for this research were conducted in the coastal processes wave flume of Texas A&M University at Galveston. A set of scale physical model testing consisting of 320 wave bursts was conducted on both traditional rubble mound and hybrid structures. The main objective of the experiments was to estimate both the average and instantaneous wave overtopping discharge rates. In addition, the controlling parameters of wave overtopping rates over a hybrid coastal structure were investigated.

This chapter includes aspects of the physical modeling tests. First, a prototype is determined that represent a realistic rubble mound structure. Second, scaling requirements and limitations are discussed. Then, the testing facility and the instrumentation used in the study are briefly described. This is then followed by the details of the experimental setup and the hydrodynamic conditions of the tests. Finally, the data collection and processing methods are presented.

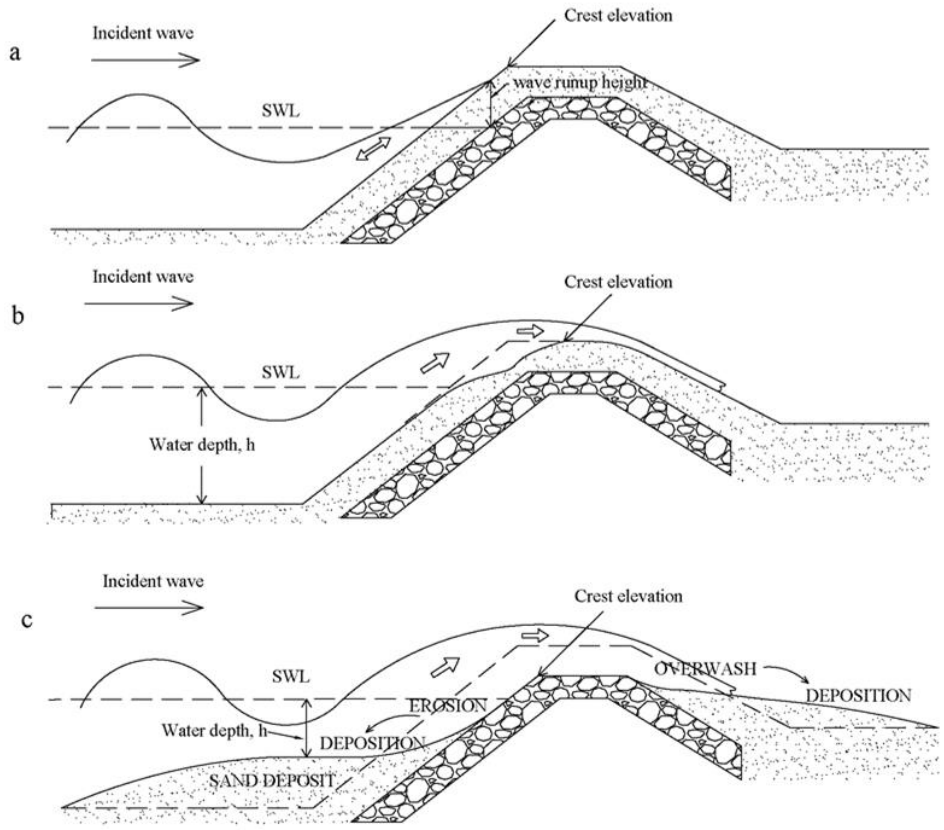

Figure 13 Schematic cross-section of a hybrid structure subject to wave runup (panel a), overtopping (panel b), and overwash (panel c).

3.1 Prototype analysis

The modeled cross-section was based on proposed prototype dimensions of a potential hybrid coastal protection system for the Houston-Galveston area along the Gulf of Mexico coast. The proposed prototype system was designed to withstand the hydrodynamic conditions created by a storm with a 100-year return period. An extreme value analysis (EVA) of historical buoy data (significant wave height and storm tide water level) approximated by a Weibull distribution was carried out. The peak-over-threshold method (POT) (Goda, 2000) was applied to obtain the extreme values used in the analysis (Almarshed, 2015). The peak wave period associated with the design wave height was estimated using a joint probability distribution approach (Kamphuis, 2010). The obtained design wave height and peak wave period at the buoy location were transformed to onshore values using the MIKE 21 Spectral Wave Module (SW) by Danish Hydraulic Institute (DHI) (DHI, 2011). The two-dimensional SW model was used to transfer the design wave conditions from buoy 42035 located at 29°13'54" N 94°24'46" W East of Galveston, where the water depth is 15.8 m, to the shoreline of Galveston Island. Figure 14 shows the location of buoy 42035 and the location of maximum wave height along the Galveston shoreline.

One primary aspect in designing any coastal structure is the stability of the structure when exposed to hydrodynamic design conditions. Hydrodynamic loads on the structure are the main concern when designing rigid structures such as vertical walls. However, for rubble mound structures the main concern is the armor unit size which needs to be able to withstand the design hydrodynamic conditions. The geometric design for a simple slope rubble mound structure using the modified Van der Meer formula (Van Gent et al., 2003). Prototype design conditions and rubble mound configurations were determined as printed in Table 3.

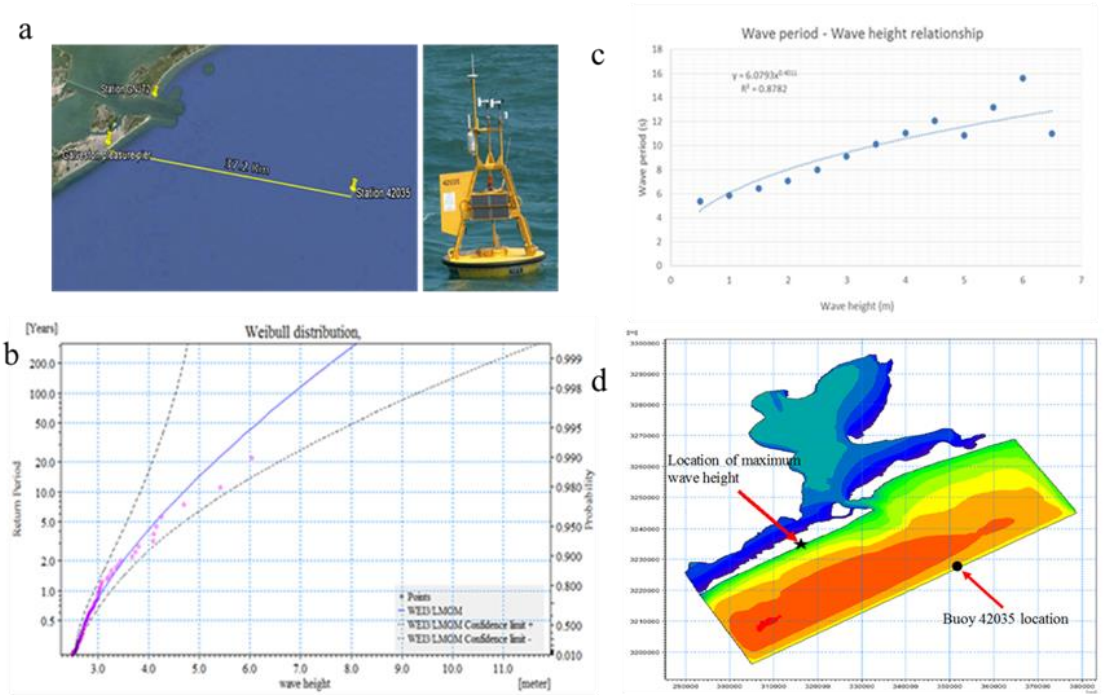

Figure 14 Procedures to obtain the prototype design wave conditions. Historical data from buoy station shown in panel (a) were downloaded and processed. Applying an extreme value analysis of available historical buoy data using the Peak-over-Threshold (PoT) method (panel b). Estimating wave period assigned with the 100-year significant wave height using a joint probability distribution (panel c). Using 2D MIKE21 spectral wave model to transfer waves to the near shore.

Table 3 Prototype parameters for rubble mound

Variable	Values
Significant wave height, H_s (m)	4.59
Wave height exceeded by 2% of the waves, $H_{2\%}$ (m)	4.62
Peak wave period, T_p (s)	12.88
Spectral wave period, $T_{m-1,0}$ (s)	10.85
Wave steepness, $S_{m-1,0}$	0.02
Relative density, Δ	2.00
Nominal diameter of armor layer, D_{n50} (m)	1.00
Mass of rocks, M_{50} (kg)	3109
Structure height (m)	6.40
Berm width, B (m)	3.00
Side slope of structure, tan(α)	0.50

3.2 Physical model setup

A scaled model can produce prototype parameters precisely when the criteria of similitude are met. Criteria of similitude are mathematical conditions governing the similarity between the model and prototype. There are three laws of similitude 1) Geometric 2) Kinematic, and 3) Dynamic. Geometric similarity pertains to the length ratio similarity between model and prototype. For kinematic similarity, the ratios of the velocities and accelerations in both the model and prototype must be equal. Ratios of forces between the model and prototype must be the same to satisfy dynamic similarity. Maintaining kinematic and dynamic similarity requires the existence of fluid forces. These forces are related to pressure, gravity, viscosity, surface tension and compressibility. The ratio of inertia force to the gravity force is called the Froude number, while the ratio of inertia force to the viscosity force is called the Reynolds number. The scale factor selection is influenced by the wave generation capability and wave flume dimensions. The typical scale factors for a physical modeling in coastal engineering ranges from 1:10 to 1:100 (Hughes, 1993). The larger scale factors produce less viscous forces compared to smaller scale factors. For smaller scale factors the accuracy of the prototype conditions decreases. In general scale effects are due to the differences between prototype and model response that may arise from the difficulties to simulate all relevant forces in a model.

In the case of water flow with a free surface, the gravitational effects predominate. The impact of other factors can be significant only for specific conditions. For example, the surface tension effects can be essential when the wave period is smaller than 0.35 s or the water depth is less than 2 cm (Hughes, 1993). Thus, Froude scaling criteria is the most applicable for modeling

wave parameters and beach/coastal structure dimensions. The Froude number expresses the relative influence of inertia to gravity forces in the hydraulic flow (Eq. 3.1).

$$F_r = \frac{U}{\sqrt{gd}} \tag{3. 1}$$

where U is the characteristic velocity such as the particle velocity or the wave celerity (m/s), g is the acceleration of gravity (m/s^2), and d is the water depth (m). The model and prototype are related as follows

$$\left(\frac{U^2}{gd}\right)_m = \left(\frac{U^2}{gd}\right)_p = K \tag{3. 2}$$

From geometric similarity,

$$\frac{(d)_p}{(d)_m} = K \tag{3. 3}$$

where, K is the scale factor for the model. Therefore,

$$\frac{(U)_p}{(U)_m} = K^{0.5} \tag{3. 4}$$

The wave length is estimated as $L = \frac{gT^2}{2\pi}\tanh(kd)$. From the dispersion relationship the wave length is a function of water depth and wave period. Wave number k is defined as $\frac{2\pi}{L}$. For deep water, the wave length ratio is $\frac{L_p}{L_m} = \frac{T_p^2}{T_m^2}$. Hence, prototype and model wave periods and wave heights are related by,

$$\frac{(T)_p}{(T)_m} = K^{0.5} \tag{3. 5}$$

$$\frac{(H)_p}{(H)_m} = K \quad (3.\ 6)$$

The prototype structure was scaled down using the Froude law and the geometric similarity with undistorted scale of 1:20. This is the largest scale factor possible in the testing facility due to the physical constraint of the flume dimensions and wave generator capabilities. The geometric undistorted scaling of the model extends to provide a reasonable approximation of the shape and size distribution of the armor and filter layers for the prototype. However, the sediment cannot be scaled geometrically because the model sediment will result in diameters typical of a cohesive material (e.g., clay). It should be noted that when dealing with physical model tests involving sediment movement all the main features of sediment transport are included (Hughes, 1993). In the current study, the used sediment grain size is equivalent to coarse sand in the prototype scale. In geometrically undistorted models, macro scale features of turbulence are in similitude with the prototype. Thus, the characteristic of the hydrodynamic processes such as wave breaking can be reproduced by the model (Hughes, 1993). Comparison of the prototype and the modeled design conditions and rubble mound configurations are displayed in Table 4.

Table 4 The prototype and the model parameters for rubble mound

Variable	Prototype values	Model values
Significant wave height, H_s (m)	4.59	0.23
Peak wave period, T_p (s)	12.88	2.88
Spectral wave period, $T_{m-1,0}$ (s)	10.85	2.43
Nominal diameter of armor layer, D_{n50} (m)	1.00	0.05
Structure height (m)	6.40	0.32
Berm width, B (m)	3.00	0.15
Side slope of structure, tan(α)	0.50	0.50

As part of this study, the performance of a hybrid coastal structure under storm conditions is assessed and compared with a rubble mound structure through physical model experiments. To this end, a set of 32 trials were conducted on both rubble mound and hybrid structures. Those trials were divided into four groups based on the sand cover (Table 5). Each trial consists of 8 individual tests. In each test, the effects of different hydrodynamic conditions on the wave overtopping were investigated (

Table 6). The generated hydrodynamic conditions were not site-specific or scaled down from a prototype condition. They were generic with the purpose of generating wave overtopping over the tested hybrid structures. Nevertheless, those hydrodynamic conditions could be scaled up to prototype conditions using the geometric scaling. A test contains 10 wave bursts with a duration of 3.5 min. Each test in the trials was labeled by two letters (HS) followed by two numbers. The first number referred to the sand cover thickness, while the second number express the different permutation of testing hydrodynamic conditions.

The modeled hybrid coastal structure consists of a rubble mound covered by a sand layer. The height of the hard structure is 23 cm above the initial beach profile, and the width of the crest is 15 cm (Figure 15). The rubble mound consists of three layers. A sand core layer with a thickness of 10 cm (Figure 16a) was covered by a geotextile fabric (Figure 16b) to prevent the sediment from washing out, topped by a filter layer with a thickness of 3 cm (Figure 16c) and an armor layer with a thickness of 10 cm (Figure 16d). The porosity of the armor layer was 0.42. In the hybrid structure trials four different sand cover thicknesses (S_t) were tested (0, 5, 7, and 9 cm). The total height of the structure at the beginning of each test was 23, 28 cm, 30 cm, and 32 cm respectively (Figure 16e). The sand used to construct the hybrid structure is poorly sorted fine sand with a

nominal diameter of 0.014 cm. The measured specific gravity and fall velocity are 1.59 and 0.75 cm/s respectively. The nominal diameter of the filter layer and armor layer stones was 2 cm and 5 cm, respectively (Figure 16f). The seaward slope of the rubble mound was 1v:2h and the foreshore slope was 1v:50h. A wooden board was inserted between the crest and the back slope of the structure (Figure 15). The board height above the initial beach profile and width were 23 cm and 60 cm, respectively. The wooden board helped in preventing water seepage through the pores of the rubble mound structure simulating a prototype scenario with an internal sheet pile barrier to manage seepage flow. The vertical wall also provided a rigid surface to attach the overtopping channel at a fixed elevation which is important when assessing overtopping discharge rates.

Table 5 Trial labels and numbers

Trial #	Sand cover thickness (S_t) (cm)	trial labels
0	0	HS 01 – HS 08
1	5	HS 11 – HS 18
2	7	HS 21 – HS 28
3	9	HS 31 – HS 38

Table 6 Summary of hydrodynamic conditions near wavemaker for individual test.

Test #	Spectral significant wave height, H_{m0} (cm)	Spectral peak wave period, T_p (s)	Water depth (cm)
1	9	1.9	104.3
2	9	1.9	102.3
3	12	1.9	104.3
4	12	1.9	102.3
5	9	1.64	104.3
6	9	1.64	102.3
7	12	1.64	104.3
8	12	1.64	102.3

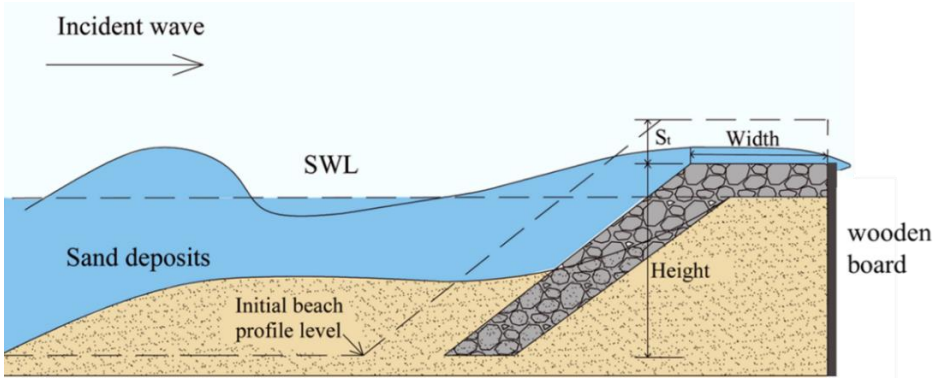

Figure 15 Schematic of hybrid structure cross section illustrates the height and width of rubble mound and the initial sand cover thickness (S_t).

Figure 16 Photos detailing the hybrid structure construction procedure. The sandy core of the rubble mound (a) was covered by a geotextile fabric (b) to prevent the movement of sediment underneath the rocks. Gravel with a nominal diameter of 2 cm was used to construct the filter layer (c). Rubble mound structure before applying the sand cover (d). Finished hybrid coastal structure with sand cover of 9 cm thickness before the first wave run (e). Used materials are shown in Panel f.

Water free surface elevation during the wave bursts was measured at nine locations using capacitance-style wave gauges. Three wave gauges were placed in the deep-water section of the wave flume to separate incident and reflected wave trains using the Mansard and Funke (1980) approach. Four wave gauges were placed at strategic locations along the beach face to capture wave transformation from deep to shallow water. The overflow layer thickness and associated velocity were calculated by two wave gauges that were placed 10 cm apart at the crest of the modeled hybrid structure. A receptacle with a sediment trap was placed behind the structure to collect the overtopped volumes of water and overwashed sediment. The sand trap as shown in Figure 17 was made from nylon plastic fabric with a micron rating of 37. This setup retained grain diameters exceeding 0.037 mm, that corresponds to very fine sand in Wentworth (1922) scale, and allowed water to pass through. A recirculating pump was used to maintain a constant water level during each wave burst.

Figure 17 Photo showing the sediment trap and overtopping channel at the landward side of the hybrid structure.

The tests were conducted to explore the effects of varying water depth, wave height, and wave period on wave overtopping discharge rates, morphological evolution, and energy dissipation rates of hybrid coastal structures subject to storm conditions. Water depths near the wave maker varied between 102.3 cm and 104.3 cm, depending on the wave height H_{m0} limited to some extent by the flume geometry (Table 7). It should be noted that the tested wave height listed in (Table 7) represents 39% and 52% of the model wave height (H_{m0}) shown in Table 4. Irregular waves following a JONSWAP spectral shape were used. The investigated parameters in this study were the incident wave height and wave period at the toe of the hybrid structure, overtopping layer

thickness over the crest of the hybrid structure, flow velocity of overtopped waves, water and swash velocity near the hybrid structure, as well as dune erosion and overwash volumes.

Table 7 Hydrodynamic test conditions

Parameter	Measured value (near wavemaker)
Spectral significant wave height, H_{m0}	9 cm, 12 cm
Spectral peak wave period, T_p	1.64 s, 1.9 s
Water depth	102.3 cm, 104.3 cm

3.3 Instrumentation and data collection

3.3.1 Wave Flume

The tests were conducted in a wave flume with dimensions of 0.6 m width, 1.2 m depth and 15 m length. The flume is divided into two sections, a deep-water wave section of 3 m length, and a sloped section of 12 m length filled with 6 m^3 of fine sand (D_{50} = 0. 14 mm) on top of a false plywood bottom to allow for simulation of the cross-shore beach and dune processes as shown in Figure 18. The flume is comprised of steel bottom plates and a steel frame to support thick glass panel side walls. The flume is equipped with a flap-type wave generator at one end. A pump is used to drain the water after the tests through polyvinyl chloride (PVC) pipes. The pump is removed from the tank during the wave bursts to avoid any obstruction to the wave motion.

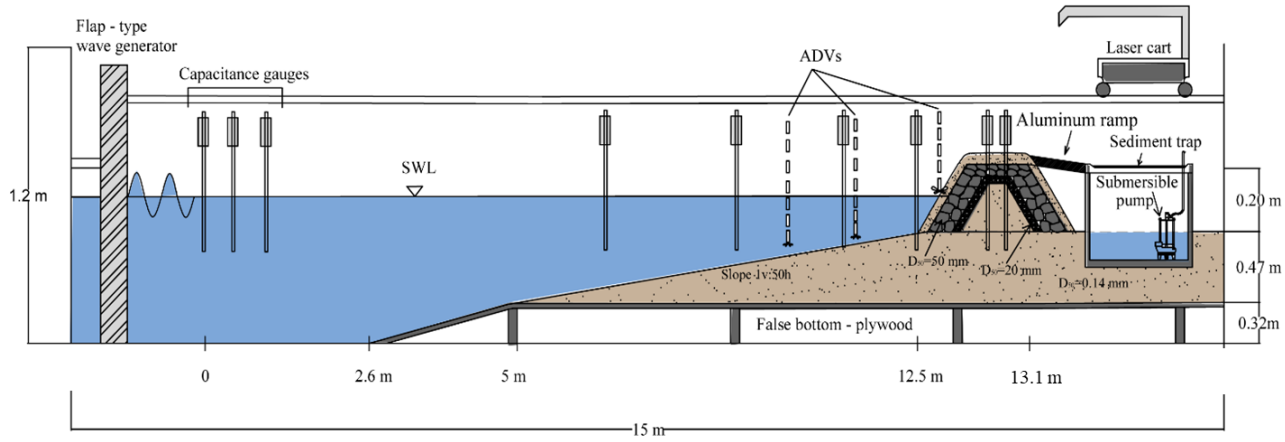

Figure 18 Schematic of movable-bed wave flume. A flap-type wave maker generates irregular wave trains. Capacitance wave gauges are strategically placed near the centerline of the flume at cross-shore locations indicated by vertical bars. Acoustic Doppler velocimeter profilers (ADVs) were placed in front and along the slope of the structure to capture three-dimensional water velocity and turbulence characteristics. A laser line scanner mounted on a moveable cart above the flume is used to measure beach and dune surface elevation between wave burst.

3.3.2 Wave Generator

The flap-type wave generator (Figure 19a) can produce regular and irregular wave trains. The flap paddle oscillates about an axis located at the flume bed. It is driven by an electric motor mounted at the back side of the flume. The wave generator is connected to a National Instruments (NI) controller and data logger hooked up to a desktop computer (Figure 19b). NI LabVIEW software controls the wave generator motion. Moreover, the software enables the user to generate a variety of wave spectra by specifying significant wave height, peak wave frequency, water depth, and the duration of a test. In addition, it saves the collected data during each wave burst. The generator is not equipped with active wave reflection control. Therefore, reflected and re-reflected waves contribute to the total wave energy in the tank. This is not an issue as long as low-frequency

oscillations (seiching motions) are not initiated during wave bursts and tank resonance frequencies are not excited. The experiment described herein utilize relatively short duration wave bursts and peak wave frequencies much different from tank resonance frequencies to avoid such issues.

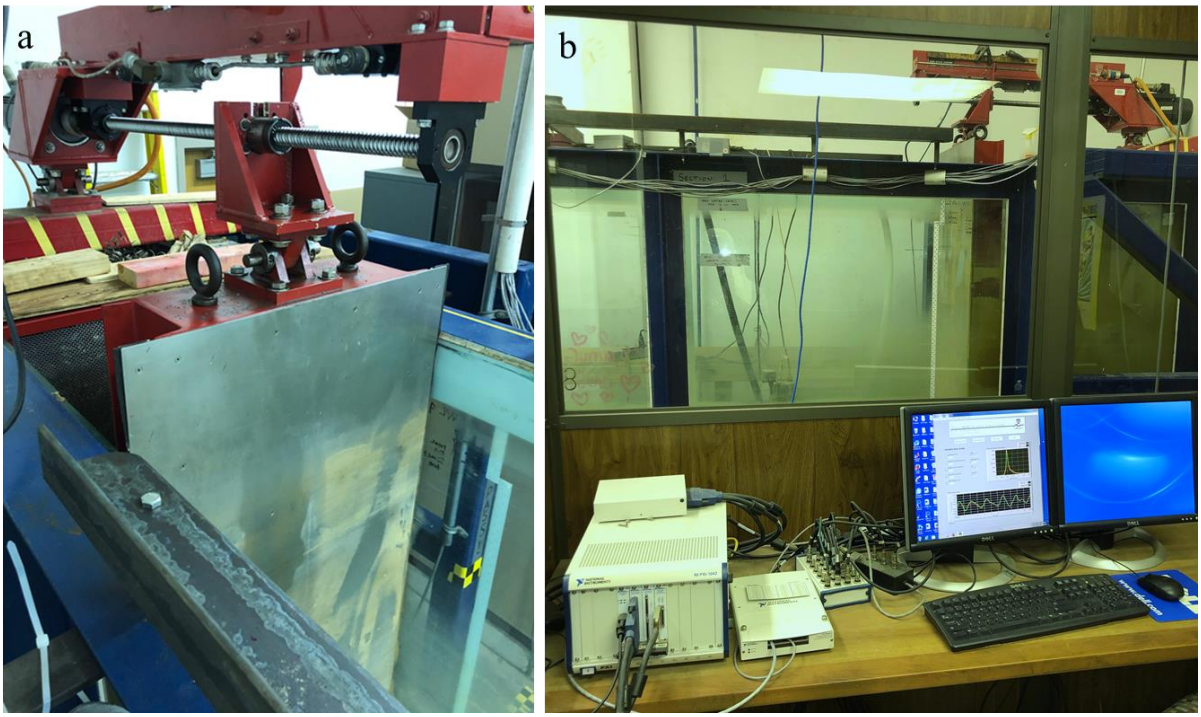

Figure 19 Photos of the wave generator and control system. The flap-type wave maker (a) is controlled through NI LabView software installed on a desktop computer (b). The software controls the wave maker, generates wave spectra, and stores the collected data during each wave burst on the hard drive.

3.3.3 Wave Gauges

Capacitance-style wave gauges with a sampling rate of 20 Hz were used to record free surface elevation during wave bursts. The gauge wires are held taut by a stainless-steel rod as

shown in Figure 20. The wire insulation acts as a capacitor between the inside conducting wire and the water that acts as the ground. During a wave burst the capacitance changes linearly with water free surface elevation. The variation in the capacitance is determined via electronic circuits. The relation between the free surface elevation and the capacitance is obtained after a voltage-to-frequency conversion and the application of an appropriate calibration constant. All the wave gages were calibrated before the tests to find the calibration coefficients relating measured voltage to water level. The wave gauges were placed in the flume, and the voltage was measured using the data acquisition board for each 1 cm rise in the water level for 10 elevations. The voltage at each free surface elevation was plotted against the corresponding water level. The plotted data were fitted using a least-squares linear regression to obtain an equation to convert the voltage to water level. Figure 21 shows an example of the relationship between the recorded voltage and the water level for each wave gauge.

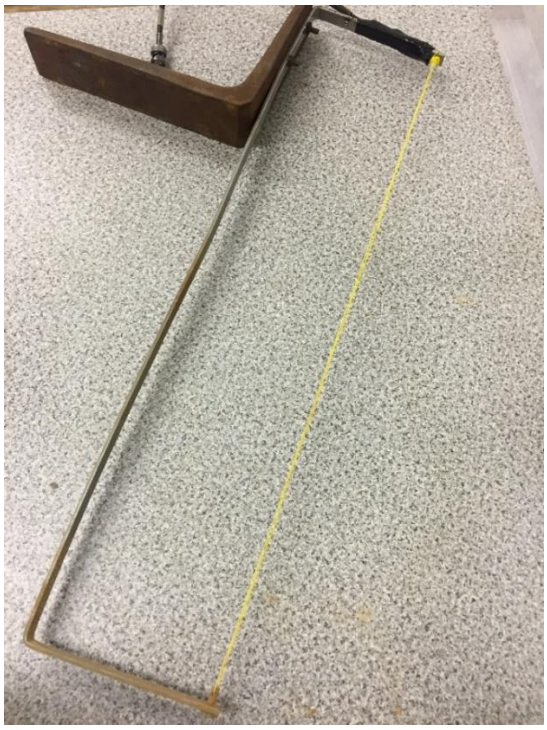

Figure 20 Photo of capacitance wave gauge used in the experiment.

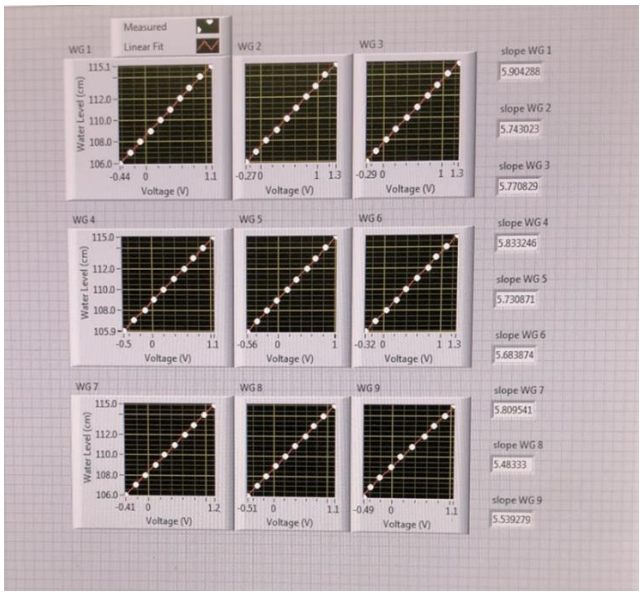

Figure 21 Output of calibration processes of the nine wave gauges. The obtained calibration coefficients are used to convert the voltage to water level for each test.

3.3.4 Acoustic Doppler Velocimeters (ADV)

Nortek Vectrino acoustic Doppler velocimeter profilers were used to measure three-dimensional water velocity and turbulence characteristics. The profilers emit an acoustic pulse at a known frequency from a transducer located at the center of the probe. Moving water particles reflect the sound wave with a different frequency. The difference between the emitted and reflected frequency is proportional to the water velocity (i.e. Doppler effect) (Nortek, 2017). The flume is equipped with two types of Vectrino profilers, Vectrino II and Vectrino+. Vectrino II has a downward-looking head with one central transducer and four receivers (Figure 22). The Profiler can record velocity components ($\vec{u}, \vec{v}, \vec{w}$) simultaneously in a vertical profile up to 31 mm in height with a sampling cell height of 1 mm (Nortek, 2009). For the experiment, the bounding velocity range was set ±1 m/s and the sampling frequency was set to 100 Hz. The Vectrino+ has a side-looking head with one transducer and four receivers (Figure 23). The profiler can record three-dimensional velocity at a shallower water depth (down to 2 cm) with a sampling rate of 200 Hz. The velocity range was set to ±0.3 m/s with a reported velocity accuracy of ±0.1 mm/s (Nortek, 2009). All the profilers were mounted on down-spouts fixed to movable carts on top of the flume for maximum deployment flexibility.

In this study, the Vectrino II profilers were used to measure the water velocity and determine turbulent kinetic energy near the hybrid system. The Vectrino+ profiler was placed along the center of the seaward slope of the structure to measure the swash velocity and associated kinetic energy. The Vectrino data were post-processed with a MATLAB script to filter the raw data. Then the filtered data were used to plot the velocity components and construct the power spectral density.

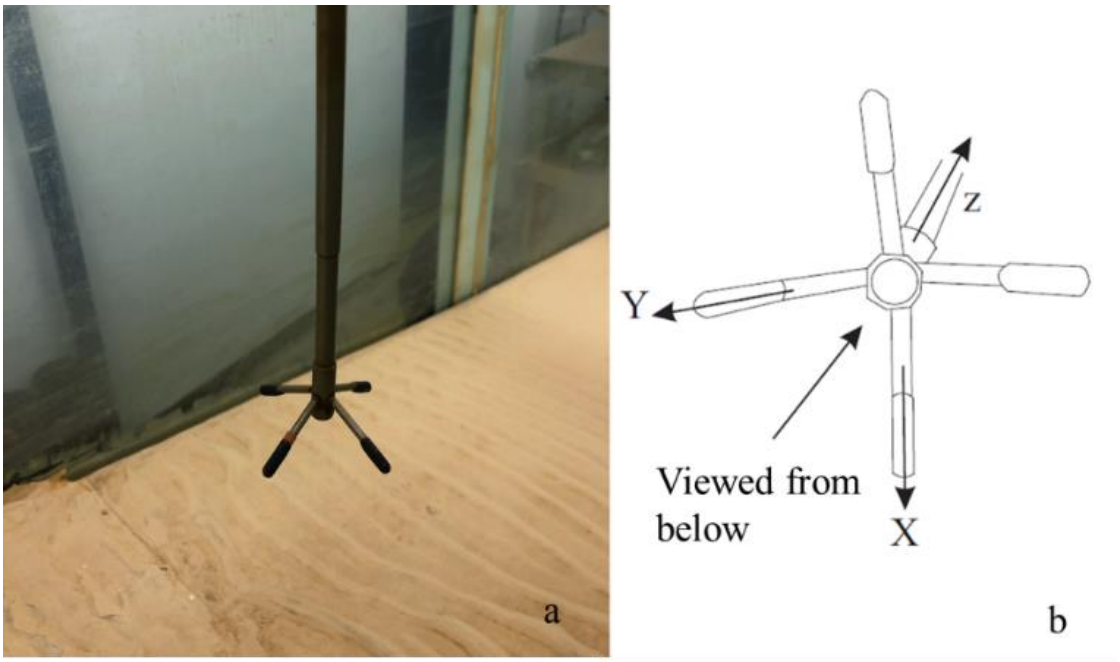

Figure 22 Photo (a) and coordinate system (b) of Vectrino II profiler.

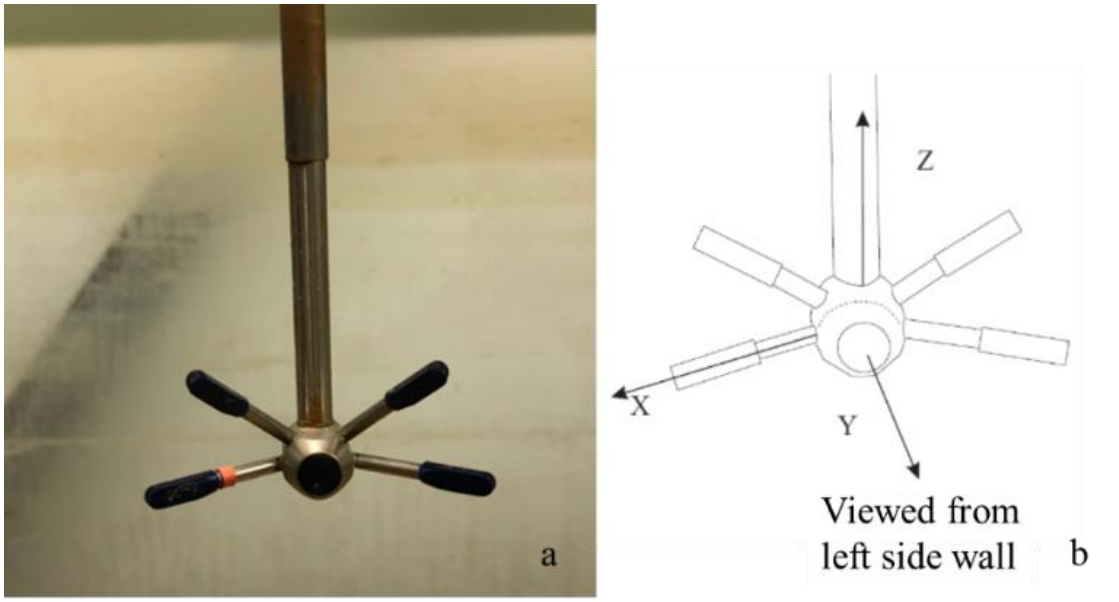

Figure 23 Photo (a) and coordinate system (b) of Vectrino+ profiler.

3.3.5 Laser Scanner

An Acuity AP820-1000 laser line scanner system mounted on a moveable cart above the flume was used to measure the beach and dune profile (Figure 24). The system utilizes a blue laser diode (540 nm wavelength) in concert with a 200 Hz 2D charge-coupled device (CCD) detector to measure the vertical elevation of the beach and hybrid structure. The laser was set up to project an alongshore blue laser line vertically downward toward the bed. The CCD detector collects the reflected laser light to calculate the elevations of each point on the illuminated alongshore transect at a cross-shore interval of 1 cm. Alongshore lines are scanned as the cart moves at continuous slow speed (~ 1 cm/s) on its tracks above the flume. The data collected from the detector are used to construct a 3D digital elevation models of the bed and structure elevations. These 3D elevation plots are then used to verify alongshore uniformity in bed level changes before being averaged to produce representative 2D cross-shore profiles at each scanned time step.

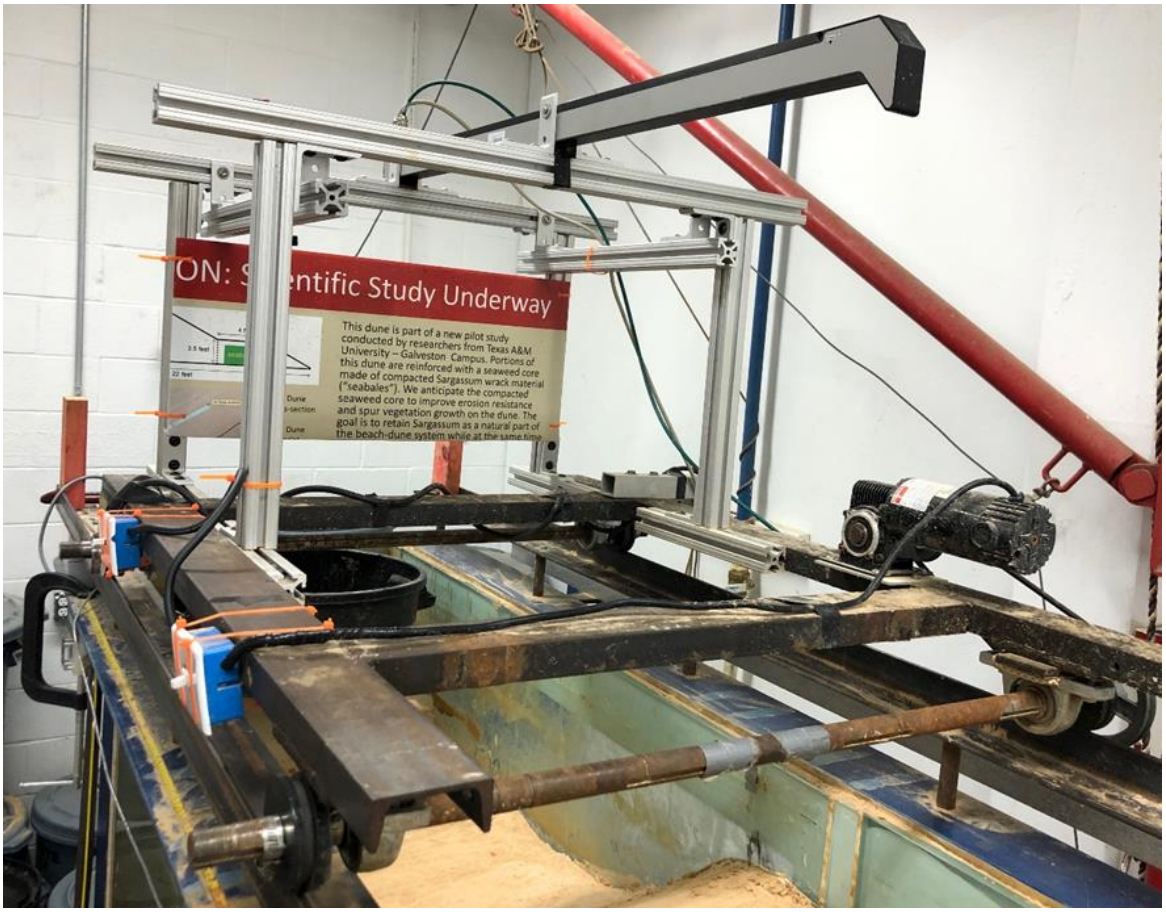

Figure 24 Photo of the laser line scanner system consisting of a blue laser diode and a detector collecting the reflected laser light. The entire system is mounted on a motorized cart as shown.

3.3.6 Water recirculation System and sediment trap

A water recirculation system, consisting of a pump, flow meter, and pipes was needed to pump overtopped water back into the main portion of the flume to maintain a constant water level during each wave burst. A submersible water pump was placed in a collection basin with a sediment trap at the back end of the modeled structure (Figure 25a, b). The sediment trap made of plywood and nylon plastic fabric was used to retain the overwashed sediment and allowed water

to pass through it. The pump was used to circulate the overtopped water from the collection basin back into the flume. The pump has a vertical float switch that allows the pumping to start when the basin is filled to a specified water level. A flow meter (Figure 25c) was connected to the pump via pipes to measure the volume of water being pumped back to the tank.

Figure 25 Photo of the exposed rubble mound at the end of a test wave burst (a). On the landward side of the structure, an aluminum ramp and the collection basin are shown. During wave overtopping event the overtopped water is collected in the basin (b), overwashed sediment is retained by the sediment trap (c), the water pump recirculates water back into the flume. The amount of the pumped water is measured by a flow meter (d).

3.4 Data processing

Measuring the wave overtopping discharge was the main task in the physical modeling experiment. Two types of wave overtopping discharge were calculated; the average wave overtopping (*q)* and the instantaneous, wave-by-wave, *q(t)* wave overtopping per unit length during a wave burst (3.5 min). The instantaneous wave overtopping per unit length was calculated by multiplying the time series of the water layer thickness *h(t)* above the structure crest and the time series of the overflow velocities *u(t)*. The time series of the water layer thickness was determined from WG9 located near the landward end of the crest. A reference water level (h_r) was recorded at the beginning of each wave bursts (total water depth from the structure toe up to the crest of the vertical wall). This water level was then used to determine the thickness of the overtopped water layer. An overtopping event was recognized whenever the water level at WG9 $h_{WG9}(t)$ was greater than h_r. Time series of the water layer thickness *h(t)* above the structure crest was calculated by evaluating the difference between the $h_{WG9}(t)$ and h_r as shown in the hatched area in Figure 26. In this study, a small water layer thickness was generated during most of the overtopping events. This is why it was challenging to collect real-time velocity data using a Vectrino+ profiler. Therefore, two wave gauges (WG8 – WG9), a known cross-shore distance apart, were mounted at the crest of the structure to estimate the overflow velocity during an overtopping event (Figure 26). The overflow velocities were determined using the time lag recorded by the two wave gauges resulting from a wave crest or roller front passing them in short succession. It should be noted that the presented velocity measurement technique is sensitive to position where the time lag is evaluated. A MATLAB algorithm was written to detect wave fronts

for each wave overtopping event and estimate the time lag (Figure 26). Then the time series of overflow velocities was obtained by dividing the distance between the gauges by the lag duration. The average wave overtopping volume per wave burst was measured by two techniques; (1) the overtopping collection basin (2) averaging instantaneous wave overtopping discharge per unit depth, *q(t),* over time. The result of overtopping measurements consists of 207 data points where the overtopping measurements during the first wave bursts (24 data points) and 9 null data points (due to technical issue with the wave gauge) were excluded. To test the accuracy of the measurement techniques of wave overtopping volumes, the total volumes from the collection basin and total volumes obtained from the flux measurement over the crest of the structure were compared (Figure 27). The comparison of 207 wave overtopping events showed a very good agreement with squared correlation coefficient $R^2 = 0.997$.

The measured average and instantaneous overtopping were used to develop a new prediction formula for overtopping of a hybrid structure. A non-Linear regression analysis was used to generate the prediction models for wave overtopping rates of a hybrid structure. To this end, it was essential to investigate the impact of several hydrodynamic including (H_{m0}, $T_{m-1,0}$, h_t) and total structure height and freeboard (R_c) on overtopping rates. Those hydrodynamic and geometrical parameters are not well examined for hybrid coastal structures unlike the traditional coastal structures.

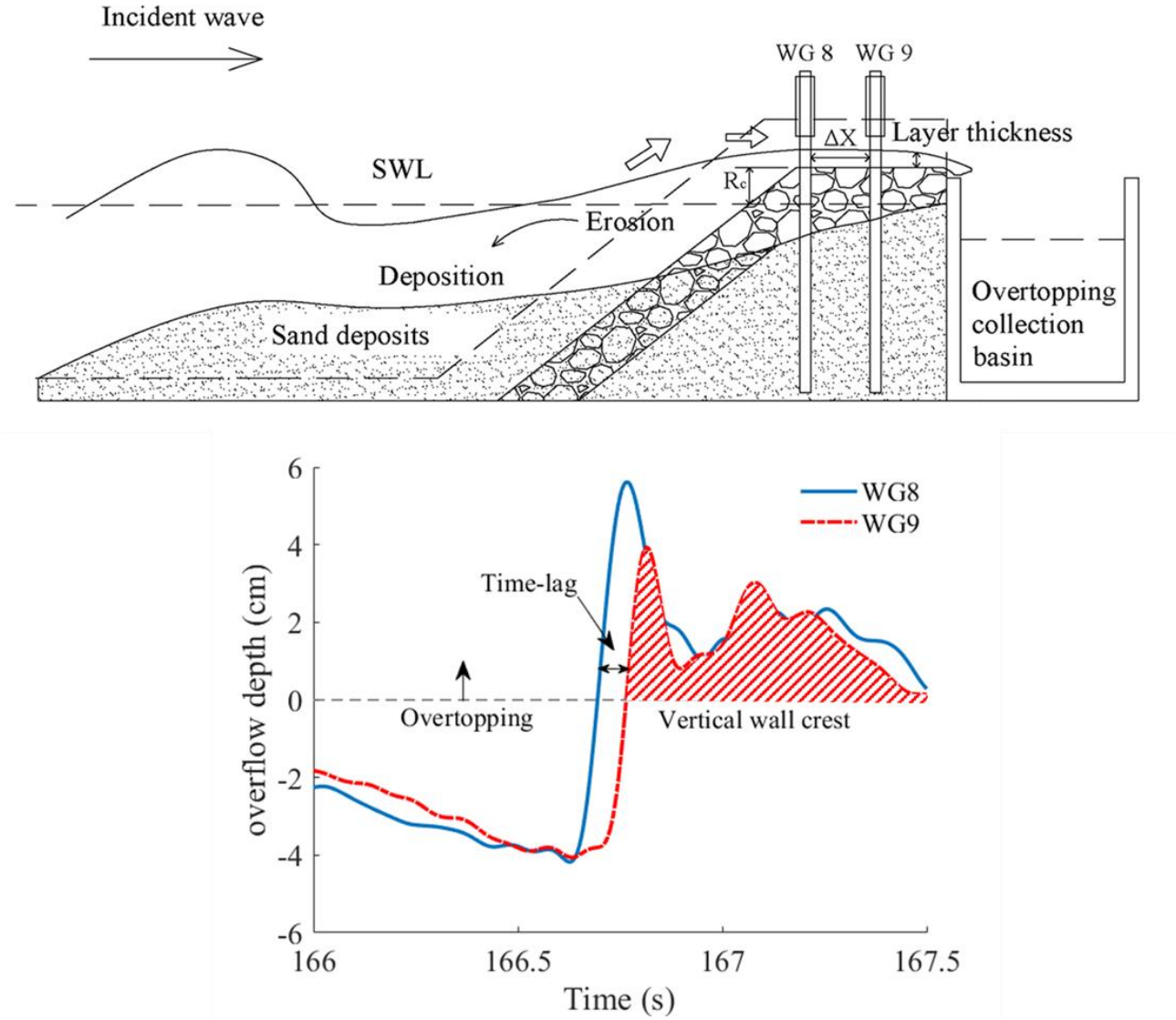

Figure 26 Top panel: Schematic of the setup to measure overtopping flow using two wave gauges on the crest of the structure detecting wave front/bore progression. Bottom panel: Sample time series measured by the two wave gauges showing the lag between the two signals created by the passing wave front/bore.

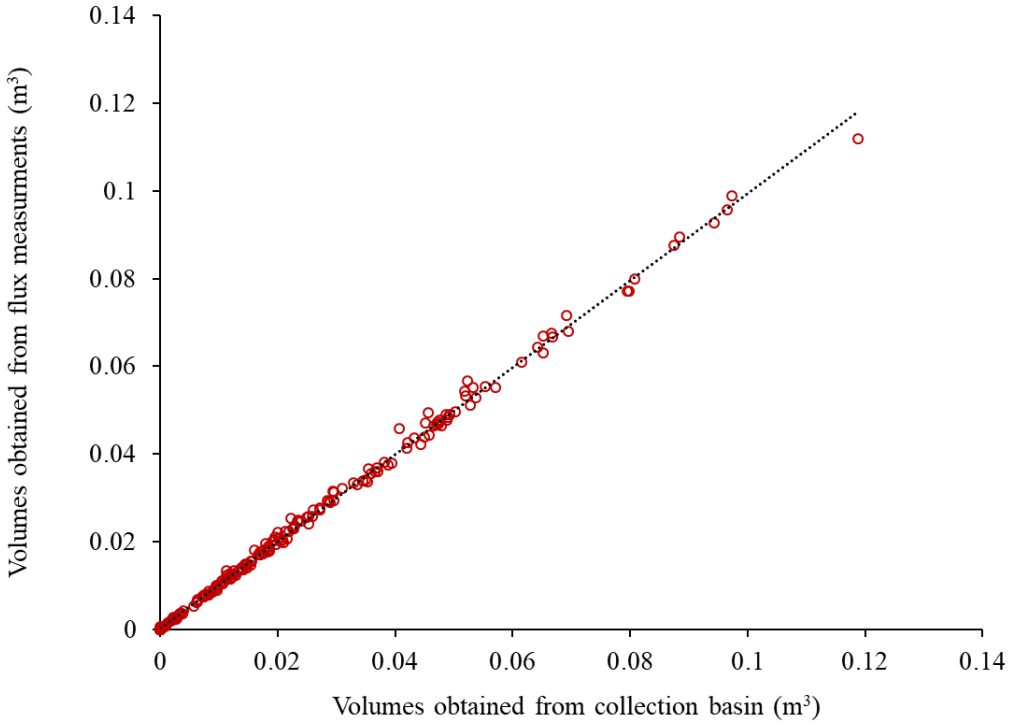

Figure 27 Comparison of total wave overtopping volumes obtained from the collection basin and the flux measurements over the crest.

The variations of the beach profile and water depth in front of the structure were estimated for each test. The wave hydrodynamic conditions were determined for each wave burst in order to assess the direct effects of wave height and wave period on the overtopping volumes for a hybrid structure.

The hybrid structure profiles were measured initially before the start of tests (P0) and then after 3.5 min (P1), 7 min (P2), 10.5 min (P3), 14 min (P4), 21 min (P6), 28 min (P8), and 35 min (P10) of wave burst. In order to perform a laser scan, the flume must be drained. The laser scanner can collect alongshore slices of profile data at cross-shore intervals of 1 cm. Each line scan was averaged and post-processed to get a representative elevation for each cross-shore position. Then,

the averaged cross-shore elevations were combined to form a 2-D profile for each of the eight profile scans collected during a test. The wave-induced erosion and deposition volumes per unit width were calculated by finding the difference between the area under each profile and the initial beach profile using the trapezoidal method. The overwashed volumes were estimated by the weight of the accumulated sediments on the sediment trap.

The wave hydrodynamic conditions were determined using spectral analysis of the recorded free surface elevations along the flume. Fast Fourier Transformation (FFT) was used to convert free surface elevation $\eta(t)$ into variance spectral density function *S(f)*. Fourier transform of free surface elevation can be determined as follow

$$F[\eta(t)] = \int_{-\infty}^{\infty} \eta(t) e^{-i2\pi ft}\, dt \tag{3. 7}$$

where *f* is the frequency and *t* is the time.

Multiplying the Fourier transform times its complex conjugate and divided by its duration shall give you the two-sided spectrum. The two-sided spectrum displays half energy at the positive frequency and half energy at the negative frequency. Therefore, to convert a two-sided spectrum to one-sided spectrum, the two-sided spectrum was truncated at the Nyquist frequency (f_N) and multiply every single point by 2 (Figure 28). The Nyquist frequency (f_N) is the highest frequency that can be defined from a time series of *N* sampled points and Δf increments ($f_N = \frac{N}{2}\Delta f$). Then the calculated *S(f)* was used to obtain the significant wave height H_{m0}, peak wave period T_p, and spectral wave period $T_{m-1,0}$. The energy-based significant wave height H_{mo} is computed from the energy spectrum of the incident waves as follows

$$H_{m0} = 4\sqrt{m_0} \tag{3. 8}$$

$$m_n = \int_0^{\infty} f^n S(f) df \quad n = -1, 0, 1, 2.. \tag{3. 9}$$

where m_n is defined as the n[th] moment of the variance spectrum, f is the sampling frequency in (Hz), and $S(f)$ is the energy density (m^2/Hz).

The T_p is the wave period associated with the peak frequency (f_p) of the spectrum where the largest variance of the spectrum is displayed. The $T_{m-1,0}$ is computed from -1 and 0 moments of the spectrum.

$$T_p = \frac{1}{f_p} \tag{3. 10}$$

$$T_{m-1,0} = \frac{m_{-1}}{m_0} \tag{3. 11}$$

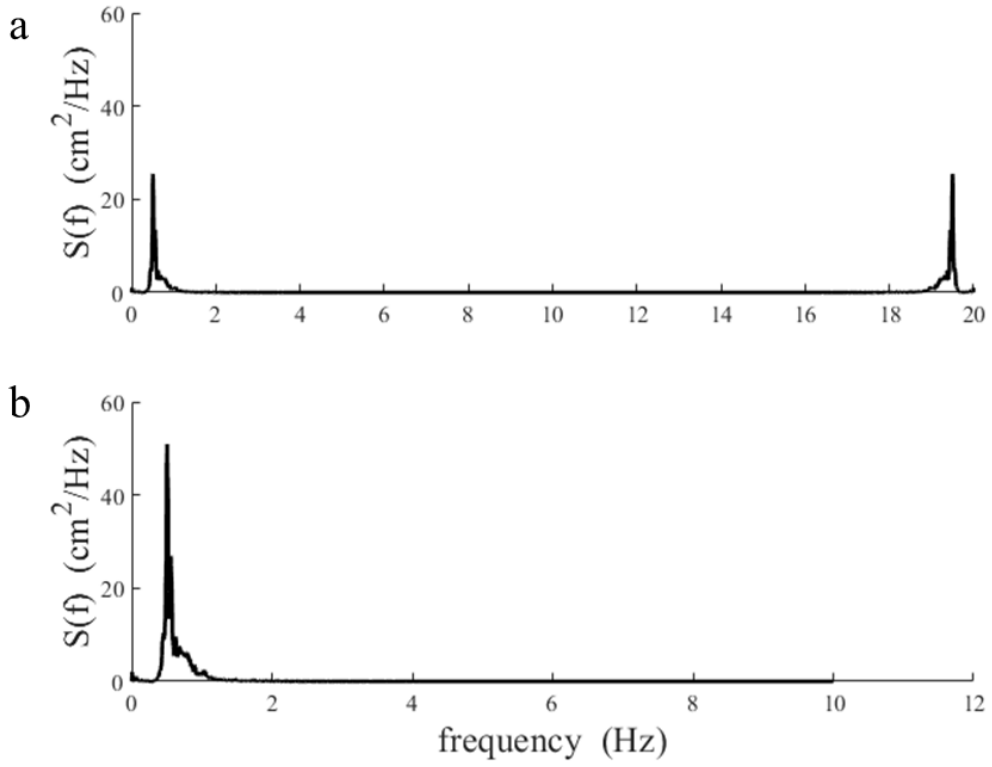

Figure 28 Two-sided spectrum (a) and one-sided spectrum (b) of a time-domain signal.

The wave field consists of both incident and reflected waves. Separating the incident and the reflected waves is essential for investigating the wave-structure interactions. The incident and reflected wave energy was used to evaluate the energy dissipation of the tested hybrid structure. Low reflected wave energy values indicate higher levels of wave energy dissipation through the adjusted beach face. The measured free surface elevations from WG1 – WG3 were used to separate the incident and the reflected spectra utilizing the method outlined by Mansard and Funke (1980). Then the measured incident wave heights, near the toe of the structure, were used to develop an empirical function to estimate wave overtopping over the hybrid structure.

The Vectrino profilers measured three-dimensional velocities during the wave bursts. The recorded velocities were filtered by removing data with an average correlation less than 70% and signal-to-noise ratio (SNR) less than 5 dB (Martin et al., 2002). Figure 29 shows an example of the raw velocity data before and after applying the filter. Filtering the data by removing spike data can help in removing the aliasing effects (phase shift of the emitted and the reflected pulses) of the Doppler signal (McLelland and Nicholas, 2000; Goring and Nikora, 2002). Spectral analysis using method outlined in Welch (1967) was performed on the filtered time series velocity data. The turbulent kinetic energy density was computed using a MATLAB script. The recorded velocities decomposed into a mean $\bar{u}, \bar{v}, \bar{w}$ and fluctuating u', v', w', then the variation of turbulent kinetic energy and Reynold stress with depth were calculated (Guerra and Thomson, 2017).

$$TKE = \frac{1}{2}\left(\overline{u'^2} + \overline{v'^2} + \overline{w'^2}\right) \quad (3.\ 12)$$

where u', v', w' are the fluctuating velocity components in the x, y, and z directions respectively, and defined as

$$u' = u - \bar{u} \quad (3.\ 13)$$

$$v' = v - \bar{v} \tag{3. 14}$$

$$w' = w - \bar{w} \tag{3. 15}$$

u, v, and w are the individual velocities and $\bar{u}, \bar{v}$, and $\bar{w}$ are the average velocities.

The spatial distribution of Reynold stress, τ_{uw} per unit mass in the near shore area was determined as follow:

$$\tau_{uw} = -\overline{u'w'} \tag{3. 16}$$

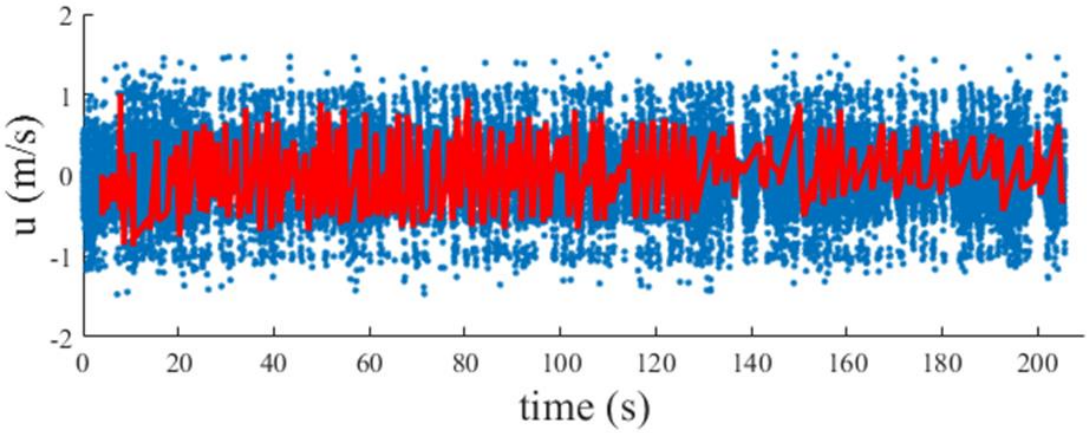

Figure 29 Raw and filtered velocity data in the x-direction. The raw velocities (blue dots) was filtered and linearly interpolated to obtain the filtered velocity components (red line).

CHAPTER 4

RESULTS AND DISCUSSION

In this chapter, results of the physical experiment are given and discussed. First and foremost, the key observations of this experiment are summarized. Next, the morphodynamic evolutions of the hybrid structure including erosion, deposition, and overwashed volumes are presented. After that, the results of hydrodynamic analysis involving significant wave heights, wave periods, reflection coefficients, kinetic energy measurements, and Reynolds stresses are shown. Then, the wave overtopping rates including the average and the instantaneous are given. After that, the new empirical overtopping formulae for wave overtopping discharge rates of a hybrid structure are presented. Finally, the effects of testing variables on wave overtopping are discussed.

4.1 Experiment observations

As explained in section 3.2, a set of 32 physical model trials was conducted with varying significant wave height, peak wave period, water depth, and sand cover thickness (Table 5 and Table 6). The performance of hybrid structures in reducing wave overtopping volumes were investigated. More insight was drawn towards morphological evolution of hybrid structure profile and its effects in enhancing the wave energy dissipation and its impact in reducing wave height and the overtopping discharge rates.

Wave overtopping discharge rates obtained from HS0 tests were compared with those volumes measured from HS1, HS2, and HS3. It was observed that hybrid structures with a thicker sand cover generate a lower wave overtopping discharge rate per unit length. Figure 30 compared

the average wave overtopping discharge rates during a wave burst per unit length for different trials during test 2. It was noted that wave overtopping discharge rates were larger during the first wave burst (t= 3.5 min) of the test, due to the existence of sand cover layer (Figure 30). The sand cover provided a smooth surface that enhanced the wave overtopping volumes. After the sand cover eroded or overwashed by wave actions, large waves continued to overtop the crest of the exposed rubble mound structure. However, hybrid structures HS3, with the initial sand layer thickness of 9 cm, fared batter in reducing the overtopping discharge rates compared to the other tested structures. In HS3 tests only few waves overtopped the hybrid structure during the first wave burst. Then the waves mainly scarped the face of the hybrid structure gradually. It was obvious during each test that the thicker sand layer provided better protection against wave overtopping.

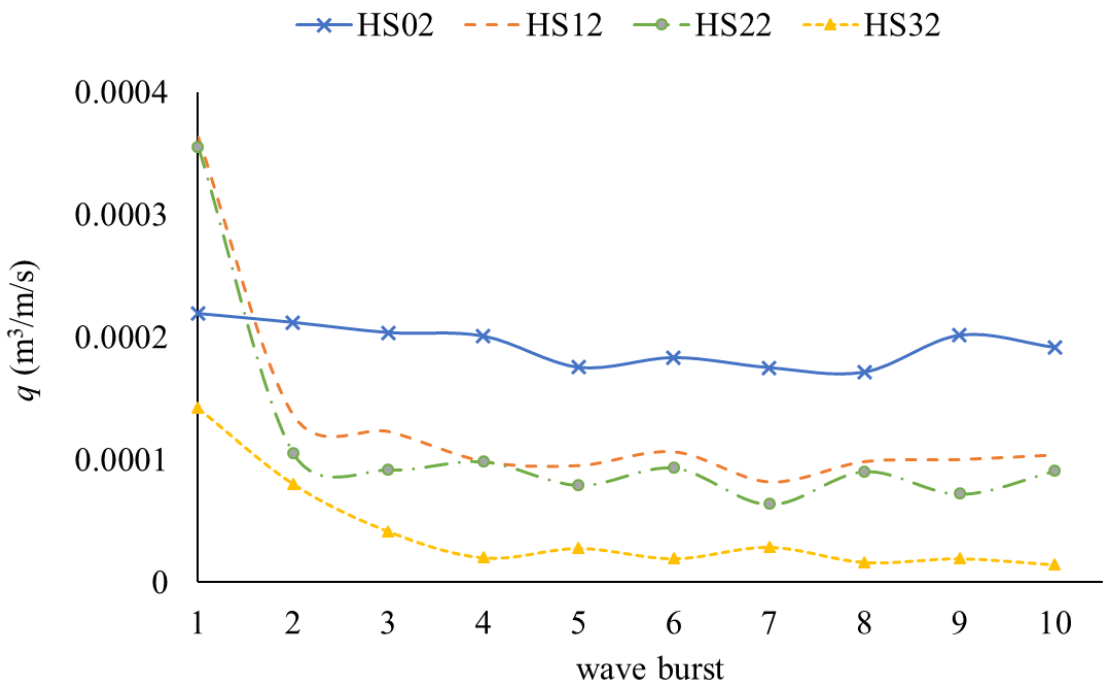

Figure 30 A comparison between wave overtopping discharge rates obtained from different trials during test 2.

A clear difference in morphological evolution was noted between the different sand layer thicknesses. In the hybrid trials with thinner sand cover HS1 (S_t = 5 cm), sediment eroded rapidly due to runup and overwash processes, exposing the rubble mound. Owing to the permeability of the rubble mound structure, part of sediment settled through the pores of the structure by the end of the first wave burst. The rest of the sediments deposited in front of the structure. The sand deposits in front of the hybrid structure can affect the slope of the beach profile, the water depth, and consequently the incident wave height near the toe. During wave bursts 2 through 10 in each test, the down rush of the waves penetrated through the pores of the exposed rubble mound, causing erosion. Wave actions continued to erode the sediment from the pores of the structure and caused

slight changes in the water depth in the front of the structure. Figure 31 shows the beach profile after the first wave burst (t = 3.5 min) of the test HS33 (blue dashed line), the final beach profile after the end of the test (t = 35 min) (red dashed line), and the settled sediment that was eroded from the structure voids by wave actions (hatched area). It was observed during the hybrid trials that, the thicker the sand layer covering the rubble mound, the more sand deposit can accumulate near the toe. The sand deposits enhanced the dissipation of wave energy reaching the toe of the structure by forcing the wave to break before hitting the structure.

A few observations were monitored regarding wave breaking during tests. The formation of submerged sand bar/berm in front of the structure forced the wave to break within a surface zone (a region where the waves are breaking, extending from the structure face to the breaker line) of 30 – 40 cm length. It was noted that there was a continuum of breaker type blending from waves spilling to plunging breaking depending on the variation of beach slope near the structure and characteristics of waves. Plunging breaker occurred when the slope of the beach changed from mild to steep. Plunging wave was distinguish by the wave curling forward and impinging onto water surface (Figure 32a). A spilling breaking was noticed over a mild beach slope. The spilling wave breaking was distinguished by white bubbles on the wave crest that were approaching the structure (Figure 32b). The turbulence generated by the plunging wave breaking lead to resuspension of the beach sediment. The fine suspended sediment then was transported in the offshore direction via undertow. It was obvious during the trials that spilling waves had a limited tendency to resuspended sediment compared to plunging waves. The plunging wave breaking generates more turbulence that can resuspend the sediment.

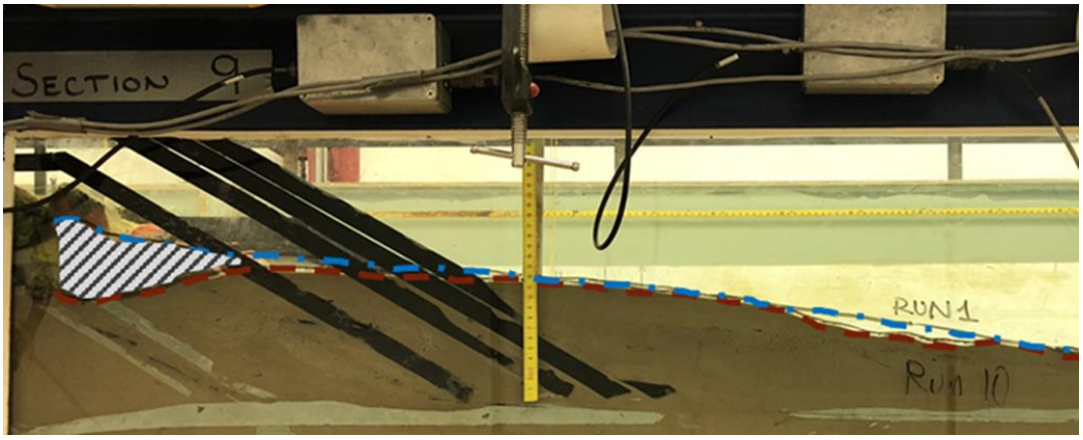

Figure 31 A photo of the beach profile variation between the first and last wave burst of a hybrid structure trial HS23.

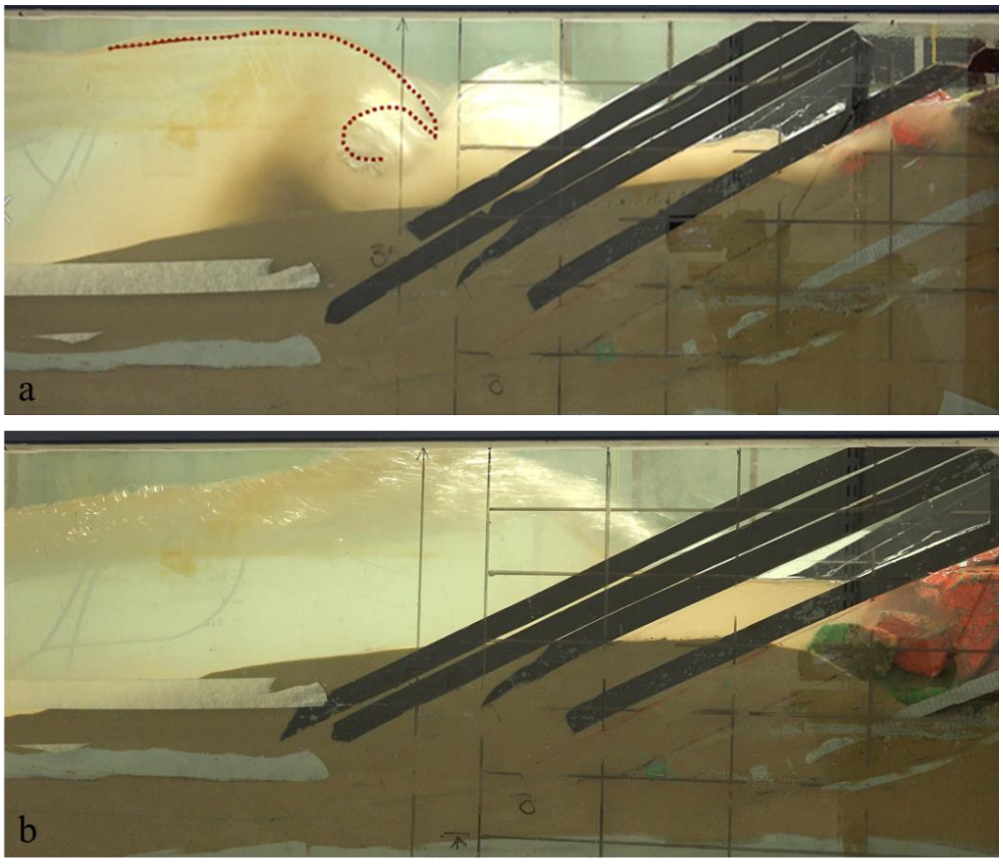

Figure 32 wave breaking on the beach face fronting a hybrid structure. (a) Plunging breaker of waves during test HS21 occurred when beach slope varies from mild to steep. (b) Spilling breaker during HS14 on a flat slope.

4.2 Morphodynamics

The profile evolution of the hybrid structure and fronting beach were captured via a laser scanner during the tests as explained in section 3.4. Figure 33 shows an example of the hybrid structure and beach profile before and after several wave bursts. The solid black line represents the initial profile of the hybrid structure. The rubble mound structure is buried under the dune initially and is represented by the gray circles. As discussed earlier, the rubble mound was partially exposed due to the gradual wave-induced erosion and overwash. The eroded sediment was deposited mostly in front of the hybrid structure raising the height of the submerged beach profile (Figure 33). The wave-induced erosion and overwash volumes were investigated with varying incident wave height, wave period, and water depth. Sediment properties including particle size, specific density, and fall velocity can influence the erosion and deposition pattern (e.g., Van Rijn, 1993; Julien, 2010). The experiment explained herein were conducted by utilizing fine sand with one sediment size (D_{50} = 0.014 cm). Therefore, exploring the effects of different sediment sizes on erosion and deposition pattern is outside the scope of this study.

The changes in beach profile were investigated to find the total erosion and frontal deposition volumes. All beach profiles were compared with the original beach profile at t = 0 min (P0). The variation of crest elevation (R_c) throughout the test was tracked since the height of the structure can significantly influence wave overtopping rates. The volume of overwashed sediment was captured by the sediment trap (section 3.3.6). The wet mass of the accumulated sand in the trap was measured first, then a sample of the collected sand was dried to obtain total dry weight and moisture content of the overwashed sediment. The changes in water depth (h_t) and the

foreshore affected significant wave height (H_{m0}) that can influence wave overtopping rates. It was found during the tests, the sand cover thickness (S_t) directly influences the water depth.

The volume of erosion and frontal deposition per unit width were calculated by finding the difference between the area under each profile and the original beach profile at t = 0 as explained in section 3.4. Erosion and overwash volumes per unit width were for different hybrid structures are summarized in Table 8, Table 9, and Table 10.

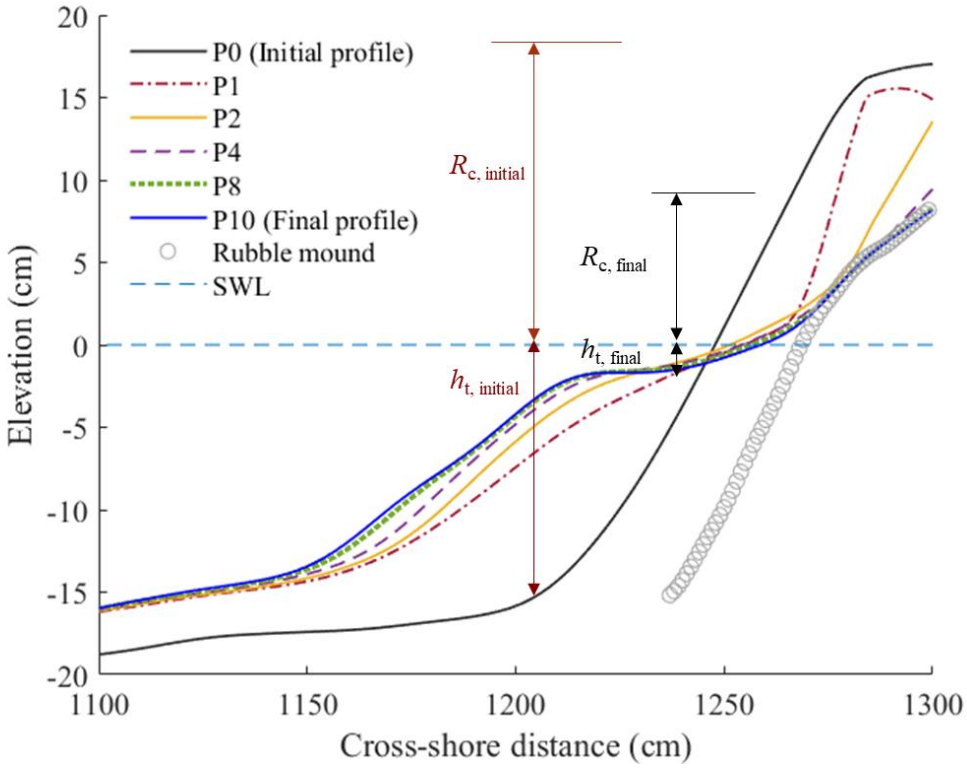

Figure 33 Measured beach and sand cover profile changes of a hybrid coastal structure with a sand cover thickness of 9 cm (HS36).

Table 8 Effects of varying water depth on overwash, erosion, and accretion volumes of hybrid structure tests after the first wave burst.

Test #	Initial sand cover (S_t)	initial Water depth (h_t)	Total overwash volume per unit width	Total erosion volume per unit width	Total frontal deposition volume per unit width	Water depth (h_t)
	(cm)	(cm)	(cm^3/cm)	(cm^3/cm)	(cm^3/cm)	cm
HS11	5	19	23.32	-357.54	290.82	10.03
HS12	5	17	18.91	-339.36	306.48	8.46
HS21	7	19	26.56	-458.14	382.31	8.72
HS22	7	17	23.00	-452.24	348.95	7.67
HS31	9	19	30.11	-448.14	430.79	7.53
HS32	9	17	20.78	-487.62	414.37	7.29

Table 9 Effects of varying wave height on overwash, erosion, and accretion volumes of hybrid structure tests after the first wave burst.

Test #	Initial sand cover (S_t)	Wave height (H_{m0})	Total overwash volume per unit width	Total erosion volume per unit width	Total frontal deposition volume per unit width	Water depth (h_t)
	(cm)	(cm)	(cm^3/cm)	(cm^3/cm)	(cm^3/cm)	cm
HS11	5	9	23.32	-357.54	290.82	10.03
HS13	5	12	15.94	-375.97	229.86	9.91
HS21	7	9	26.56	-458.14	382.31	8.72
HS23	7	12	23.63	-482.63	418.87	8.50
HS31	9	9	30.11	-448.14	430.79	7.53
HS33	9	12	28.64	-510.64	470.53	7.54

Table 10 Effects of varying wave period on overwash, erosion, and accretion volumes of hybrid structure tests after the first wave burst.

Test #	Initial sand cover (S_t)	Wave period (T_p)	Total overwash volume per unit width	Total erosion volume per unit width	Total frontal deposition volume per unit width	Water depth (h_t)
	(cm)	(s)	(cm^3/cm)	(cm^3/cm)	(cm^3/cm)	cm
HS11	5	1.9	23.32	-357.54	290.82	10.03
HS15	5	1.64	19.47	-351.50	324.36	10.11
HS21	7	1.9	26.56	-458.14	382.31	8.72
HS25	7	1.64	24.62	-423.98	330.20	8.92
HS31	9	1.9	30.11	-448.14	430.79	7.53
HS35	9	1.64	24.50	-441.05	345.43	8.17

Comparing tests with the same initial sand cover thickness (e.g., HS11 and HS12, HS21 and HS22), for a constant wave period (T_p = 1.9 s), and wave height (H_{m0} = 9 cm), a reduction in the initial water depth near the toe of the structure by 2 cm led to a reduction in erosion and overwash volumes per unit width as summarized in Table 8. However, for hybrid coastal tests with thicker sand cover layer (e.g., HS31 and HS32) the erosion volume increased by 8.8% with the decrease of the initial water depth by 2 cm. The enhancement of the erosion volumes can be interpreted as follows: the thicker sand cover provides more protection against wave overtopping; only a few larger waves can overtop the structure, while the smaller waves continue to scarp the face of the dune gradually.

For a constant wave period (T_p = 1.9 s) and a constant initial water depth near the structure (h_t = 19 cm), an increase in wave height led to an average increase in erosion volumes by 8.2% for hybrid tests with the same initial sand cover layer (e.g., HS11 and HS13, HS21 and HS23, HS31 and HS33) as shown in Table 9. However, the overwashed volumes decreased as the wave height increase (e.g., HS31 and HS33). Larger waves erode more sediment and tend to break faster than the smaller waves. The eroded fine sediment was carried by the wave flow and deposited in the weak turbulence area. This will allow the growth of the sand feature in front of the structure. Therefore, wave energy dissipation rate will increase and wave overtopping volumes over the structure crest will decrease (less overwashed sediment).

As the wave period (T_p) increased, with constant initial water depth (h_t = 19 cm) and wave height (H_{m0}= 9 cm), the erosion and overwashed volumes increased as shown in Table 10. On average the higher wave period (T_p = 1.9 s) increased the erosion and overwash volumes by 3.6% and 14%, respectively.

4.3 Hydrodynamics

The wave free surface elevation was recorded by 7 capacitance wave gauges along the wave flume. The recorded voltage at a wave gauge location was processed to generate time series with a temporal frequency of 20 Hz. The recorded time series of water fluctuations around the still water level was analyzed using a spectral method to calculate significant wave height and wave period at each wave gauge location. Each time series consists of 4200 data points. The first 200 data points in each file encounter water surface disturbance due to a ramp-up of wave generation before reaching the fully developed wave state. These 200 data points were excluded from the analysis and the calculations to avoid a ramp-up effect on the results.

As discussed in section 3.4, wave spectrum represents the distribution of wave energy for sea surface as a function of frequency. From the wave spectrum, various wave period parameters can be found including peak wave period T_p, the mean wave period T_m, significant wave period $T_{1/3}$, and the spectral wave period $T_{m-1,0}$. The peak period T_p is the period associated with the peak of the spectrum. The mean spectral wave period T_m is the average wave period of the incident waves ($T_m = m_0 / m_1$). The significant wave period $T_{1/3}$ is the mean period of the highest 1/3 of wave. The significant wave period is used in the analysis of many coastal processes with a standard spectral shape and deep-water conditions. In shallow water depth where the wave spectrum tends to be flatter or multi-peaked due to the non-linear wave processes near the shore, the spectral wave period ($T_{m-1,0} = m_{-1} / m_0$) is used rather than the significant wave height (e.g., Van Gent et al., 2003; Van der Meer et al., 2016). The $T_{m-1,0}$ is used in describing processes relevant to wave-structure interactions including wave runup, wave overtopping, wave reflection, and structure stability. The first negative moment of the spectral wave period is used to account for the increased relevance of

lower wave frequencies in the spectrum to runup and overtopping processes. For hybrid coastal structures investigated herein the spectral significant wave height H_{mo} and the spectral wave period $T_{m-1,0}$ near the structure toe are used in wave overtopping calculations. The existence of the dynamic sand cover layer in the hybrid structure can affect the foreshore slope. The sediment eroded by wave action during a storm changes the initial water depth in front of the structure to a shallower water depth.

As waves propagate from deep water condition to the toe of the structure, the wave spectrum shape evolves from a single peak spectrum to a double- or multi- peaked spectrum. An example of the cross-shore evolution of the wave power spectrum from WG1 – WG6 (Figure 34). As the waves approach the hybrid structure at WG7 the wave spectrum shape changes into a multi-peaked spectrum. As shown in Figure 35, the energy is distributed between a primary peak at f = 0.52 Hz, a sub-harmonic (lower frequency) at f = 0.178 Hz, and a first super-harmonic (higher frequency) at f = 0.92 Hz, a second super-harmonic at f = 1.02 Hz. The multi-peaked spectrum occurs as a result of the non-linear wave transformation in shallow water depth, wave breaking, and wave-wave interaction near a structure (triad interaction). Sub-harmonic frequencies can cause long period oscillation, slow drift motion, and an offshore sand bar feature due to sediment transport. Super-harmonic frequencies can cause a sharp peaked wave crest and flatter trough that can impact the sediment transport (Klopman and Van Leeuwen, 1990). The non-linear energy transferred from the incident peak frequency to sub- and super- harmonics (Figure 35). The pattern of the cross-shore evolution of the wave power spectral density from WG1 – WG6 was similar in other hybrid tests. However, the power spectral density near the structure toe (WG7) of the thinner sand cover (HS1) had two sub-harmonics at $0.3f_p$, and $0.5f_p$ and super-harmonics at $2f_p$, and $2.5f_p$

(Figure 36a). For the thicker sand cover tests (HS3) had a sub-harmonic at $0.23f_p$ and three super-harmonics around $1.6f_p$, $1.3f_p$, and $1.9f_p$ as shown in Figure 36b. Wave interactions showed that energy transfer to sub- and super-harmonic prior to breaking leading to significant changes in the spectral shape with a subsequent dissipation of the wave energy in the surf zone

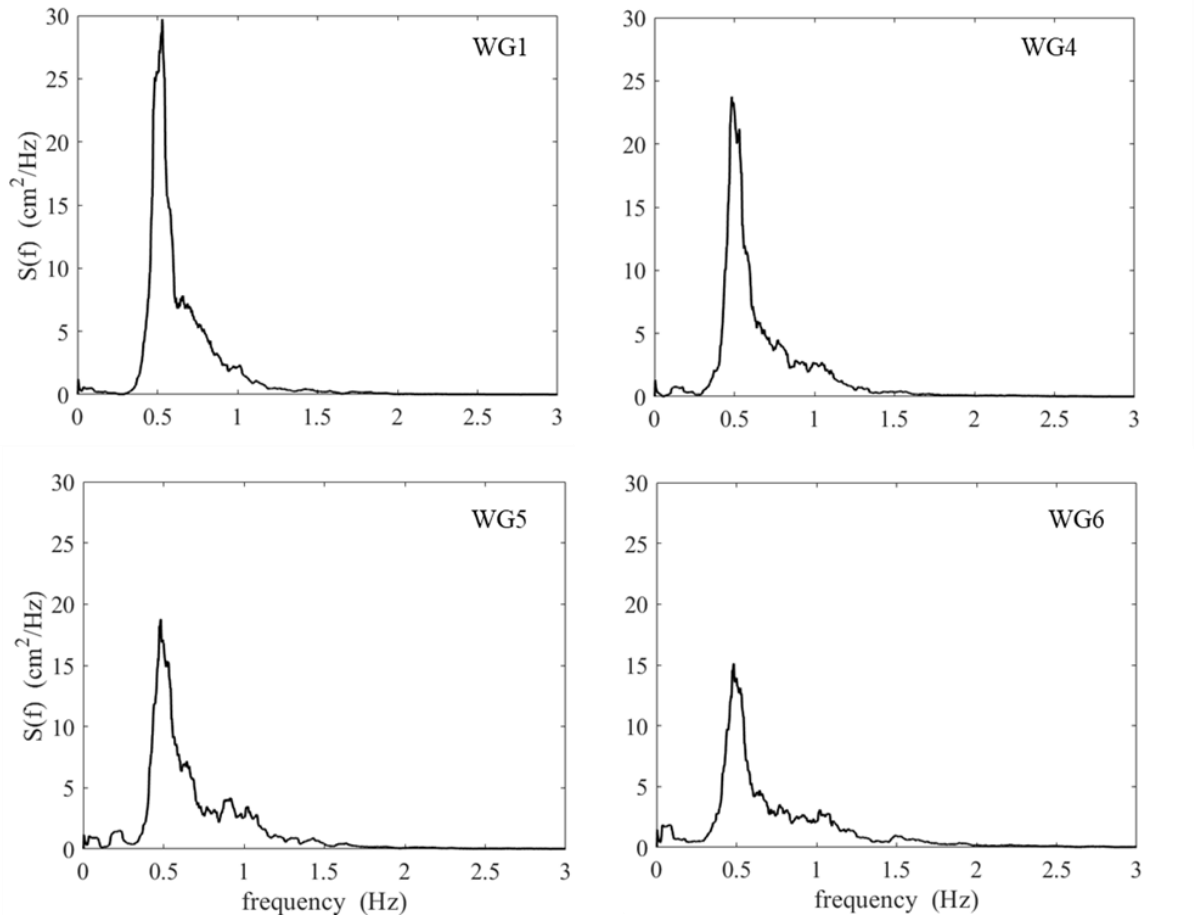

Figure 34 Cross-shore evolution of the wave power spectral density for HS21 test

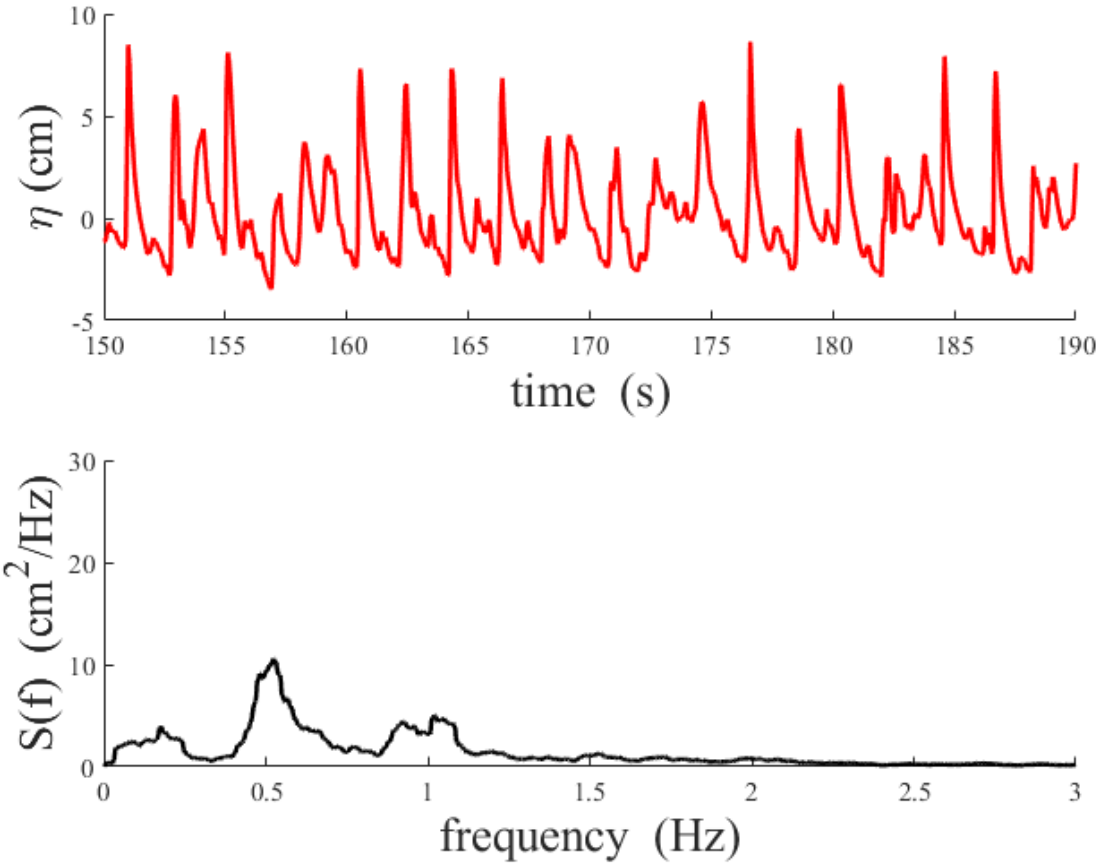

Figure 35 Upper panel: 40-second segment of measured free surface elevation near the cross-shore location of the structure toe (test HS21). The jagged nature of the time series is indicative of breaking waves, steep wave fronts and surf zone interactions. Lower panel: Corresponding spectral wave energy density in shallow water depth and generating of sub- and super- harmonics where energy transfer can occur and overall energy dissipation.

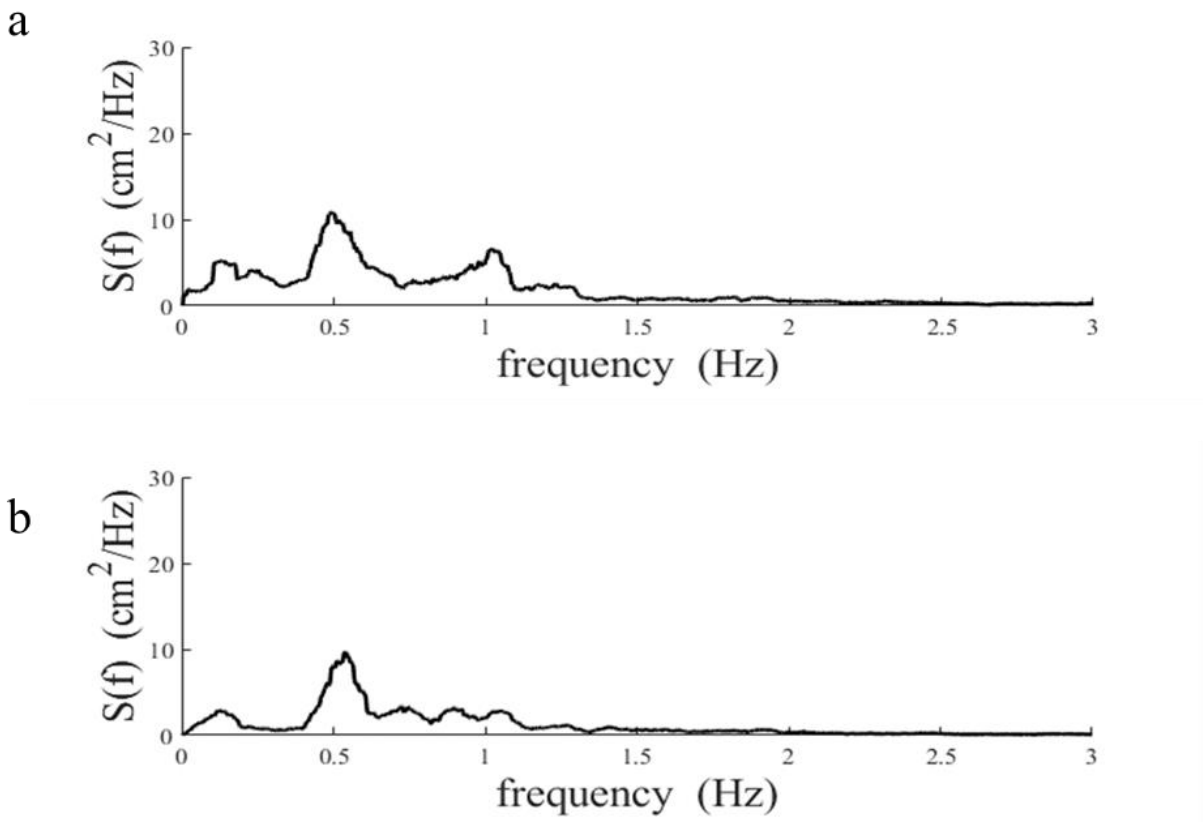

Figure 36 Power spectral density near the toe of the structure for (a) HS11 (b) HS31.

The measured time series at each wave gauge location includes both incident and reflected waves. In order to separate the incident from the reflected waves, the Mansard and Funke (1980) method was applied using the three most offshore-located wave gauges. The reflected and incident spectra were calculated to assess the degree of energy reflection. Wave reflection can increase wave velocities and shear stresses that can lead to a larger sour depth near the toe of a structure. Rubble mound dissipate a portion of the incident wave energy while reflect the remaining energy back towards offshore direction. The incident wave energy may be transmitted over the rubble

mound or dissipated via turbulence within the voids (e.g., Allsop and Hettiarachchi, 1988).The reflection coefficient, C_r is expressed by the following formula

$$C_r = \frac{H_r}{H_i} \quad (4.\ 1)$$

where H_r is the reflected wave height in (cm), H_i is the incident wave height (cm).

The reflection coefficients were calculated during wave bursts for each test, and their values are presented in Table 11. The values of the reflection coefficient vary between 0.16 and 0.5. Initially hybrid coastal structures (HS1, HS2, and HS3) produced higher reflection coefficients compared with the rubble mound structure (HS0) as shown in Table 11. The higher reflection coefficients can be explained by the presence of the smooth sand cover layer before the wave-induced erosion took place. Once the sand cover is eroded, these coefficients dropped to lower values. The modification of these reflection coefficients for hybrid structure tests can be clarified by the adjustment in their profiles throughout the tests. Also, the presence of the submerged sand feature that was responsible of dissipating the wave energy. After the adjustment of hybrid structure profiles (through wave bursts 3 – 10) the reflection coefficient reduced by 4% – 23% on average compared with rubble mound structure test. It was found that the reflection coefficients of rubble mound remain almost constant during each test as shown in Table 11. Reflection coefficients depends on the hydrodynamic and geometrical parameters of a coastal structure (Zanuttigh and van der Meer, 2008). However, for hybrid structures reflection coefficients were affected by variation of the water depth near the structure. Thus, reflection coefficients varied through wave burst 1 – 2 (Table 11).

Table 11 Wave reflection coefficients

Wave burst Test	1	2	3	4	5	6	7	8	9	10
HS01	0.27	0.27	0.27	0.27	0.27	0.27	0.27	0.27	0.27	0.27
HS02	0.27	0.27	0.27	0.27	0.27	0.27	0.27	0.27	0.28	0.28
HS03	0.27	0.27	0.27	0.27	0.27	0.27	0.27	0.27	0.27	0.27
HS04	0.28	0.28	0.28	0.28	0.28	0.28	0.28	0.28	0.28	0.28
HS05	0.26	0.25	0.26	0.26	0.25	0.25	0.25	0.25	0.25	0.25
HS06	0.28	0.27	0.27	0.27	0.27	0.27	0.27	0.27	0.27	0.27
HS07	0.25	0.25	0.25	0.25	0.25	0.25	0.25	0.25	0.25	0.25
HS08	0.26	0.26	0.26	0.26	0.26	0.26	0.26	0.26	0.26	0.26
HS11	0.43	0.24	0.23	0.23	0.23	0.22	0.22	0.22	0.23	0.23
HS12	0.43	0.25	0.24	0.24	0.23	0.23	0.23	0.23	0.23	0.23
HS13	0.41	0.23	0.23	0.23	0.23	0.22	0.22	0.22	0.22	0.22
HS14	0.37	0.24	0.23	0.23	0.22	0.22	0.22	0.22	0.22	0.22
HS15	0.45	0.27	0.24	0.24	0.23	0.23	0.23	0.22	0.22	0.22
HS16	0.48	0.31	0.26	0.25	0.24	0.23	0.23	0.23	0.23	0.23
HS17	0.44	0.25	0.24	0.23	0.23	0.22	0.22	0.22	0.22	0.22
HS18	0.44	0.26	0.24	0.23	0.23	0.22	0.22	0.22	0.22	0.22
HS21	0.47	0.25	0.24	0.24	0.23	0.23	0.23	0.23	0.23	0.23
HS22	0.45	0.25	0.22	0.22	0.22	0.22	0.22	0.22	0.22	0.22
HS23	0.44	0.24	0.24	0.23	0.23	0.23	0.23	0.23	0.23	0.23
HS24	0.42	0.23	0.21	0.21	0.22	0.21	0.22	0.21	0.21	0.22
HS25	0.45	0.22	0.21	0.21	0.20	0.20	0.20	0.20	0.19	0.19
HS26	0.48	0.26	0.22	0.21	0.20	0.20	0.20	0.20	0.20	0.20
HS27	0.43	0.22	0.21	0.21	0.21	0.21	0.21	0.20	0.21	0.21
HS28	0.43	0.23	0.20	0.19	0.19	0.19	0.19	0.19	0.18	0.18
HS31	0.50	0.24	0.20	0.20	0.20	0.20	0.20	0.20	0.20	0.20
HS32	0.47	0.26	0.21	0.21	0.21	0.21	0.21	0.21	0.20	0.20
HS33	0.44	0.22	0.20	0.20	0.20	0.20	0.20	0.20	0.20	0.20
HS34	0.46	0.24	0.20	0.20	0.20	0.20	0.20	0.20	0.20	0.20
HS35	0.50	0.23	0.16	0.16	0.16	0.16	0.17	0.17	0.17	0.17
HS36	0.46	0.25	0.20	0.19	0.18	0.18	0.18	0.18	0.18	0.18
HS37	0.45	0.20	0.17	0.17	0.17	0.17	0.18	0.17	0.17	0.17
HS38	0.44	0.22	0.18	0.17	0.17	0.17	0.17	0.17	0.17	0.16

Nortek Vectrino acoustic Doppler velocimeters (1) and profilers (2) measured the water velocities at three different cross-shore locations in the approach to the hybrid structure as shown

in Figure 18. The two profilers with a down-looking head were placed at a cross-shore distance of 11.68 m and 11.19 m from WG1, respectively. Both profilers were placed 6 cm above the sea bed before each wave burst where the sampling depth was 3.1 cm. Hence, all the velocity measurements can capture the inner flow at the near-bed region where z/h < 0.2 (ratio of sampling depth to flow depth). TKE per unit mass was measured by obtaining the root-mean-square (RMS) velocities as explained in section 3.4. The TKE represents the intensity of the turbulence in the water flow. The noticeable increase in TKE within the sampling depth represents the generation of turbulence fluctuations by the wave flow. The changes of TKE depend on the wave phase and location of the breaking where under the crest of the wave the TKE increases. While at the location of the breaking more TKE was generated near the surface then it was diffused along the depth. In this study, the TKE was transferred toward the structure in the upper sampling volume while it was transferred in the offshore direction near the bed as shown in Figure 37 and Figure 38. The Reynolds stresses per unit mass (τ_{uw}) were calculated for each wave burst in the tests using the equation (3.16). τ_{uw} stresses then were time averaged along constant depths to construct a single stress profile of the calculated spatial values. The distribution of τ_{uw} can be an indication of the net increase or decrease of in momentum flux and can provide a qualitative insight of the vertical mixing of the sediment. τ_{uw} will then be expected to become positive near the bed, representing transport of high momentum from the overlying flow. Variations of TKE and Reynolds stresses with depth under the profiler head are shown through Figure 37 - Figure 40.

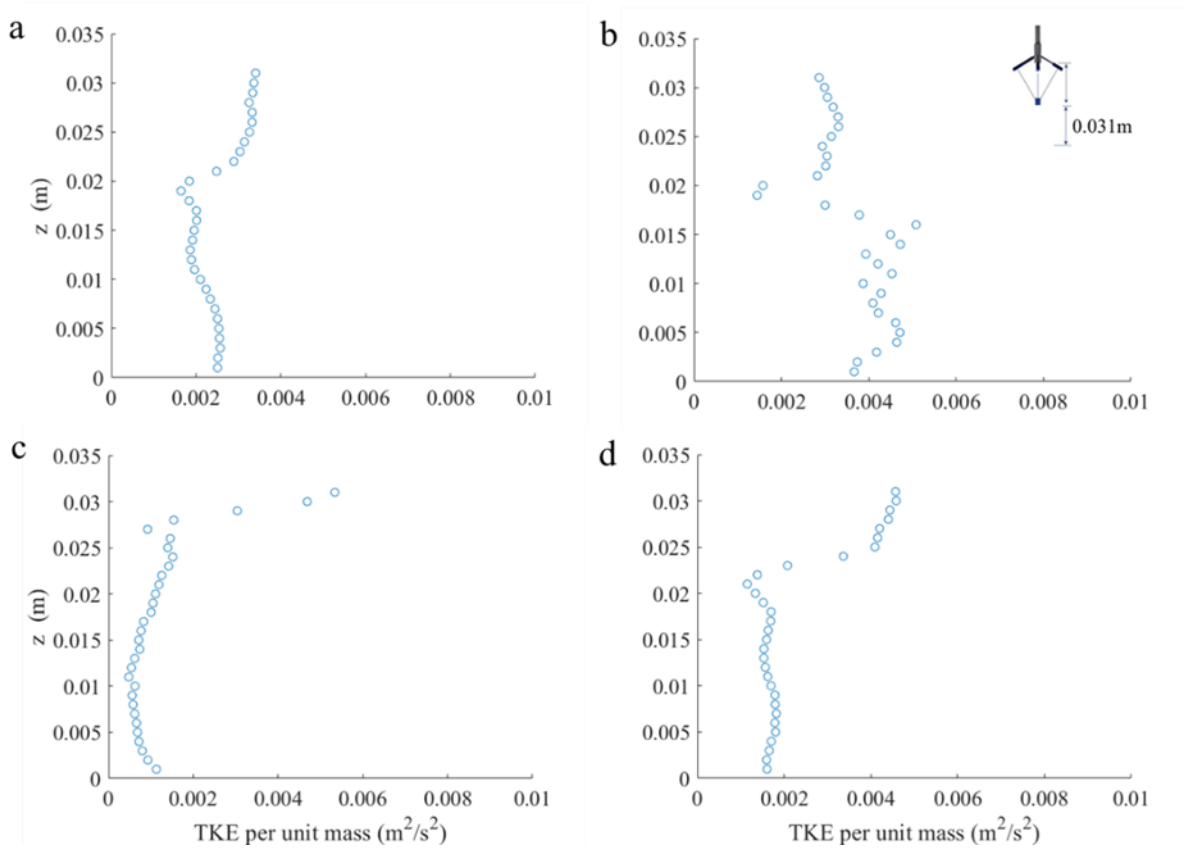

Figure 37 Variation TKE per unit mass with depth during the first wave burst of test (a) HS01 (b) HS11 (c) HS21 (d) HS31.

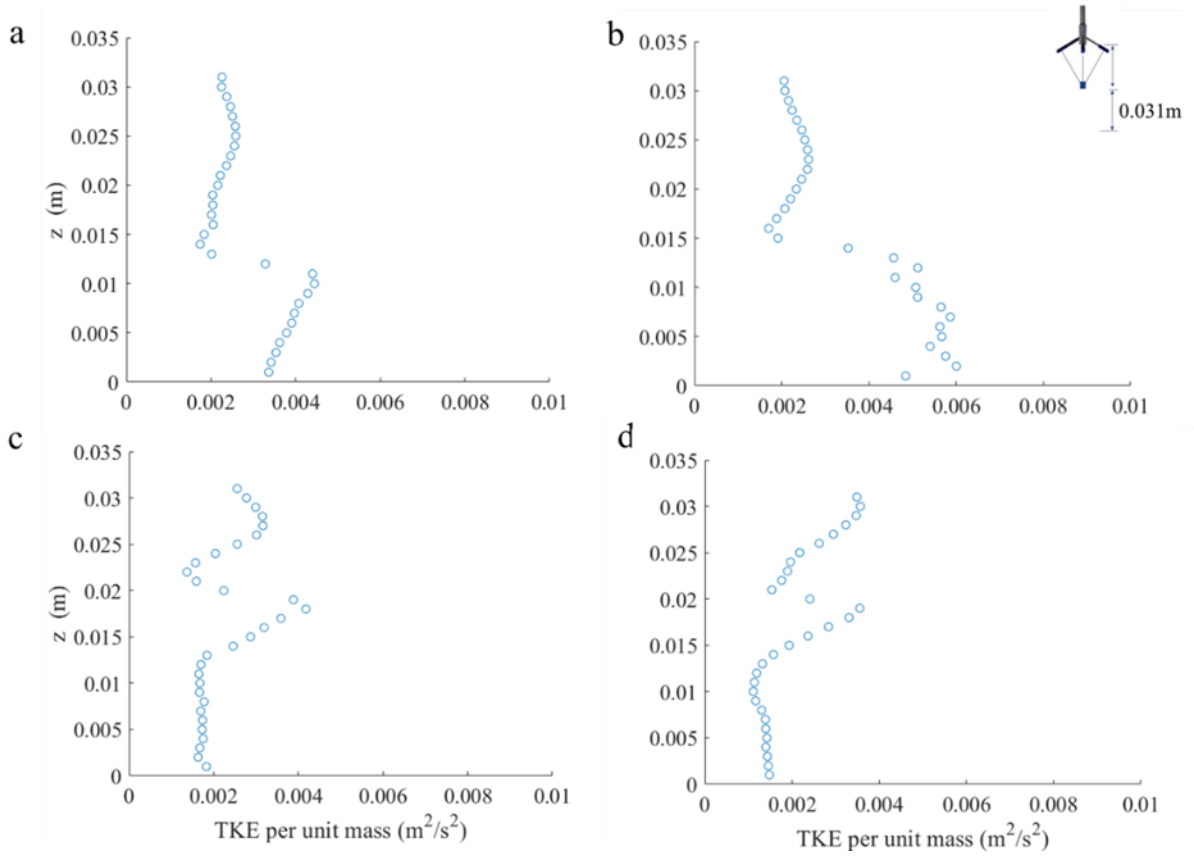

Figure 38 Variation TKE per unit mass with depth during the last wave burst of test (a) HS01 (b) HS11 (c) HS21 (d) HS31.

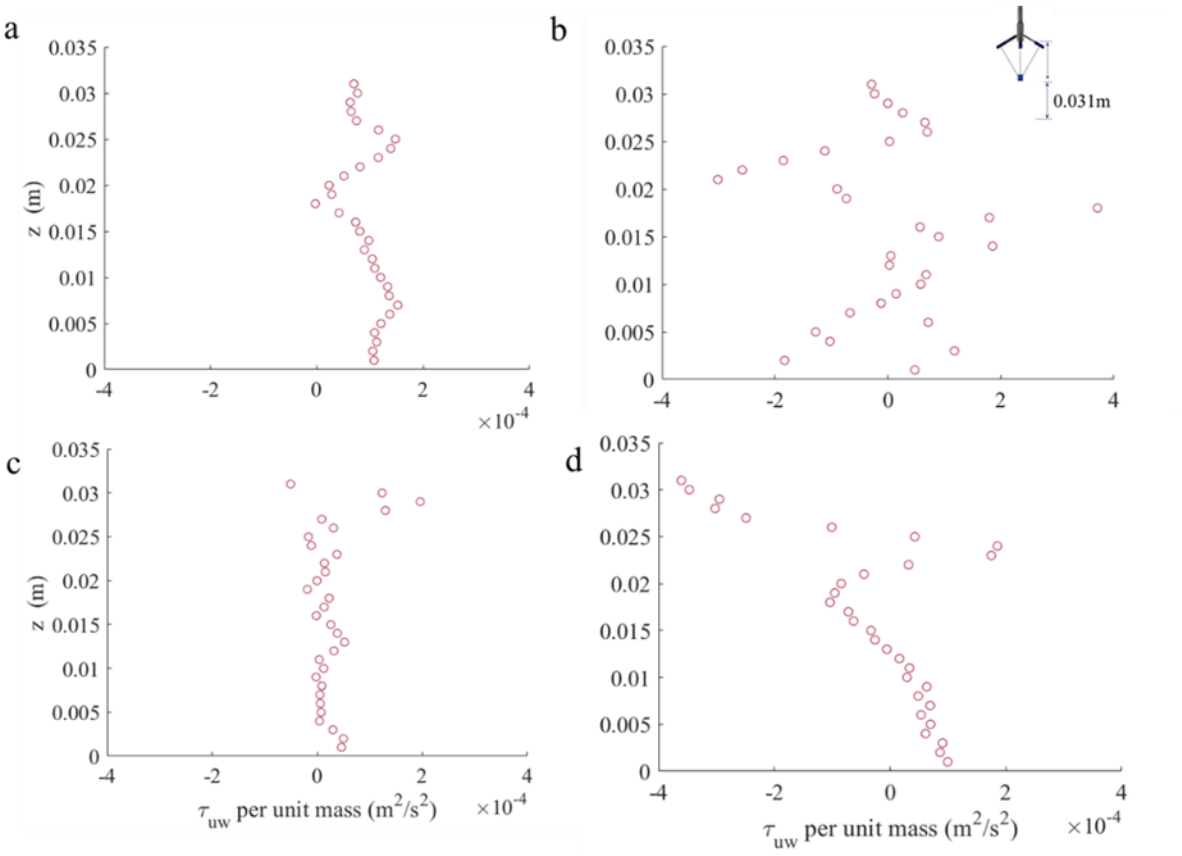

Figure 39 Variation τ_{uw} per unit mass with depth during the first wave burst of test (a) HS01 (b) HS11 (c) HS21 (d) HS31.

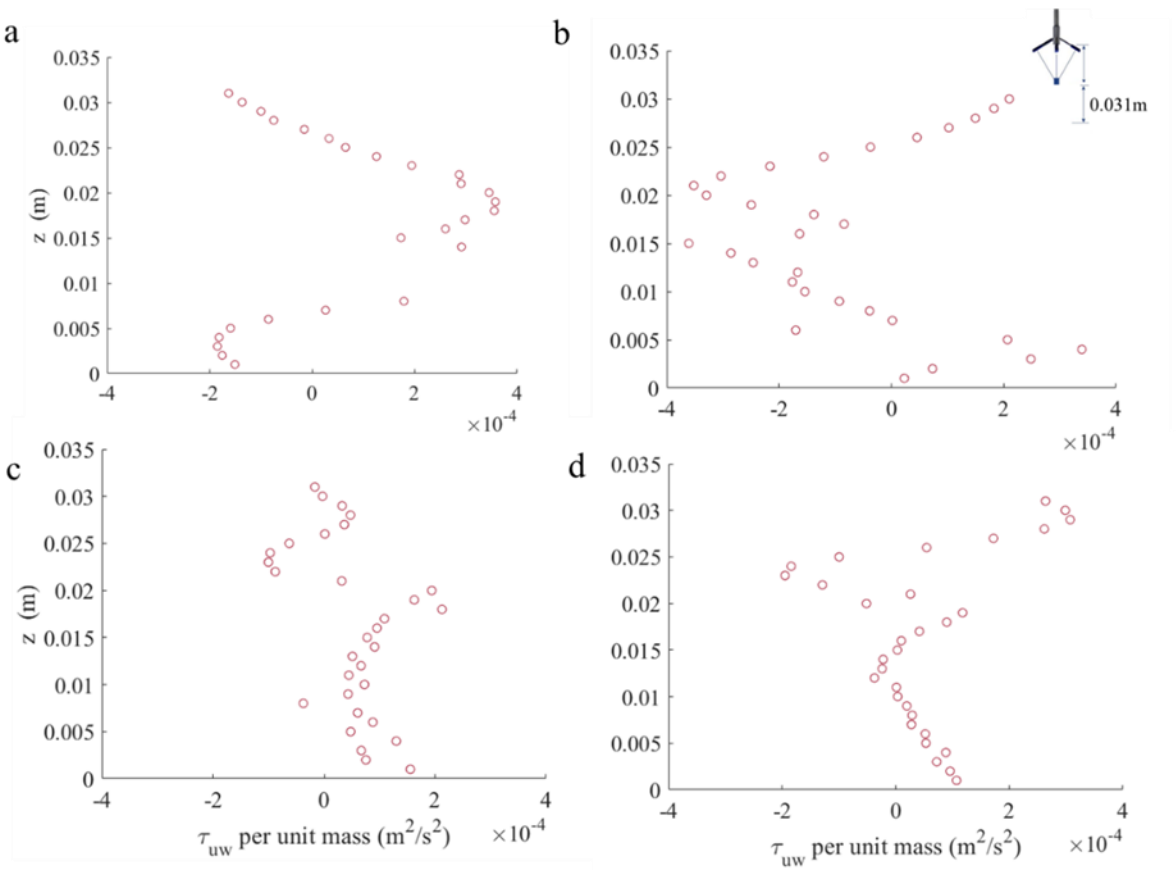

Figure 40 Variation τ_{uw} per unit mass with depth during the last wave burst of test (a) HS01 (b) HS11 (c) HS21 (d) HS31.

The Vectrino+ profiler with a side-looking head was placed along the slope of the hybrid structure at a cross-shore distance of 12.73 m from WG1. The collected data from the profilers were filtered out by removing spikes and excess noise and created a set of clean data as explained in section 3.4. Spectral analysis was applied to investigate the TKE characteristics in the swash zone. Nortek Vectrino+ profiler data was first filtered and then the energy density of the horizontal velocity component was determined. The turbulent kinetic energy in the swash zone was calculated from the power spectral density. In general, the TKE spectrum consists of three sub-ranges 1) the

energy containing sub-range, 2) the inertial sub-range, and 3) the dissipation sub-range. In the inertial sub-range, the energy transfers from larger to small scale while in the dissipative range the energy dissipates through viscosity (Katul et al., 1995). The measured TKE spectrum (Figure 41) lay within the inertial energy sub-range that showed a similar decay to $f^{-5/3}$ law by Kolmogorov et al. (1991). Similar variation of TKE spectrum was found for other hybrid structures with different sand cover thickness (HS1, HS2, and HS3).

The recorded flow velocities in the swash zone were not symmetrical where the uprush velocities were not simply the reverse of the backrush velocities. When the wave uprush reaches the structure crest the velocity increase from zero to the value of the overflow velocity where part of the sediment was overwashed. Throughout the remainder of the uprush velocity decreases to zero. The flow velocity during the backrush increases as the water flows downward until it reaches the maximum backrush velocity (Figure 41). It should be noted that most of the data collected through the first wave burst were not suitable for the data analysis due to poor quality (low SNR) and gaps in data record (Vectrino receivers were not submerged completely). On average the uprush velocities were affected by the wave energy dissipation through wave breaking at the location of submerged sand bar feature. On average the uprush velocities decreased during thicker sand cover trails (HS3 and HS2) compared pure rubble mound tests (HS0). While the average uprush velocities measured during the testing of hybrid structures with thinner sand cover were larger than other trials. Capturing the detailed hydrodynamics will be essential for the future numerical model studies.

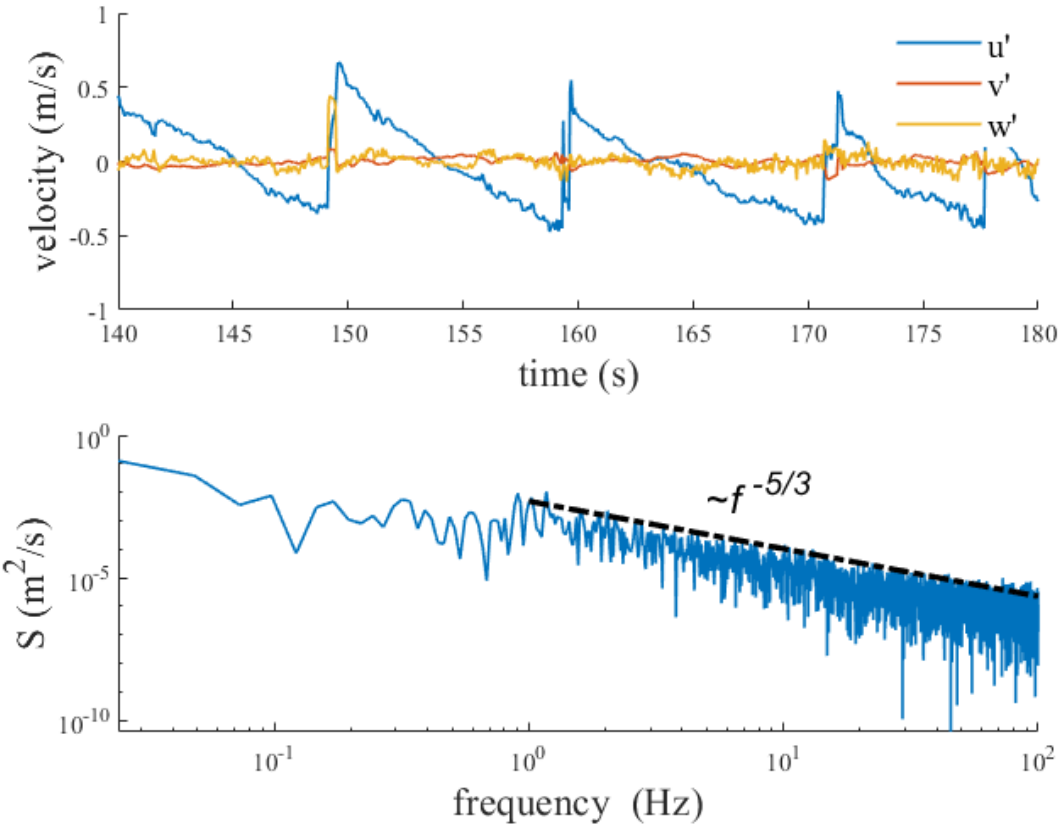

Figure 41 Upper panel shows 30-second segment of measured turbulence velocity components along the seaward structure slope during the third wave burst of test HS31. Lower panel shows the power spectral density of TKE that lies within the inertial sub-range.

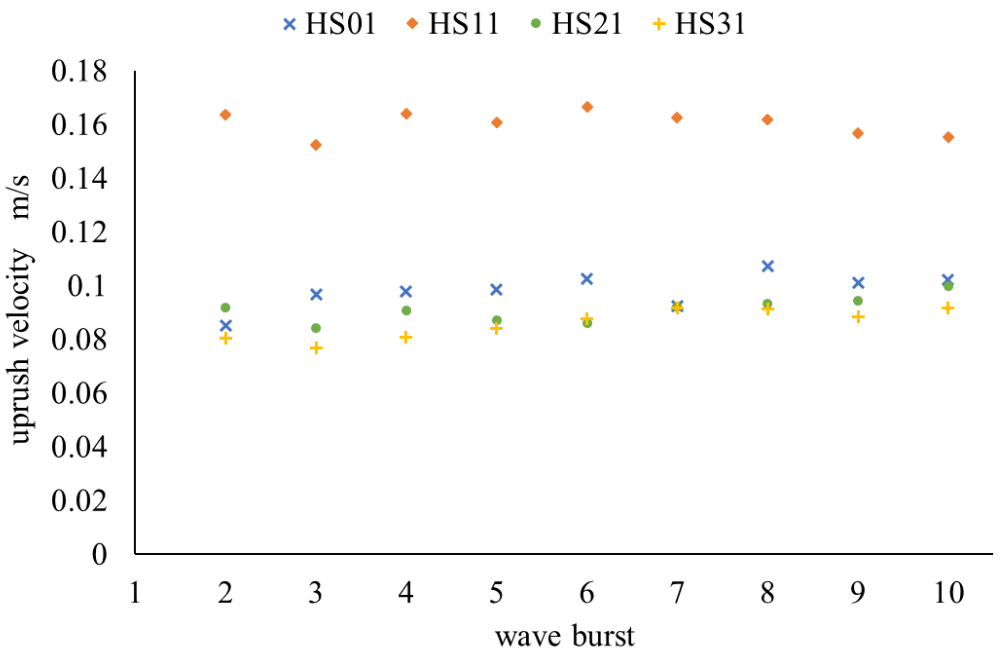

Figure 42 Uprush velocities obtained during wave burst for different hybrid structure trials.

4.4 Wave Overtopping

The main focus of the experimental investigation was to develop applicable wave overtopping equations for a hybrid structure. The average (over a wave burst duration) and the instantaneous (Figure 43) wave overtopping discharge rates per unit length were obtained as explained in section 3.4. The time series of instantaneous wave overtopping discharge rates for different hybrid structure tests are shown through Figure 44 - Figure 46. As shown from the experimental results the average wave overtopping rate is smaller than the maximum individual wave overtopping rate. The average wave overtopping rates are affected by multiple parameters including R_c, h_t, H_{m0}, $T_{m-1,0}$, $s_{m-1,0}$ (ratio of wave height to wave length), seaward slope of the structure (tan α), and the roughness of the structure surface (Van der Meer et al., 2016). In this

experimental investigation, only one side slope of 1v:2h was tested. Thus, the effect of the side slope is outside of the scope of this study. It should be noted that overtopping measurements during the first wave bursts were excluded from the analysis of overtopping empirical formulation. During the first wave burst, rapid variations in R_c and h_t were encountered before the hybrid structure reach its equilibrium status.

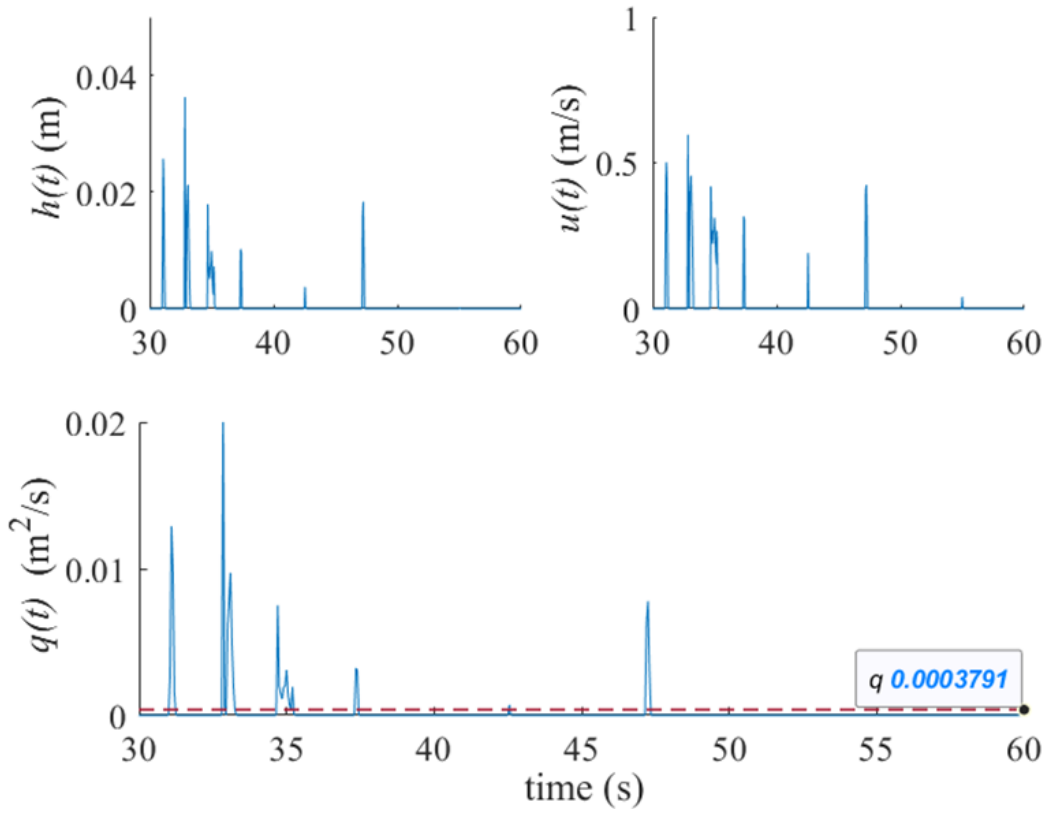

Figure 43 30-second segment of the instantaneous wave overtopping rates for HS21.

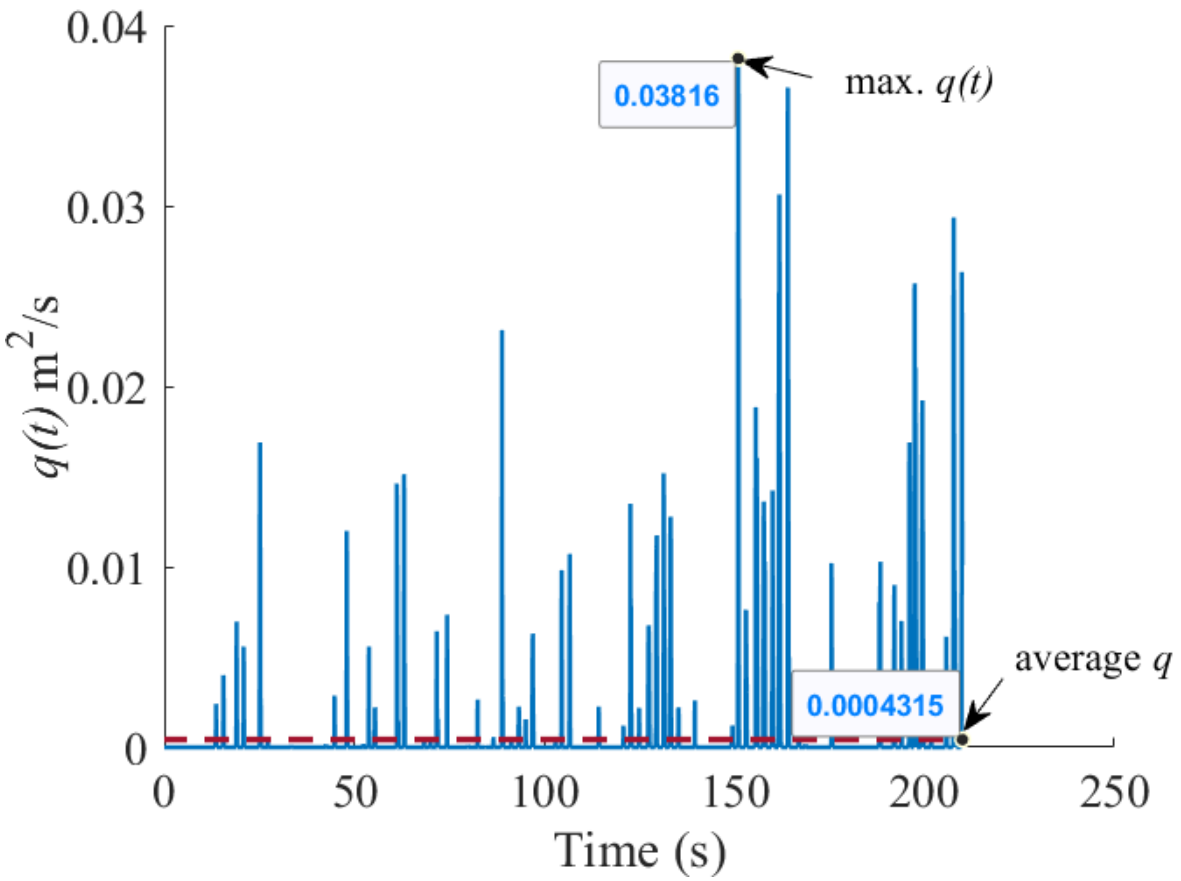

Figure 44 Instantaneous wave overtopping rate and the average wave overtopping over the duration of a wave burst during HS11.

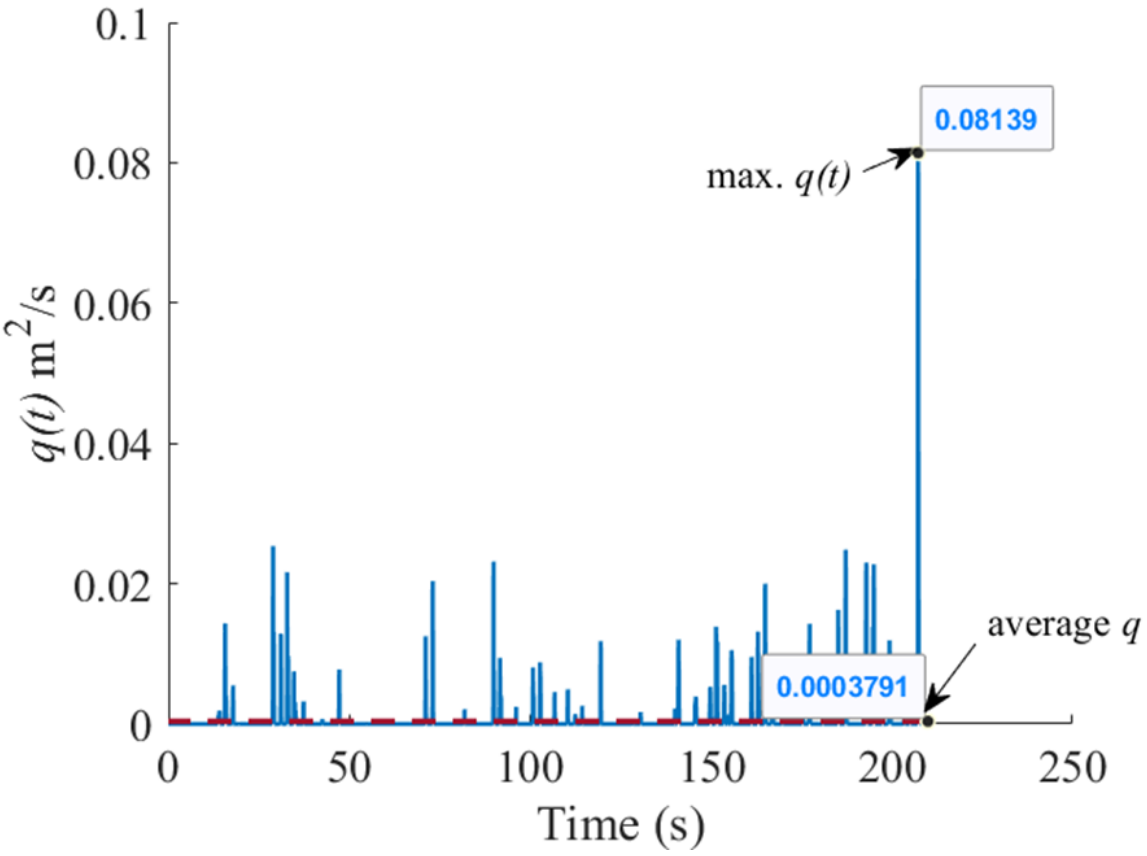

Figure 45 Instantaneous wave overtopping rate and the average wave overtopping over the duration of a wave burst during HS21.

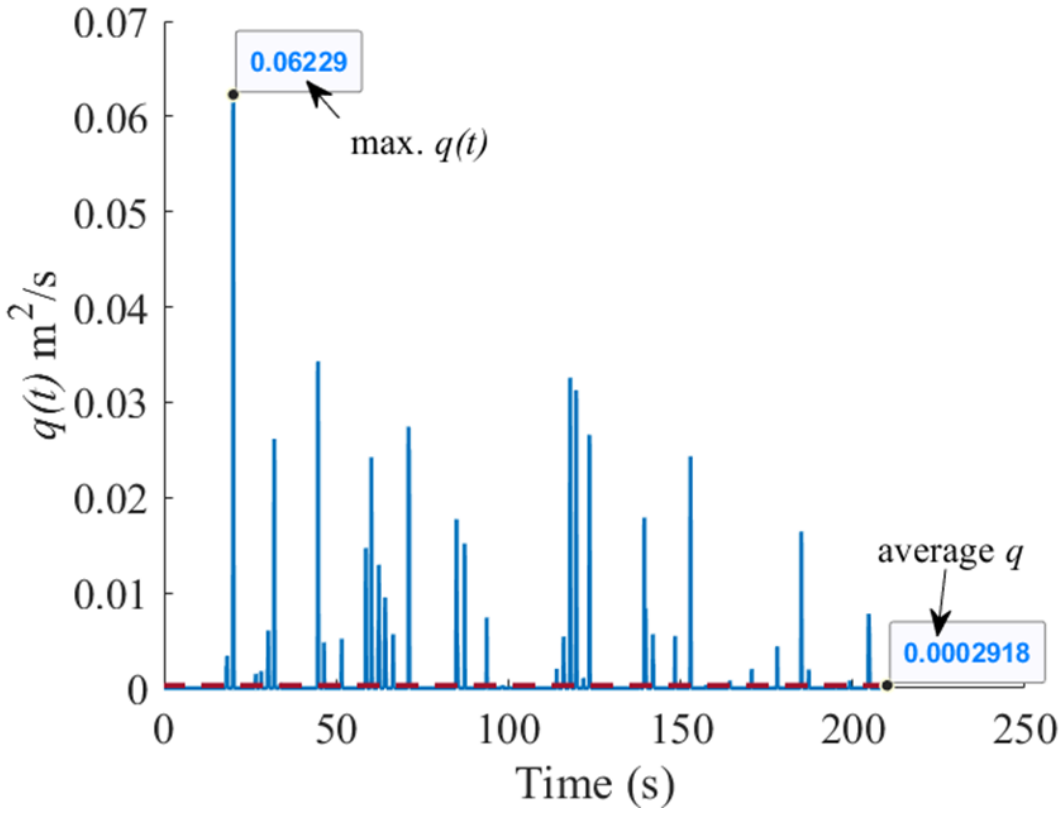

Figure 46 Instantaneous wave overtopping rate and the average wave overtopping over the duration of a wave burst during HS31.

4.4.1 Average Wave Overtopping Rates

The average wave overtopping rates were clearly dependent on the crest freeboard and water depth in this physical model study. A data set of 207 average overtopping rates was used to develop a prediction model for overtopping of hybrid structures. Using dimensional analysis, a non-dimensional average wave overtopping model was formulated as shown in Eq. (4.3.1)

$$\frac{q}{\sqrt{gH_{m0}{}^3}} = f\left(\frac{R_c}{H_{m0}}, \frac{h_t}{H_{m0}}, \frac{L_{m-1,0}}{H_{m0}}, tan\alpha\right) \tag{4.3.1}$$

The impact of the tanα on overtopping volumes was neglected as it was fixed in all trials. Also, the effects of $\frac{L_{m-1,0}}{H_{m0}}$ were assumed to be minor as its values varied slightly between tests. Eq. (4.3.1) was simplified to the following expression:

$$\frac{q}{\sqrt{gH_{m0}{}^3}} = f\left(\frac{R_c}{H_{m0}}, \frac{h_t}{H_{m0}}\right) \tag{4.3.2}$$

The results show that the non-dimensional average wave overtopping rate decays exponentially as the non-dimensional number $R_c h_t / H_{mo}^2$ increases (Figure 47). Hence an empirical formula for the average wave overtopping rate was developed [Eq. (4.3.3)]. The three dimensionless parameters of Eq. (4.3.3) *a*, *b*, and *c* were determined by non-linear regression analysis to be 0.00553, 3.087, and 2.133, respectively. Comparing the measured data with predicted data obtained from Eq. (4.3.3) yields a squared correlation coefficient, R^2, of 0.72.

$$\frac{q}{\sqrt{gH_{m0}{}^3}} = a \times Exp\left[-b\left(\frac{R_c\, h_t}{H_{m0}{}^2}\right)^c\right] \tag{4.3.3}$$

Rearranging Eq. (4.3.3), the dimensional average wave overtopping rate q per unit length is presented in Eq. (4.3.4).

$$q = 0.00553\sqrt{gH_{m0}{}^3} \times Exp\left[-3.087\left(\frac{R_c\, h_t}{H_{m0}{}^2}\right)^{2.133}\right] \tag{4.3.4}$$

where g is gravitational acceleration, H_{m0} is energy-based significant wave height, R_c is the crest freeboard, and h_t is the water depth at the toe of the structure.

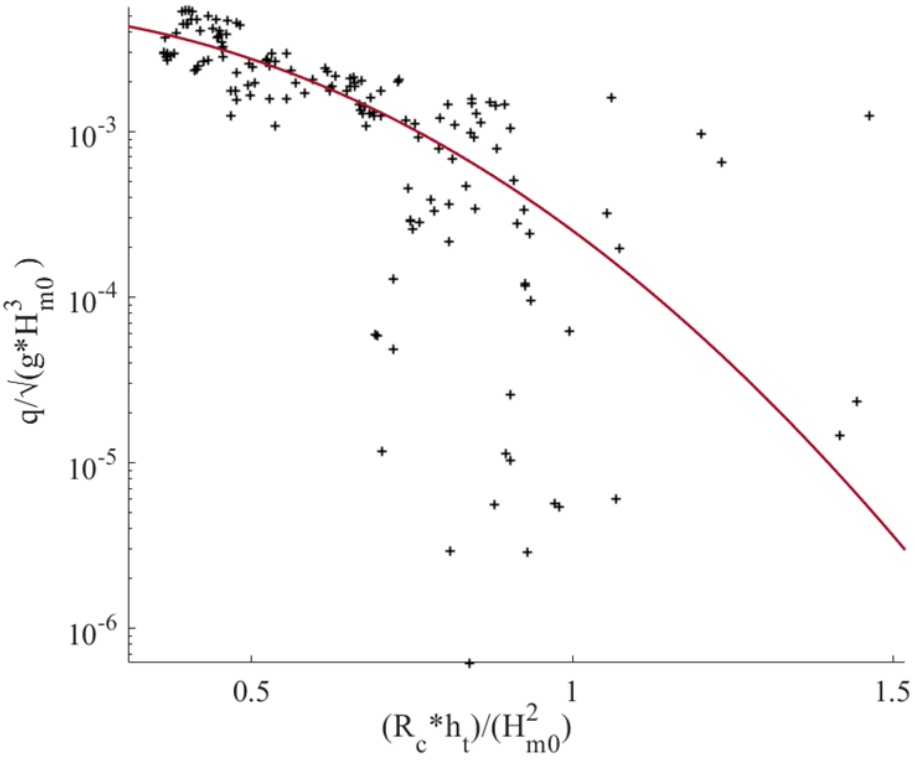

Figure 47 Measured data (crosses) and exponential model fit (line) relating nondimensional average wave overtopping rate to the non-dimensional group including crest freeboard, water depth at the toe, and spectral significant wave height for a hybrid coastal structure.

4.4.2 Instantaneous Wave Overtopping Rates

The maximum instantaneous wave overtopping rate can be several times greater than the average wave overtopping rate. Although the maximum instantaneous overtopping rate occurs over a short duration, it is responsible for the instability of armor units and sediment erosion (Hughes and Thornton, 2016). Therefore, accurate prediction of instantaneous overtopping rates is important for the design of hybrid coastal structures. The time series of overtopping discharge rate was calculated at the crest of the hybrid structure. The instantaneous discharge rates per unit length *q(t)* obtained from each wave burst were divided by the total overtopped water volume per

unit length (V_T). A data set of 49422 individual overtopping measurements were fitted by several distributions (Rayleigh, Exponential, and Weibull) to assess the best mathematical form that can represent the instantaneous discharge rates (Figure 48). As seen in Figure 48, Rayleigh and Exponential probability distribution do not fit the data well. The instantaneous wave overtopping rates are best represented by a Weibull distribution. The probability distribution of instantaneous wave overtopping rates is shown in Figure 49 and is expressed by the following mathematical form

$$q(t) = V_T \frac{\beta}{\alpha}\left(\frac{t}{\alpha}\right)^{\beta-1} Exp\left[-\left(\frac{t}{\alpha}\right)^{\beta}\right] \tag{4.3.5}$$

Integrating Eq. (4.3.5) with time yields the probability distribution for cumulative overtopping volume as shown in Eq. (4.3.5)

$$V(t) = V_T\left[1 - Exp\left(-\left(\frac{t}{\alpha}\right)^{\beta}\right)\right] \tag{4.3.6}$$

where *q(t)* is the instantaneous wave overtopping rate per unit length, *V(t)* is the cumulative overtopping volume per unit length, *t* is time, α is a scale factor, and β is a shape factor. The shape factor, scale factor, and the coefficient of determination, R^2,are found to be 0.6277, 0.0495 s^{-1}, and 0.998, respectively.

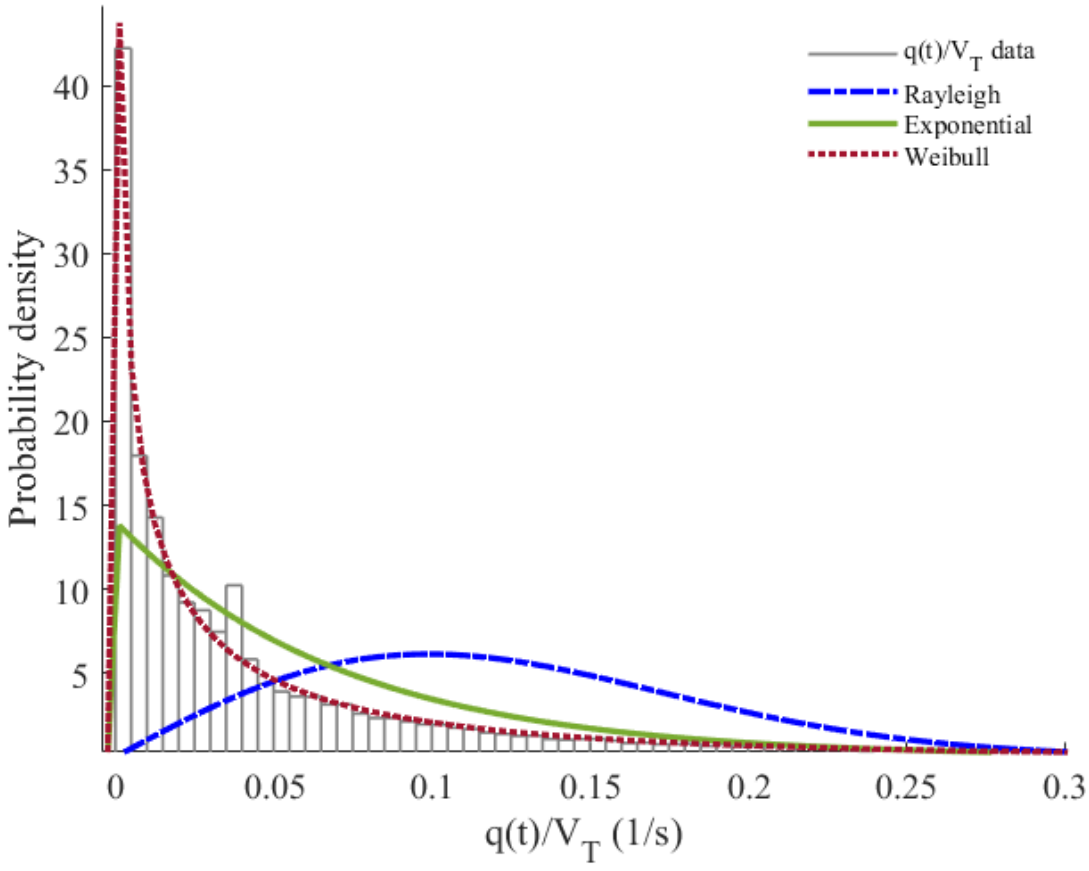

Figure 48 Probability density plot for the ratio of instantaneous wave overtopping discharge and total volume comparing several distribution models.

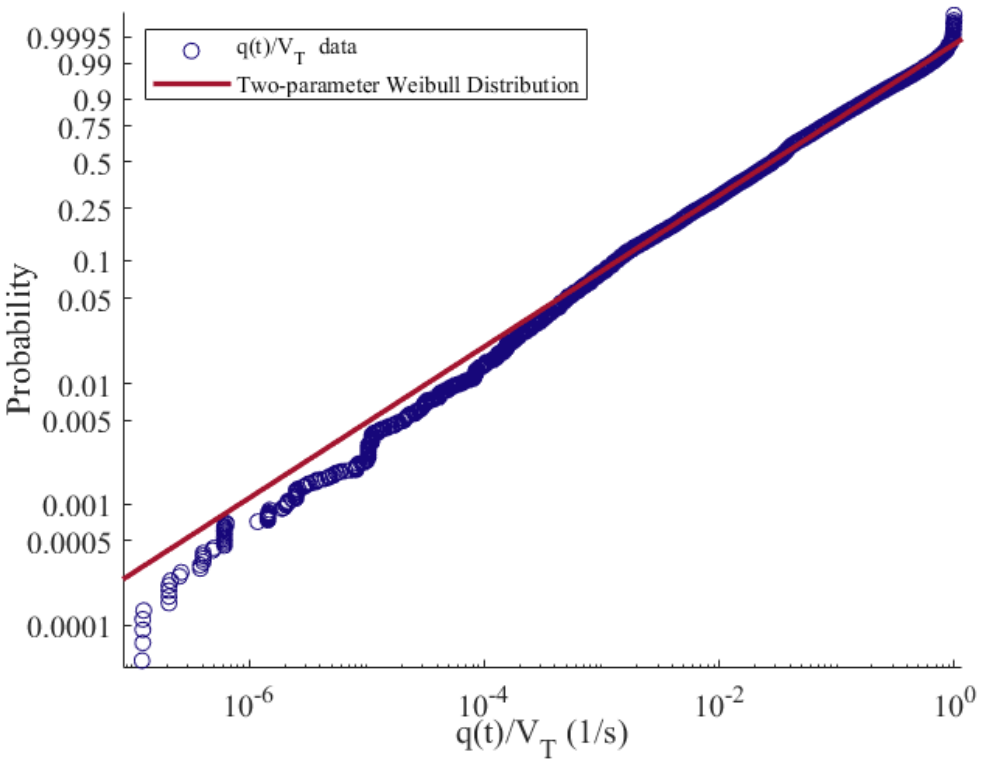

Figure 49 Weibull distribution probability plot for ratio of instantaneous wave overtopping discharge and total volume for hybrid structure bursts.

The wave overtopping rate over a hybrid structure is influenced by many factors, including the crest freeboard, water depth, the incident hydrodynamic conditions, and seaward slope of the structure. In the experimental model trials, the height of the rubble mound structure was fixed, and R_c was adjusted by placing sand layers with varying initial thickness and changing the water level in the tank. The data and the analysis show that the wave overtopping rate decreases as the crest freeboard height (R_c) increases. Also, it was found that the smooth sand cover layer, as shown in Figure 50a, initially increases the R_c and reduces the surface roughness. Larger wave overtopping volumes were generated during the first wave burst (3.5 min). Initially, the sand cover increases

the overtopping volumes by 40% to 60% when compared to rubble mound tests under the same hydrodynamic conditions. However, during actual storms the water level increases gradually, allowing for profile adjustments potentially without the detrimental increase in initial overtopping volumes. After the rubble mound was partially exposed due to wave-induced erosion and overwash processes (Figure 50b), wave overtopping rates become 20% – 90% less than those of the plane rubble mound trial. These findings agree with the first research hypothesis where hybrid coastal structures with thicker sand cover layer provide better protection against flooding compared to traditional coastal structures under wave attack. The results of the experiment showed that the incident wave height affects wave overtopping volume significantly. For a constant wave period, T_p, and water depth, h_t, increasing the wave height leads to an increase the wave overtopping rates by 73% on average. Nevertheless, it was found that the accumulated sand deposits near the toe of the hybrid structure (Figure 50c) enhance the wave energy dissipation. The wave energy in the hybrid structure trails was 80% less than that of the rubble mound trial leading to a reduction in wave overtopping volumes. Thus, the presence of the mobile sand cover over the rubble mound structure (hybrid structure) influenced the water depth and the hydraulic conditions after wave-induced erosion and accretion occurred.

Figure 50. Photos of the physical model hybrid structure with a sand cover of 7 cm and its evolution during HS22 tests. Initially, the hybrid structure looks like an engineered sand dune (a). After 7 minutes of wave impact, the sand cover above the crest was completely eroded (b). The water depth and the foreshore slope were altered due to the erosion and deposition processes (c).

The mean wave period near the toe, $T_{m-1,0}$, is an important hydraulic parameter for wave overtopping volume. The effect of wave period is considered in the wave steepness parameter, $S_{m-1,0}$. In rubble mound trials with constant wave height, an increase in wave period increases the wavelength and the wave steepness reduces resulting in higher overflow velocities and higher overtopping volumes. However, in the hybrid coastal structure tests wave breaking, runup, and

overtopping characteristics were influenced by both wave period and the evolution of sand deposits (Figure 50c) throughout all tests.

The proposed empirical formula for the average wave overtopping rate was influenced mainly by the relative freeboard and relative water depth near the toe. The proposed overtopping equation can predict the discharge rates based on hydrodynamic conditions and morphodynamic changes near the structure. Two main concerns should be addressed when treating a hybrid structure; 1) the variation of water depth and 2) the beach slope near the structure toe. More insight is required into the effect of beach and dune evolution during extreme storms on the overtopping discharge rates, especially in coastal communities prone to frequent storms, where the sediment can be lost from the hybrid system. Thus, larger overtopping volumes can be generated. Also, there is a need to investigate the ability of a hybrid structure to recover after a storm event and to assess the required the replenishment plans to provide the desired protection level.

The resulting instantaneous and cumulative wave overtopping discharge rates were fitted to a Weibull distribution model as shown in Eq. (4.3.5) and Eq. (4.3.6). Both models depend on the total overtopping volume per unit length (V_T) during a storm event and the time of occurrence of individual overtopping rates (t). The time variation in the instantaneous wave overtopping rates can feature an increase in the discharge rate to the maximum value, then gradual reduction to zero. During this short duration, rapid changes occur on the hydrodynamic forcing hitting a structure. Therefore, more attention is needed to be directed toward the effects of the instantaneous wave overtopping discharge on the structural stability and erosion of a hybrid structure.

CHAPTER 5

CONCLUSION AND RECOMMENDATIONS

Hybrid structures integrate well into local coastal systems and can include nourishment and dune restoration strategies. It is understood that hybrid structures consisting of sand-covered hard structures cannot function exactly as natural dunes since the existence, shape, and behavior of natural dunes is directly linked to the governing geomorphic processes and sediment supply. Thus, general sediment scarcity in certain coastal areas of the world remains an important consideration when creating hybrid systems. However, hybrid systems can be integral parts of coastal sediment feeder systems (i.e., mega nourishments) and play a vital role in erosion control and habitat creation. They can be viable Engineering-with-Nature® solutions that provide flexible coastal defense systems instead of fixed, rigid structures. The system's flexibility is essential in adapting to future climate and environmental changes. The addition of a mobile sand layer on top of existing hard coastal structures can reduce damages associated with extreme storms. This was shown, for example, through the performance of a hybrid structure (relic seawall) in reducing erosion and overwash at Bay Head, New Jersey. That level of protection was attained by strengthening the existing hard structure with an extra sand cover layer. Existing hybrid structures in the Netherlands also provide evidence that such hybrid approaches can easily adapt to environmental changes, especially sea-level rise. It is worth noting that hard coastal structures can protect coastal areas from future environmental changes. However, the construction cost of massive seawalls or dikes and the often-limited space may favor soft protection measures or hybrids if feasible.

Hybrid approaches can be applied in locations with limited space while still providing traditional coastal risk reduction. Design optimization of hybrid coastal structures has the potential to lower the overall cost of defense systems by reducing hard structure component design requirements (e.g., freeboard, material volume), wave runup and overtopping through the targeted use of sediment material. The question is how to select the optimum sand cover volume and core structure. Research efforts on hybrid concepts still have many gaps, especially in estimating hydrodynamic responses, erosion and overwash processes, and its environmental impact. The interaction between the soft and hard components of a hybrid structure is still not well understood. Knowledge gaps associated with the needed elevation of the hard structure elements of hybrid systems should be filled in by conducting more large- and small-scale physical model experiments and by conducting further numerical model studies. Those studies can provide more insight on the performance of those structures and to utilize them in coastal communities better. More investigations are needed into dune and beach profile evolution during extreme events and into the potential benefits of hybrid systems in controlling flooding and scouring associated with hard structures. Maintenance plans and techniques to estimate the costs and benefits of innovative hybrid structures are also needed to investigate the feasibility of such structures. The presented study contributes significantly toward a better understanding of wave overtopping phenomena above the crest of a hybrid structure.

This dissertation investigates the average and instantaneous wave overtopping over a hybrid coastal structure with the objectives to fill the research gaps for such structures and propose prediction formulae of wave overtopping. The hybrid approaches described herein combine traditional hard coastal structures (rubble mound) and sand covers mimicking dunes into single

systems. This type of structure can offer socioeconomic, ecological, and environmental benefits along with protection against flooding, surge, and wave attack.

It is essential to improve the knowledge base, tools, and expertise needed to develop new and sustainable ways to prepare the world's coastlines for extreme storms and relative sea level rise. The present research sets the stage for further hybrid structure research and design efforts. It raises awareness of the lack of proper criteria and formulae to design hybrid coastal structures. Also, it draws more attention to the need of such design methods combining aspects from the functional design of hard coastal structures and knowledge of morphodynamic evolution of beach and dune systems under hydrodynamic forcing conditions.

Empirical formulae for wave overtopping rate over a hybrid coastal structure were proposed based on the results and analysis of physical experiments. The physical model experiments of a hybrid coastal structure consisting of a rubble mound dike with a varying sand cover thickness were performed under different hydrodynamic conditions. The average and time varying wave overtopping rates were measured at the crest of the tested hybrid structure. The average wave overtopping rate for the hybrid structure was clearly dependent on the relative freeboard and relative water depth near the structure's toe. The new proposed empirical formula predicts the average wave overtopping rate per unit length for a hybrid structure concept combining a rubble mound dike and a sand cover layer. The individual wave overtopping (instantaneous wave overtopping) rates for the same hybrid structure were found to be represented by the two-parameter Weibull probability distribution.

Hybrid coastal structures with different sand cover layer thicknesses enhance the reduction of the overtopping volumes after the erosion or overwash of the sand layer. Initially, sand cover layer increases the overtopped volume compared to those overtopped the rubble mound dike. The eroded sediment is deposited near the toe of the hybrid structure and alters the water depths. The sand deposits affect hydrodynamic conditions and decrease overtopping volumes. As a result, hybrid structures on a prototype scale will eventually reduce, or at least delay, the flooding expected during extreme storms. In addition, significant wave energy dissipation is noticed after the sand layer thickness is eroded. This leads to lower wave forces on the structure and increases its stability.

The available data and the analysis of the results could be used to develop or improve the existing numerical models that predict wave overtopping rates. The inclusion of the sand cover layer in a validated numerical model open the space to investigate a wider range of scenarios such as different wave conditions, different types of structures, different types and sizes of sediments, and different structure slopes.

Advances in incorporating the response of hard and soft coastal defense approaches into design considerations during extreme storms should be studied because there are currently only limited data on how hybrid approaches perform during extreme storms. The effects of the sand cover layer on the geometrical design of the hard structure (i.e., height of the structure, stability of the structure, wave transmission, etc.) is still a topic of investigation. The structural stability of a hard structure buried in a dune may need to be evaluated based on the hybrid setup and modified critical failure mechanisms (e.g., overtopping, piping, instability of the structure via infiltration and erosion, etc.). Wave overtopping and its spatial distribution behind the crest are still needed

for hybrid structures. Investigating the spatial destruction of wave overtopping can help in estimate the load on the inner slope and evaluate the erosion of back slopes.

Only a few studies have been conducted on hybrid structures to investigate the influence of hard structures on dune erosion or to predict the erosion volume of hybrid structures. However, a prediction formula to estimate the erosion rates of hybrid structures is not proposed or investigated yet. The limited number of prototype examples and targeted research efforts for hybrid coastal structures highlights the need for physical and numerical model investigations that aim to utilize design tools for hybrid defenses.

Following are some research topics that are recommended to be addressed in the future investigation of hybrid structure behavior and design, specifically as it pertains to sand-covered rubble mound structure:

1. Wave runup characteristics and wave-induced morphological evolution.
2. Exploring the effect of other geometrical parameters of structure, including the side slope, height of the rubble mound, etc., on the average and instantaneous wave overtopping rates.
3. Establishing a prediction model of erosion rates for such hybrid structure.
4. Investigating hybrid structures numerically. This will allow investigation of many storm event scenarios and collection of more data to enhance the developed empirical formulae for wave overtopping.
5. Investigating the combined effect of wave and wind on wave overtopping rates.
6. Conducting large-scale experiments to eliminate any constraints related to scaling.

REFERENCES

Ahrens, J.P. and Heimbaugh, M.S., 1989. Seawall overtopping model, Proceedings of the twenty-first coastal engineering conference. ASCE, New York, 1988, Costa del Sol-Malaga, Spain, pp. 795-806.

Ahrens, J.P., Seelig, W.N., Ward, D.L. and Allsop, N.W.H., 1993. Wave runup on and wave reflection from coastal structures. Proceedings of Ocean Wave Measurement and Analysis (Waves '93) Conference, New Orleans, Louisiana, pp. 489-502.

Allsop, N.W.H. and Hettiarachchi, S.S.L., 1988. Reflections from coastal structures. 1988(21).

Almarshed, B., 2015. Extreme value analysis of significant wave height and storm tide, galveston,tx (unpublished report), Texas A&M University, Number of 32 pp.

Aminti, P. and Franco, L., 1988. Wave overtopping on rubble mound breakwaters, Proceedings of the twenty-first Coastal Engineering Conference. ASCE, New York, Malaga, pp. 770-781.

Andersen, T.L. and Burcharth, H.F., 2006. Landward distribution of wave overtopping for rubble mound breakwaters, Proceedings of the First International Conferece on the Application of Physical Modelling to Port and Coastal Protection Department of Civil Engineering, Aalborg University, pp. 401-411.

Arcadis, 2012. Kustwerk katwijk: Ontwerp- projectplan kustversterking katwijk. , In nauwe samenwerking met: Gemeente katwijk provincie zuid-holland, *Technical report*, Hoogheemraadschap van Rijnland, Number of 89 pp.

Basco, D.R., 1998. The economic analysis of "soft" versus "hard" solutions for shore protection: An example, Proceedings of the 26th International Conference on Coastal Engineering. ASCE, New York, pp. 1449-1460.

Bauer, B.O. and Davidson-Arnott, R.G.D., 2003. A general framework for modeling sediment supply to coastal dunes including wind angle, beach geometry, and fetch effects. Geomorphology, 49(1): 89-108.

Besley, P., 1999. Overtopping of seawalls: Design and assessment manual, 178. HR Wallingford Ltd, Environment Agency, North East Region, 51 pp.

Blenkinsopp, C., Matias, A., Howe, D., Castelle, B., Marieu, V. and Turner, I., 2016. Wave runup and overwash on a prototype-scale sand barrier. Coastal Engineering, 113: 88-103.

Boers, M., 2012. Technisch rapport duinwaterkeringen en hybride keringen 2011 Deltares, 140 pp.

Boers, M.B., Van Geer, P.F.C. and Van Gent, M.A., 2011. Dike and dune revetment impact on dune erosion, The Proceedings of the Coastal Sediments 2011 World Scientific Publishing Company, Miami, FL, pp. 810-823.

Boudreau, R., Sloop, R., Holloway, A. and Rivera, J., 2018. Maui's resilient living shoreline project provides adaptation strategy for critical infrastructure. Journal of the American Shore & Beach 86(4): 26-35.

Bradbury, A. and Allsop, N., 1988. A hydraulic effects of breakwater crown walls, Proceedings of the Breakwaters '88 Conference, Institution of Civil Engineers. Thomas Telford Publishing, London, UK, pp. 385-396.

Bruun, P., 1998. Dunes — their function and design. Proceedings of the plam beach international coastal symposium. Journal of Coastal Research, Special Issue No. 26: pp. 26-31.

Christiansen, M.B. and Davidson-Arnott, R., 2004. Rates of landward sand transport over the foredune at skallingen, denmark and the role of dune ramps. Geografisk Tidsskrift-Danish Journal of Geography, 104(1): 31-43.

CIRIA, 2007. Manual on the use of rock in coastal and shoreline engineering. Construction Industry Research and Information Association, London, United Kingdom, 639 pp.

CIRIA, CUR and CETMEF, 2007. The rock manual. The use of rock in hydraulic engineering (second edition). Construction Industry Research & Information Association (CIRIA), London, 1304 pp.

Coulton, P.K., Dean, C.B., Hatheway, D., Honeycutt, C.M., Johnson, J., Jones, P.C. and Komar, P.P., 2005. Fema coastal flood hazard analysis and mapping guidelines, *Focused Study Report*, Number of 84 pp.

D'Alessandro, F. and Tomasicchio, G.R., 2016. Wave–dune interaction and beach resilience in large-scale physical model tests. Coastal Engineering, 116: 15-25.

Davidson-Arnott, R., 2010. Introduction to coastal processes and geomorphology. Cambridge University Press Cambridge, New York, Melbourne, Madrid, Cape Town, Singapore, São Paulo, Delhi, Dubai, Tokyo, 442 pp.

de Waal, J. and Van der Meer, J., 1992. Wave runup and overtopping on coastal structures, Coastal Engineering Proceedings, pp. 1758-1771.

Dewberry and Davis, I., 1989. Basis of assessment procedures for dune erosion in coastal flood insurance studies report Washington, D.C.: Federal Emergency Management Agency, Number of 95 pp.

DHI, 2011. Mike 21 spectral waves fm module.

Donnelly, C., Kraus, N. and Larson, M., 2006. State of knowledge on measurement and modeling of coastal overwash. Journal of Coastal Research, 22(4): 965-991.

Ebersole, B.A., Massey, T.C., Hendon, D.L., Richardson, T.W. and Whalin, R.W., 2015. Interim report—ike dike concept for reducing hurricane storm surge in the houston-galveston region. Jackson State University.

Federal Emergency Management Agency, 1995. Guidelines and specifications for wave elevation determination and v-zone mapping., Washington, D.C. (unpublished). Number of 303 pp.

Federal Emergency Management Agency, 2011. Coastal construction manual: Principles and practices of planning, siting, designing, constructing, and maintaining residential buildings in coastal areas, FEMA P-55 (Volume I). Federal Emergency Management Agency, Washinghton DC, USA, 253 pp.

Figlus, J., Kobayashi, N., Gralher, C. and Iranzo, V., 2011. Wave overtopping and overwash of dunes. Journal of Waterway, Port, Coastal, and Ocean Engineering, 137(1): 26-33.

Figlus, J., West, N.A., Almarshed, B. and Jonkman, S.N., 2015. Conceptual design and physical model study of core-enhanced dunes as hybrid coastal defense structures, *Proceedings of Coastal Structures and Solutions to Coastal Disasters Joint Conference*, (Boston, MA: ASCE).

French, P., 2001. Coastal defences: Processes, problems and solutions. Routledge, London.

Goda, Y., 2000. Random seas and design of marine structures. Advanced series on ocean engineering, vol. 15. World Scientific Publishing company, Singapore.

Goring, D.G. and Nikora, V.I., 2002. Despiking acoustic doppler velocimeter data. Journal of Hydraulic Engineering, 128(1): 117-126.

Guerra, M. and Thomson, J., 2017. Turbulence measurements from five-beam acoustic doppler current profilers. Journal of Atmospheric and Oceanic Technology, 34(6): 1267-1284.

Hallermeier, R. and Rhodes, J., 1986. Description and assessment of coastal dune erosion. Dewberry & Davis, Inc.

Hancock, M.W. and Kobayashi, N., 1994. Wave overtopping and sediment transport over dunes, Proceedings of the 24th Coastal Engineering Conference. American Society of Civil Engineers 1995, Kobe, Japan, pp. 2028-2042.

Hanley, M.E., Hoggart, S.P.G., Simmonds, D.J., Bichot, A., Colangelo, M.A., Bozzeda, F., Heurtefeux, H., Ondiviela, B., Ostrowski, R., Recio, M., Trude, R., Zawadzka-Kahlau, E. and Thompson, R.C., 2014. Shifting sands? Coastal protection by sand banks, beaches and dunes. Coastal Engineering, 87: 136-146.

Harter, C. and Figlus, J., 2017. Numerical modeling of the morphodynamic response of a low-lying barrier island beach and foredune system inundated during hurricane ike using xbeach and cshore. Coastal Engineering, 120: 64–74.

Hedges, T. and Reis, M., 2004. Accounting for random wave run-up in overtopping predictions. Maritime Engineering Journal, 157: 113-122.

Houser, C., 2009. Synchronization of transport and supply in beach-dune interaction. Progress in Physical Geography: Earth and Environment, 33(6): 733-746.

Houser, C. and Hamilton, S., 2009. Sensitivity of post-hurricane beach and dune recovery to event frequency. Earth Surface Processes and Landforms, 34(5): 613-628.

Houser, C., Hapke, C. and Hamilton, S., 2008. Controls on coastal dune morphology, shoreline erosion and barrier island response to extreme storms. Geomorphology, 100(3–4): 223-240.

Houser, C., Wernette, P., Rentschlar, E., Jones, H., Hammond, B. and Trimble, S., 2015. Post-storm beach and dune recovery: Implications for barrier island resilience. Geomorphology, 234: 54-63.

Hughes, S.A., 1993. Physical models and laboratory techniques in coastal engineering, 7. World Scientific.

Hughes, S.A., 2004. Estimation of wave run-up on smooth, impermeable slopes using the wave momentum flux parameter. Coastal Engineering, 51(11–12): 1085-1104.

Hughes, S.A. and Thornton, C.I., 2016. Estimation of time-varying discharge and cumulative volume in individual overtopping waves. Coastal Engineering, 117: 191-204.

Hunt, I.A., 1959. Design of seawalls and breakwaters. Journal of Waterway Harbors Division: 123–152.

Irish, J., L Lynett, P., J Weiss, R., Smallegan, S.M. and Cheng, W., 2013. Buried relic seawall mitigates hurricane sandy's impacts. Coastal Engineering, 80: 79-82.

Jensen, O.J., 1984. A monograph on rubble mound breakwaters. Danish Hydraulic Institute (DHI).

Johnson, B.D., Kobayashi, N. and Gravens, M.B., 2012. Cross-shore numerical model cshore for waves, currents, sediment transport and beach profile evolution, Engineer research and development center Vicksburg MS coastal and hydraulic lab, Number of.

Julien, P.Y., 2010. Erosion and sedimentation. Cambridge University Press, 371 pp.

Kamphuis, J.W., 2010. Introduction to coastal engineering and management, 30. World Scientific, 437 pp.

Katul, G.G., Parlange, M.B., Albertson, J.D. and Chu, C.R., 1995. Local isotropy and anisotropy in the sheared and heated atmospheric surface layer. Boundary-Layer Meteorology, 72(1): 123-148.

Kim, H.D., 2017. Coastal protection techniques for storm damage experimental and numerical study on rock seawall in swash zone to reduce wave overtopping and overwash of sand beach, University of Delaware, 162 pp.

Kim, H.D., Kobayashi, N. and Cardenas, X.C., 2017. Comparison of rock seawall and dune for storm damage reduction, Proceedings of the 35th International Conference on Coastal Engineering ASCE, Reston, VA, pp. 1-13.

Klopman, G. and Van Leeuwen, P.J., 1990. An efficient method for the reproduction of non-linear random waves. Coastal Engineering(22): 478-488.

Kobayashi, N., 2016. Coastal sediment transport modeling for engineering applications. Journal of Waterway, Port, Coastal, and Ocean Engineering, 142(6): 03116001.

Kobayashi, N., Buck, M., Payo, A. and Johnson, B.D., 2009. Berm and dune erosion during a storm. Journal of Waterway, Port, Coastal, and Ocean Engineering, 135(1): 1-10.

Kobayashi, N. and Kim, H.D., 2017. Rock seawall in the swash zone to reduce wave overtopping and overwash of a sand beach. Journal of Waterway, Port, Coastal, and Ocean Engineering, 143(6): 04017033.

Kobayashi, N., Tega, Y. and Hancock, M.W., 1996. Wave reflection and overwash of dunes. Journal of Waterway, Port, Coastal, and Ocean Engineering, 122(3): 150-153.

Kolmogorov, A.N., Levin, V., Hunt, J.C.R., Phillips, O.M. and Williams, D., 1991. The local structure of turbulence in incompressible viscous fluid for very large reynolds numbers. Proceedings of the Royal Society of London. Series A: Mathematical and Physical Sciences, 434(1890): 9-13.

Kriebel, D.L. and Dean, R.G., 1985. Numerical simulation of time - dependent beach and dune erosion. Coastal Engineering, Volume 9(3): 221-245.

Larson, M., Erikson, L. and Hanson, H., 2004. An analytical model to predict dune erosion due to wave impact. Coastal Engineering, 51(8): 675-696.

Larson, M. and Kraus, N.C., 1989. Sbeach: Numerical model for simulating storm-induced beach change report 1: Empirical foundation and model development, Department of Water Resources Engineering Institute of Science and Technology, University of Lund, Vicksburg, Mississippi, Number of 115 pp.

Lee, G.-h., Nicholls, R.J. and Birkemeier, W.A., 1998. Storm-driven variability of the beach-nearshore profile at duck, north carolina, USA, 1981–1991. Marine Geology, 148(3): 163-177.

Mansard, E.P. and Funke, E., 1980. The measurement of incident and reflected spectra using a least squares method. Coastal Engineering Proceedings, 1(17).

Martin, V., S. R. Fisher, T., Millar, R. and C. Quick, M., 2002. Adv data analysis for turbulent flows: Low correlation problem, 1-10 pp.

Matias, A., Masselink, G., Castelle, B., Blenkinsopp, C.E. and Kroon, A., 2016. Measurements of morphodynamic and hydrodynamic overwash processes in a large-scale wave flume. Coastal Engineering, 113: 33-46.

McLelland, S.J. and Nicholas, A.P., 2000. A new method for evaluating errors in high-frequency adv measurements. Hydrological Processes, 14(2): 351-366.

Mertens, T., Verwaest, T., Delgado, R., Trouw, K. and De Nocker, L., 2011. Coastal management and disaster planning on the basis of flood risk calculations. Coastal Engineering Proceedings, 1(32): 12.

Miche, M., 1944. Mouvements ondulatries de la mer en profondeur constant on decroissante. Annales des Ponte et Chaussees, 114e Année: 25–78, 131–164, 270–292, 369–406.

Miller, J.K., Mahon, A.M. and Herrington, T.O., 2009. Development of the stevens dynamic underwater coastal surveying (ducks) system, Davidson Laboratory Technical Report, Coastal Protection Techanical Assistance Service, Number of.

Muller, J.R.M., 2017. A hybrid solution for galveston seawall: A study on the reduction of the hydraulic loads by a sand cover at the galveston seawall with the use of xbeach., Delft University of Technology and Texas A&M University – Galveston Campus, 87 pp.

Muller, J.R.M., Figlus, J. and Vries, S.d., 2018. Xbeach simulation of a hybrid coastal risk-reduction measure: A galveston seawall test case. Proceedings of 36th International Conference on Coastal Engineering, 1(36): 100.

Nederhoff, C., 2014. Modeling the effects of hard structures on dune erosion and overwash: Hindcasting the impact of hurricane sandy on new jersey with xbeach. Master's Thesis, Delft University of Technology, 169 pp.

Nederhoff, C.M., Lodder, Q.J., Boers, M., Den Bieman, J.P. and Miller, J.K., 2015. Modeling the effects of hard structures on dune erosion and overwash: A case study of the impact of

hurricane sandy on the new jersey coast, *The Proceedings of the Coastal Sediments 2015*. World Scientific, pp. 1-17.

Nordstrom, K.F., 2018. Coastal dunes with resistant cores. Journal of Coastal Conservation.

Nordstrom, K.F. and Arens, S.M., 1998. The role of human actions in evolution and management of foredunes in the netherlands and new jersey, USA. Journal of Coastal Conservation, 4: 169-180.

Nordstrom, K.F., Lampe, R. and Vandemark, L.M., 2000. Re-establishing naturally functioning dunes on developed coasts. Environmental Management, 25(1): 37-51.

Nortek, 2009. Vectrino velocimeter: User guide. Nortek Scientific Acoustic Development Group Inc, Norway, 41 pp.

Nortek, 2017. The comprehensive manual: Awac| aquadopp profiler | 2d horizontal profiler | vector | vectrino. Nortek Scientific Acoustic Development Group Inc, 151 pp.

Overton, M., Fisher, J. and Fenaish, T., 1987. Numerical analysis of swash forces on dunes, Proceedings of Coastal Sediments '87. ASCE 1990, New Orleans, Louisiana, pp. 632-641.

Owen, M., 1980. Design of seawalls allowing for wave overtopping, Number of 96 pp.

Pedersen, J. and Burcharth, H.F., 1992. Wave forces on crown walls, Coastal Engineering Proceedings of the twenty-third Coastal Engineering Conference. ASCE, New York, Venice, pp. 1489-1502.

Pullen, T., Allsop, N., Bruce, T., Kortenhaus, A., Sch, H. and Van der Meer, J., 2007. Wave overtopping of sea defences and related structures: Assessment manual. Kuratorium für Forschung im Küsteningenieurwesen, Hamburg, 178 pp.

Robin, G.D.D.-A., 2005. Conceptual model of the effects of sea level rise on sandy coasts. Journal of Coastal Research, 21(6): 1166-1193.

Roelvink, D.R., Van Dongeren, A., Van Thiel de Vries, J., McCall, R. and Lescinski, J., 2009. Modelling storm impacts on beaches, dunes and barrier islands. Coastal Engineering, 56(11–12): 1133-1152.

Sallenger Jr, A.H., 2000. Storm impact scale for barrier islands. Journal of Coastal Research, 16(3): 890-895.

Saye, S.E., van der Wal, D., Pye, K. and Blott, S.J., 2005. Beach–dune morphological relationships and erosion/accretion: An investigation at five sites in england and wales using lidar data. Geomorphology, 72(1): 128-155.

Sherwood, C.R., Long, J.W., Dickhudt, P.J., Dalyander, P.S., Thompson, D.M. and Plant, N.G., 2014. Inundation of a barrier island (chandeleur islands, louisiana, USA) during a hurricane: Observed water-level gradients and modeled seaward sand transport: Barrier-island inundation. Journal of Geophysical Research: Earth Surface, 119: 1498–1515.

Sigren, J.M., Figlus, J., Highfield, W., Feagin, R.A. and Armitage, A.R., 2018. The effects of coastal dune volume and vegetation on storm-induced property damage: Analysis from hurricane ike. Journal of Coastal Research: 164-173.

Smallegan, S.M., Irish, J.L., Van Dongeren, A.R. and Den Bieman, J.P., 2016. Morphological response of a sandy barrier island with a buried seawall during hurricane sandy. Coastal Engineering, 110: 102-110.

Steetzel, H.J., 1987. Systematic reserach on the effectiveness of dune toe revetments, large scale model investigation, (in dutch), report h298-i, Delft Hydraulics, Delft, The Netherlands, Number of.

Steetzel, H.J., 1991. Cross-shore transport during storm surges, Coastal engineering 1990, pp. 1922-1934.

Stronkhorst, J. and Lagendijk, O., 2012. Toekomstbestendige verharde zeeweringen in opdracht van Rijkswaterstaat, waterdienst, Number of 81 pp.

Sutton-Grier, A.E., Wowk, K. and Bamford, H., 2015. Future of our coasts: The potential for natural and hybrid infrastructure to enhance the resilience of our coastal communities, economies and ecosystems. Environmental Science & Policy, 51: 137-148.

Takada, A., 1970. On relation among wave run-up, overtopping and reflection, Proceedings of the Japan Society of Civil Engineers, pp. 19–30. (In Japanese).

Thorenz, F. and Blum, H., 2011. Implementing coastal defence strategies for sandy coasts–reinforcement of the norderney dune revetment. th 5 SCACR 2011 International Short

Conference on Applied Coastal Research, RWTH Aachen University, Germany, pp. 238-243.

U.S. Army, U.S. Navy and U.S. Air Force, 1978. Maintenance of waterfront facilities. Publication Army TM 5-622, Hyattsville.

U.S. Army Corps of Engineers, 2018. Coastal texasn protection and restoration feasibility study: Draft integrated feasibility report and environmental impact statement, 442 pp.

US Army Corps of Engineers, 2002. Coastal engineering manual. Engineer manual (in 6 volumes), 1110. U.S. Army Corps of Engineers, Washington, D.C., 2-1100 pp.

Van de Graaff, J., 1986. Probabilistic design of dunes; an example from the netherlands. Coastal Engineering, 9(5): 479-500.

Van de Graaff, J., 1989. Guide to the assessment of the safety of dunes as a sea defence. 9037600050, CUR, The Netherlands, Number of 30 pp.

Van der Meer, J., 2002. Technical report wave run-up and wave overtopping at dikes, Technical Advisory Committee on Flood Defence, Delft, The Netherlands, Number of 42 pp.

Van der Meer, J.W., 1993. Conceptual design of rubble mound breakwaters publication no. 483. Delft hydraulics, delft. 221-315.

Van der Meer, J.W., Allsop, N.W.H., Bruce, T., De Rouck, J., Kortenhaus, A., Pullen, T., Schüttrumpf, H., Troch, P. and Zanuttigh, B., 2016. Eurotop: Manual on wave overtopping of sea defences and related sturctures-an overtopping manual largely based on european research, but for worlwide application (second edition), 252 pp.

Van der Meer, J.W., Hoffmans, G. and Van der Hoven, A., 2014. Analyses grass erosion in wave run-up and wave overtopping conditions, Rijkswaterstaat, V&L. Deltares, Number of 97 pp.

Van der Meer, J.W. and Janssen, J.P., 1995. Wave run-up and wave overtopping at dikes and revetments. Wave forces on inclined and vertical structures, ASCE — Task Committee Reports (1995): 1-27.

Van der Meer, J.W., Verhaeghe, H. and Steendam, G.J., 2009. The new wave overtopping database for coastal structures. Coastal Engineering, 56(2): 108-120.

Van Doorslaer, K., De Rouck, J. and Gysens, S., 2009. Reduction of wave overtopping: From research to practice. 4th International Short Conference on Applied Coastal Research (SCACR-2009) Barcelona, Spain, pp. 337-346.

Van Geer, P., Boers, M. and Van Gent, M., 2009. Measurements on the interaction between dunes and dikes during extreme storm events, Proceedings of Coastal Dynamics 2009, (Tokyo, Japan), 10.1142/9789814282475_0086.

Van Gent, M., 2008. Large-scale tests to analyse the influence of collapsed dune revetments on dune erosion. Proceedings of the 31 st International Conference on Coastal Engineering, pp. 2583-2595.

Van Gent, M.R., Smale, A.J. and Kuiper, C., 2003. Stability of rock slopes with shallow foreshores. Proceedings of Coastal structures, pp. 100-112.

Van Gent, M.R.A., Van den Boogaard, H.F.P., Pozueta, B. and Medina, J.R., 2007. Neural network modelling of wave overtopping at coastal structures. Coastal Engineering, 54(8): 586-593.

Van Gent, M.R.A., Van Thiel de Vries, J.S.M., Coeveld, E.M., de Vroeg, J.H. and Van de Graaff, J., 2008. Large-scale dune erosion tests to study the influence of wave periods. Coastal Engineering, 55(12): 1041-1051.

Van Rijn, L.C., 1993. Principles of sediment transport in rivers, estuaries and coastal seas, 1006. Aqua publications Amsterdam.

Van Thiel de Vries, J., 2012. Dune erosion above revetments. ICCE 2012: Proceedings of the 33rd International Conference on Coastal Engineering, Santander, Spain, pp. 1-13.

Van Thiel de Vries, J.S.M., Van Gent, M.R.A., Walstra, D.J.R. and Reniers, A.J.H.M., 2008. Analysis of dune erosion processes in large-scale flume experiments. Coastal Engineering, 55(12): 1028-1040.

Vellinga, P., 1983. Predictive computational model for beach and dune erosion during storm surges, Proceedings of the Specialty Conference on Coastal Structures '83. American Society of Civil Engineers, pp. 806-819.

Verhaeghe, H., Van der Meer, J.W., Steendam, G.J., Besley, P., Franco, L. and Van Gent, M.R.A., 2003. Wave overtopping database as the starting point for a neural network prediction

method. In: J. Melby (Editor), Proceedings of the 4th Coastal Structures Conference. ASCE, Portland, Oregon, pp. 418–430.

Voorendt, M., 2015. Examples of multifunctional flood defences, Delft University of Technology, Department of Hydraulic Engineering, The Netherlands, Number of 72 pp.

Voorendt, M.Z., 2017. Design principles of multifunctional flood defences. Doctoral's Thesis, Delft University of Technology, The Netherlands, 342 pp.

Walling, K., Herrington, T.O. and Miller, J.K., 2016. Hurricane sandy damage comparison: Oceanfront houses protected by a beach and dune system with vs. Without a rock seawall. Shore & Beach, 84(3): 35-41.

Welch, P., 1967. The use of fast fourier transform for the estimation of power spectra: A method based on time averaging over short, modified periodograms. IEEE Transactions on Audio and Electroacoustics, 15(2): 70-73.

Wentworth, C.K., 1922. A scale of grade and class terms for clastic sediments. The Journal of Geology, 30(5): 377–392.

Williams, J., Buscombe, D., Masselink, G., Turner, I. and Swinkels, C., 2012. Barrier dynamics experiment (bardex): Aims, design and procedures. Coastal Engineering, 63: 3-12.

Woodruff, J.D., Irish, J.L. and Camargo, S.J., 2013. Coastal flooding by tropical cyclones and sea-level rise. Nature, 504: 44.

Wootton, L., Miller, J., Miller, C., Peek, M., Williams, A. and Rowe, P., 2016. New jersey sea grant consortium dune manual, njseagrant.org/dunemanual Number of 76 pp.

Zanuttigh, B. and van der Meer, J.W., 2008. Wave reflection from coastal structures in design conditions. Coastal Engineering, 55(10): 771-779.